

## **INFORMATION TO USERS**

This manuscript has been reproduced from the microfilm master. UMI films the text directly from the original or copy submitted. Thus, some thesis and dissertation copies are in typewriter face, while others may be from any type of computer printer.

**The quality of this reproduction is dependent upon the quality of the copy submitted.** Broken or indistinct print, colored or poor quality illustrations and photographs, print bleedthrough, substandard margins, and improper alignment can adversely affect reproduction.

In the unlikely event that the author did not send UMI a complete manuscript and there are missing pages, these will be noted. Also, if unauthorized copyright material had to be removed, a note will indicate the deletion.

Oversize materials (e.g., maps, drawings, charts) are reproduced by sectioning the original, beginning at the upper left-hand corner and continuing from left to right in equal sections with small overlaps.

Photographs included in the original manuscript have been reproduced xerographically in this copy. Higher quality 6" x 9" black and white photographic prints are available for any photographs or illustrations appearing in this copy for an additional charge. Contact UMI directly to order.

Bell & Howell Information and Learning  
300 North Zeeb Road, Ann Arbor, MI 48106-1346 USA  
800-521-0600

**UMI<sup>®</sup>**



VIOLATIONS OF ERGODICITY AS OBSERVED IN  
QUANTUM CHAOTIC SYSTEMS AND COULOMB  
BLOCKADE PEAK HEIGHTS

By

NICHOLAS ROBERT CERRUTI

A dissertation submitted in partial fulfillment of  
the requirements for the degree of

DOCTOR OF PHILOSOPHY

WASHINGTON STATE UNIVERSITY  
Department of Physics

DECEMBER 2000

UMI Number: 3007481

UMI<sup>®</sup>

---

UMI Microform 3007481

Copyright 2001 by Bell & Howell Information and Learning Company.


All rights reserved. This microform edition is protected against  
unauthorized copying under Title 17, United States Code.

---


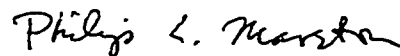
Bell & Howell Information and Learning Company  
300 North Zeeb Road  
P.O. Box 1346  
Ann Arbor, MI 48106-1346

To the Faculty of Washington State University:

The members of the Committee appointed to examine the dissertation of NICHOLAS ROBERT CERRUTI find it satisfactory and recommend that it be accepted.

A handwritten signature in cursive script, appearing to read "Steve Tompkins", written above a horizontal line.

Chair

A handwritten signature in cursive script, appearing to read "James S. Walker", written above a horizontal line.A handwritten signature in cursive script, appearing to read "Philip L. Marston", written above a horizontal line.

## ACKNOWLEDGMENTS

There are several people that I would like to thank for their help and support through out my years at Washington State University. First, I would like to acknowledge Steve Tomsovic for his patience and guidance during my doctoral work. I would also like to thank Brian Watkins and Tatsuro Nagano for many helpful discussions and general support. Working with Arul Lakshminarayan helped with the development of some of the ideas and theories presented here. Also there were several discussions with Julie Lefebvre and Michael Wolfson which proved useful. Two collaborators, Evgenii Narimanov and Harold Baranger, are appreciated for involving me in some of the research that they were doing. Finally, I would like to thank my parents for their continuing support. The work contained in this dissertation was supported by the National Science Foundation and the Office of Naval Research.

VIOLATIONS OF ERGODICITY AS OBSERVED IN  
QUANTUM CHAOTIC SYSTEMS AND COULOMB  
BLOCKADE PEAK HEIGHTS

Abstract

by Nicholas Robert Cerruti, Ph.D.  
Washington State University  
December 2000

Chair: Steven Tomsovic

Quantum systems that are classically chaotic were conjectured to follow the ergodic hypothesis stating that time averaging is equal to energy averaging. This dissertation investigates systematic deviations from this hypothesis in quantum chaotic systems and Coulomb blockade peak heights.

The first part of this dissertation contains a semiclassical analysis of the response of eigenvalues to a perturbation in quantum chaotic systems. The variance of the response is related to a classical diffusion coefficient. Also, we developed a new measure that sensitively probes phase space localization properties of the eigenstates based upon a correlation between the eigenvalues and the eigenfunctions. In the ergodic model, the correlation is predicted to be zero, i.e. no localization of the eigenfunctions. However, we find large deviations from ergodic theory based on classical orbits of the system.

The second part of this dissertation deals with quantum dots and an effect known as Coulomb blockade. Current can flow only if two different charge states of a quantum dot are

tuned to have the same energy; this produces a peak in the conductance of the dot whose magnitude is directly related to the magnitude of the wave function near the contacts of the dot. Since dots are generally irregular in shape, the dynamics of the electrons are chaotic, and the characteristics of Coulomb blockade peaks reflect those of wave functions in chaotic systems.

We developed a semiclassical theory of Coulomb blockade peak heights and showed that the dynamics in the dot lead to a large modulation of the peak heights. The corrections to the standard statistical theory, which assumes ergodicity, of peak height distributions, power spectra, and correlation functions are non-universal and can be expressed in terms of the classical periodic orbits of the dot that are well coupled to the leads. The resulting correlation function oscillates as a function of peak number in a way defined by such orbits; in addition, the correlation of adjacent conductance peaks is enhanced.



# Table of Contents

<b>Acknowledgments</b>	<b>iii</b>
<b>Abstract</b>	<b>iv</b>
<b>List of Figures</b>	<b>x</b>
<b>1 Introduction</b>	<b>1</b>
<b>2 Ergodicity</b>	<b>10</b>
<b>3 Classical Diffusion of Quantum Level Velocities: Systematic Deviations from Random Matrix Theory</b>	<b>18</b>
3.0 Abstract . . . . .	18
3.1 Introduction . . . . .	19
3.2 The Standard Map and Random Matrix Theory . . . . .	22
3.3 Semiclassical Theory . . . . .	28
3.3.1 The chaotic phase space . . . . .	28
3.3.2 The mixed phase space . . . . .	36

3.3.3	Generalizations . . . . .	41
<b>4</b>	<b>Exploring Phase Space Localization of Chaotic Eigenstates via Parametric Variations</b>	<b>50</b>
4.0	Abstract . . . . .	50
4.1	Introduction . . . . .	51
4.2	Preliminaries . . . . .	56
4.3	Ergodicity, Random Waves, and Random Matrix Theory . . . . .	61
4.4	Semiclassical Dynamics . . . . .	65
4.4.1	Level velocities . . . . .	66
4.4.2	Overlap intensities . . . . .	74
4.4.3	Weighted level velocities . . . . .	78
4.5	Stadium Billiard . . . . .	84
4.6	Conclusions . . . . .	99
4.A	Gaussian Integration . . . . .	100
4.B	Sum Rule for the Strength Function . . . . .	104
<b>5</b>	<b>Phase Space Localization of Chaotic Eigenstates: Violating Ergodicity</b>	<b>113</b>
5.0	Abstract . . . . .	113
5.1	Introduction . . . . .	114
5.2	The bakers map . . . . .	119
5.2.1	Semiclassical Evaluation . . . . .	119

5.2.2	Special case and verifications . . . . .	123
5.2.3	Classical features in the correlation . . . . .	128
5.2.4	General operators and selective enhancements . . . . .	136
5.3	The standard map . . . . .	140
5.3.1	The map and the mixed phase space regime . . . . .	140
5.3.2	Chaotic regime . . . . .	148
5.4	Summary and conclusions . . . . .	152
<b>6</b>	<b>Chaos in Quantum Dots: Dynamical Modulation of Coulomb Blockade Peak Heights</b>	<b>158</b>
6.0	Abstract . . . . .	158
6.1	Letter . . . . .	159
<b>7</b>	<b>Semiclassical Theory of Coulomb Blockade Peak Heights in Chaotic Quan- tum Dots</b>	<b>175</b>
7.0	Abstract . . . . .	175
7.1	Introduction . . . . .	176
7.2	The Height of a Conductance Peak in Coulomb Blockade . . . . .	180
7.3	Wave functions in the Dot: The Statistical Description . . . . .	182
7.4	Peak Heights Distribution . . . . .	188
7.5	Comparison with numerics and experiment . . . . .	202
7.6	Summary . . . . .	210

7.A Temperature Calculations . . . . .	212
<b>8 Conclusion</b>	<b>219</b>

## List of Figures

3.1	Variance vs. $k$ . . . . .	26
3.2	Variance vs. $k$ in mainly the mixed phase space regime . . . . .	38
3.3	Coefficient $c_2(k)$ vs. $k$ . . . . .	40
3.4	Quantum correlation between the matrix elements of two operators . . . . .	44
4.1	Strength function for the stadium billiard . . . . .	58
4.2	Illustration of ergodic behavior . . . . .	60
4.3	Random wavefunction . . . . .	63
4.4	Birkhoff coordinates . . . . .	86
4.5	Distribution of the level velocities for the stadium billiard . . . . .	88
4.6	Root mean square of the level velocities . . . . .	89
4.7	Wave packets in the stadium billiard . . . . .	90
4.8	Average overlap intensity for a Gaussian wave packet . . . . .	92
4.9	Root mean square of the overlap intensity for a Gaussian wave packet . . . . .	93
4.10	Scaling of the root mean square of the overlap intensities . . . . .	94
4.11	Overlap correlation coefficient for the stadium with energy range of 2200-2600 . . . . .	96
4.12	Trajectories corresponding to the peaks of the overlap correlation coefficient . . . . .	97

4.13	Overlap correlation coefficient for the stadium with energy range of 9200-10000	98
5.1	Correlation in the baker's map	129
5.2	Sections of the correlation	130
5.3	Classical structures in the correlation	131
5.4	Sections of the correlation to highlight the period-4 orbit	134
5.5	Correlation for $N = 128$ and $N = 200$	135
5.6	Inverse participation ratio for the bakers map	137
5.7	Correlation for the series of operators $A = \cos(2\pi 2^m q)$	139
5.8	Correlation for different harmonics $A = \cos(2\pi n q)$	141
5.9	Correlation for the operator $A = \cos(14\pi q)$	142
5.10	Quantum correlation for the standard map	145
5.11	Quantum correlation for the standard map at $\alpha = (0, 0)$	146
5.12	Quantum correlation for the standard map vs. $k$	153
6.1	Peak conductance	161
6.2	Power spectrum of peak heights	167
6.3	Conductance statistics	168
7.1	Peak conductances and power spectra	204
7.2	Peak amplitude vs. lead width	205
7.3	Peak-to-peak conductance correlation function	206
7.4	Temperature dependence of peak amplitude correlation function	208
7.5	Conductance statistics for symmetric and asymmetric lead placement	209

# Chapter 1

## Introduction

During the early development of quantum mechanics, the general notion of different “types” of quantum systems first emerged. Einstein, in 1917, recognized that classical chaotic motion such as found in the helium atom could not be quantized in the same way as hydrogen [1]. His paper and ideas seemed to go unnoticed for many decades. In the interim, Wigner was developing a statistical approach to make generalizations about the eigenvalues of complex nuclei [2]. His work later led to the concepts of ergodicity in quantum systems, whereas Einstein’s insight led to the concepts of “quantum chaos.”

It was once believed that if a classical system is chaotic, then the corresponding quantum system would obey ergodic theory. This is true as a first approximation in many asymptotic limiting processes (short wavelength, high energy, ...), but a richer display of features can be found in these systems. This dissertation examines some specific examples of how classical motion causes deviations from ergodicity in quantum mechanics. We will begin by defining chaos as it pertains to classical mechanics and then make some comments about chaos in quantum systems.

Classical dynamics can be classified with two extreme limiting cases: integrability and chaos. Most physical dynamical systems lie somewhere between the two, commonly called the “mixed” regime containing both stable and unstable motion. For integrable systems there is a constant of motion for each of the system’s degrees of freedom,  $d$ . This confines the dynamics

to a  $d$ -dimensional surface in the  $2d$ -dimensional phase space as defined by the action-angle variables. In contrast, chaotic systems have much more complicated trajectories. Measure one of the trajectories in a chaotic system are unstable, i.e. any two arbitrarily chosen nearby points will exponentially diverge from each other.

In quantum mechanics, the dynamics are solely governed by the Schrödinger equation which does not include any information about the classical orbits. The concept of a phase space does not exist in quantum mechanics. Due to the Heisenberg uncertainty principle, the solutions are probabilistic whereas in classical mechanics deterministic solutions can be found. An integrable quantum system has one good quantum number for each degree of freedom. On the other hand, there are no parallels with classical mechanics for a quantum chaotic system. It has been suggested that quantum evolution cannot exhibit chaos and, thus, there is no “quantum chaos.” This seems contrary to the many observations of quantum chaotic systems behaving differently from those that correspond to classically integrable system. For example, the distributions of the spacings of the eigenvalues obey different statistics [3]. It is these systems which are of interest to a number of physicists and engineers, since all but a handful of systems contain some regions of chaos. In addition, the theories developed for quantum chaos apply to wave chaos in general and are applicable to fields such as acoustics, oceanography and optics.

The correspondence between quantum and classical systems can be achieved by the use of semiclassical physics which utilizes classical information such as trajectories (rays) and actions (phases) to gain insight into quantum mechanical phenomena. The construction of



the wave functions is well understood for integrable systems where the quantization can be accomplished by the method of EBK (Einstein-Brillouin-Keller) [1, 4, 5], though it may be difficult to implement. For chaotic systems the quantization is complicated. Initially, only the density of the eigenvalues could be adequately reproduced [6] which involves only periodic orbits. More recently individual eigenstates could be semiclassically constructed [7] using a different set of classical orbits. These results are surprising since the orbits involved in these calculations have zero measure compared with the other trajectories that ergodically explore the available phase space in a chaotic system. The use of only small subsets of the complex trajectories in a chaotic system gave rise to some hope for describing events in quantum chaos via semiclassical mechanics. Another important accomplishment of semiclassical theory is in the propagation of states beyond times previously thought to be feasible by such methods [8].

In the next chapter we will define what it means for a quantum system to behave ergodically and briefly review some of the tools and measures used in quantum chaos to determine if a system is acting ergodically. These include the use of Wigner transforms which represent the wave functions in a pseudo-phase space. The larger than expected values of the wave function in the pseudo-phase space is known as phase space localization and is one way to observe deviations from ergodic expectations. The rest of this dissertation examines areas in quantum chaos where violations of ergodicity occur. We begin with a more abstract model using maps and infinite wells and in latter part we use a more applied model consisting of quantum dots.

The first part of this dissertation uses parametric variations to examine phase space lo-

calization in quantum chaotic systems. The parameter being varied,  $\lambda$ , is usually defined as, but not restricted to, a perturbation to the Hamiltonian,  $\hat{H} = \hat{H}_0 + \lambda \hat{H}_1$ . Parametric variations have been previously used to study the eigenstates and the statistics of the eigenvalues in chaotic systems. Many of these studies have shown agreement with the ergodic theory. Here is a partial list of some of those works. A new statistic, the parametric number variance, was developed which measures the correlation of fluctuations in energy levels as a parameter is varied [9]. The statistical properties of nonintegrable and chaotic energy spectra when parametrically varied were found to obey the ergodic model [10]. Also, the parametric motion of energy levels was statistically analyzed and was in good agreement with numerical data from the magnetized hydrogen atom and ergodic theory [11]. Certain correlators in disordered systems were discovered to depend only upon the symmetries of the systems after a rescaling was done [12, 13]. The distribution function of parametric derivatives of energy levels in quasi-1D systems (quantum kicked rotator, “domino” billiard, disordered wire, etc.) was derived [14]; the statistics of the derivatives were linked to the extent of the eigenfunctions. Phase space localization was explored using a correlation between parametrically varied eigenenergy levels and overlap intensities [15]. Parametric variations have also been used to explore the localization properties in disordered metals. The density of states using parametric variations in the Anderson model has been studied [16].

We use parametric variations of quantum chaotic systems to show how eigenvalues and eigenstates deviate from ergodicity in chapters 3-5. These chapters are papers either published in Physical Review E or in press. The two types of Hamiltonian systems studied here

are conservative continuous or time-dependent discrete quantum maps. With the help of Arul Lakshminarayan who worked out the theory for the quantum maps in detail [17] and Julie H. Lefebvre who provided the wave functions for the stadium billiard [18], we developed a new measure that quantifies phase space localization and connects the localization to classical orbits of the system. We also related the variance of the changes of the eigenenergies with respect to a parameter to classical diffusion coefficients [19].

The second part of this dissertation deals with conductance through quantum dots in the Coulomb blockade regime [20]. A quantum dot is a mesoscopic device that confines a 2D electron gas into a small region by the use of gates. When a voltage difference is applied to the leads, current would normally flow through the dot. The Coulomb blockade regime of a quantum dot consists of two tunneling barriers between the leads and the dot. Because of the tunneling barriers, electrons can become localized on the dot. This localization causes a potential barrier due to the Coulomb force that blocks the flow of additional electrons onto the dot, hence, the name “Coulomb blockade.” Current will only flow when the energy of the dot is unchanged as an additional electron is added. Thus, the conductance only occurs at discrete values of the gate voltage in the zero temperature limit. Assuming the eigenstates of the dot are ergodic, the distribution of the conductance peak heights was shown to obey Porter-Thomas statistics [21].

Applications for quantum dots, also known as single-electron transistors or artificial atoms, are fast emerging, so understanding their properties is becoming increasingly important. With the miniaturization of electronic circuits, single-electron transistors are a

very efficient way of storing data. Also, quantum dots have been used as devices that measure single charges called single-electrometers [22] and as far-infrared detectors [23]. There are still several unknown puzzles pertaining to quantum dots. Since quantum dots are usually irregular in shape they should obey the ergodic model, but deviations from ergodicity have been discovered in both the peak heights [24, 25] and peak spacings [26].

Chapters 6 and 7 which contains two more papers [27, 28] will demonstrate how the heights of the conductance peaks of quantum dots in the Coulomb blockade violate ergodicity. Evgenii E. Narimanov and Harold U. Baranger constructed a theory for quantum dots that explains a modulation of the conductance peaks. The numerical calculations that we provided for their theory demonstrated that this modulation is inconsistent for chaotic dots with a standard statistical model that depends on the eigenstates being ergodic. We showed that the modulation is a result of the classical periodic orbits that are well coupled to the leads of the dot. Interestingly, the modulation only slightly affects the distribution of the peak heights which again agrees with the standard statistical model.

We end with some concluding remarks and suggestions for further research. The results presented here only scratches the surface of quantum chaos and ergodicity. Understanding the role of chaos in quantum mechanics (or wave mechanics, in general) is becoming increasingly important as we try to comprehend our complex universe.

## References

- [1] A. Einstein, Verh. Dtsch. Phys. Ges. **19**, 82 (1917).
- [2] E. P. Wigner, Ann. Math. **53**, 36 (1951); **62**, 548 (1955); **65**, 203 (1957); **67**, 325 (1958).
- [3] O. Bohigas, M. J. Giannoni and C. Schmit, Phys. Rev. Lett. **52**, 1, (1984).
- [4] L. Brillouin, J. Phys. Radium **7**, 353 (1926).
- [5] J. B. Keller, Ann. Phys. (NY) **4**, 180 (1958).
- [6] M. C. Gutzwiller, *Chaos in Classical and Quantum Mechanics*, (Springer-Verlag, New York, 1990).
- [7] S. Tomsovic and E. J. Heller, Phys. Rev. Lett. **70**, 1405 (1993).
- [8] M. A. Sepúlveda, S. Tomsovic and E. J. Heller, Phys. Rev. Lett. **69**, 402 (1992).
- [9] J. Goldberg, U. Smilansky, M. V. Berry, W. Schweizer, G. Wunner and G. Zeller, Nonlinearity **4**, 1 (1991).
- [10] P. Gaspard, S. A. Rice, H. J. Mikeska and K. Nakamura, Phys. Rev. A **42**, 4015 (1990).
- [11] J. Zakrzewski and D. Delande, Phys. Rev. E **47**, 1650 (1993).

- [12] B. D. Simons and B. L. Altshuler, *Phys. Rev. B* **48**, 5422 (1993).
- [13] Y. Alhassid and H. Attias, *Phys. Rev. Lett.* **74**, 4635 (1995).
- [14] Y. V. Fyodorov, *Phys. Rev. Lett.* **73**, 2688 (1994).
- [15] S. Tomsovic, *Phys. Rev. Lett.* **77**, 4158 (1996).
- [16] D. J. Thouless, *Phys. Rep.* **13**, 93 (1974).
- [17] A. Lakshminarayan, N. R. Cerruti and S. Tomsovic, *Phys. Rev. E* **63** (2001) (to be published).
- [18] N. R. Cerruti, A. Lakshminarayan, J. H. Lefebvre and S. Tomsovic, *Phys. Rev. E* **63** (2001) (to be published).
- [19] A. Lakshminarayan, N. R. Cerruti and S. Tomsovic, *Phys. Rev. E* **60**, 3992 (1999).
- [20] C. W. J. Beenakker, *Phys. Rev. B* **44**, 1646 (1991).
- [21] R. A. Jalabert, A. D. Stone and Y. Alhassid, *Phys. Rev. Lett.* **68**, 3468 (1992).
- [22] T. A. Fulton and G. J. Dolan, *Phys. Rev. Lett.* **59**, 109 (1987).
- [23] S. Komiyama, O. Astafiev, V. Antonov, T. Kutsuwa and H. Hirai, *Nature* **403**, 405 (2000).
- [24] A. M. Chang, H. U. Baranger, L. N. Pfeiffer, K. W. West and T. Y. Chang, *Phys. Rev. Lett.* **76**, 1965 (1996).

- [25] S. R. Patel, D. R. Stewart, C. M. Marcus, M. Gokcedag, Y. Alhassid, A. D. Stone, C. I. Duruoz and J. S. Harris, Jr., *Phys. Rev. Lett.* **81**, 5900 (1998).
- [26] S. R. Patel, D. R. Stewart, A. G. Iuivers, C. M. Marcus, C. I. Duruoz, J. S. Harris, Jr., K. Campman and A. C. Gossard, *Phys. Rev. Lett.* **80**, 4522 (1998).
- [27] E. E. Narimanov, N. R. Cerruti, H. U. Baranger and S. Tomsovic, *Phys. Rev. Lett.* **83**, 2640 (1999).
- [28] E. E. Narimanov, H. U. Baranger, N. R. Cerruti and S. Tomsovic, (in preparation).

## Chapter 2

### Ergodicity

The general notion of ergodicity is that time averaging is equivalent to phase space averaging. In classical mechanics, this has the consequence that all but measure zero of the trajectories explore the available phase space on an ever finer scale. All the systems that are considered here are Hamiltonian and are either conservative continuous or time-dependent discrete maps. In conservative systems where the potential energy is time independent, chaos enters through extra degrees of freedom, i.e. the number of constraints is less than the number of degrees of freedom. For maps each iteration propagates the phase space points one time step and energy can be either added or taken out of the system, thus, relaxing the energy conservation constraint.

Ergodicity in quantum mechanics is not as well defined as it is in classical mechanics. For our purposes we will only examine “quantum ergodicity” as it pertains to the wave functions. One technique is to use Wigner transforms. The Wigner transform  $A(\mathbf{p}, \mathbf{q})$  of a quantum mechanical operator  $\hat{A}$  is one way of representing its projection into a pseudo-phase space. It is defined as

$$A(\mathbf{p}, \mathbf{q}) = \frac{1}{h^d} \int e^{-i\mathbf{p}\cdot\mathbf{x}/\hbar} \left\langle \mathbf{q} + \frac{1}{2}\mathbf{x} | \hat{A} | \mathbf{q} - \frac{1}{2}\mathbf{x} \right\rangle d\mathbf{x} \quad (2.1)$$

where  $d$  is the degrees of freedom of the system. For wave functions,  $\hat{A}$  is the projection operator  $|\psi\rangle\langle\psi|$  and its Wigner transform is denoted as  $\Psi(\mathbf{p}, \mathbf{q})$ . It was conjectured by Berry [1] that the wave functions of quantum chaotic systems would obey the so-called



ergodic hypothesis  $\Psi(\mathbf{p}, \mathbf{q}) \propto \delta(E - H(\mathbf{p}, \mathbf{q}))$  and that the amplitudes of the eigenstates would be Gaussian random. The ergodic hypothesis simply states that the Wigner transform of the wave function would uniformly inhabit all of the available phase space on the energy surface to within quantum fluctuations.

The strength function is another way to determine if the eigenstates are behaving ergodically [2]. It looks at aspects of the eigenstates other than their coordinate space representation. The strength function is the Fourier transform of the autocorrelation function of a state  $|\alpha\rangle$  that evolves in time,

$$\begin{aligned} S_\alpha(E) &= \frac{1}{2\pi\hbar} \int_{-\infty}^{\infty} \langle \alpha | \alpha(t) \rangle e^{iEt/\hbar} dt \\ &= \sum_n p_{\alpha n} \delta(E - E_n) \end{aligned} \quad (2.2)$$

The overlap intensities  $p_{\alpha n} = |\langle \alpha | \phi_n \rangle|^2$  where  $\phi_n$  are the eigenstates of the system. The strength function measures how similar the state  $|\alpha\rangle$  is to the eigenstates. Generally, it is of interest to choose  $|\alpha\rangle$  as a minimum uncertainty wave packet which is the closest representation of a classical particle in phase space. If the system is ergodic, then every eigenstate would exist near  $|\alpha\rangle$  and the overlap intensities would fluctuate with a  $\chi^2_\nu$  distribution. In systems with time reversal symmetry, the overlap intensity distribution is  $\chi^2_1$  (Porter-Thomas) since the eigenstate amplitudes are predicted to be Gaussian. Systems with broken time reversal symmetry have a  $\chi^2_2$  distribution. Along with the strength function, the autocorrelation function has also been used to predict ergodicity of the eigenstates [3].

A simple way to simulate locally the chaotic behavior of quantum eigenstates is to use

a random superposition of plane waves [4]. In a classically chaotic system, there exist an infinite number of rays passing through each point in coordinate space. The rays have random directions and can be constructed as plane waves using semiclassical theory. The plane waves are created each having a Gaussian random amplitude with random phase and direction but a fixed magnitude of the wave number,  $k$ . This model is consistent with having a rapid decay of the two-point correlation in the wave function. The correlation for the two-dimensional case is given by

$$C(\mathbf{x}, \mathbf{x} + \delta) = \int \psi^*(\mathbf{x})\psi(\mathbf{x} + \delta)d\mathbf{x} = AJ_0(k\delta) \quad (2.3)$$

where  $A$  is a constant and  $J_0$  is the zero order Bessel function. The superpositions are disorganized but there is a strong similarity between them and structures in classically chaotic Hamiltonian systems known as “scars” [5, 6]. A quantum eigenstate has a scar of a periodic orbit “if its density on the classical invariant manifolds near the periodic orbit differs significantly from the statistically expected density” [7]. The ridges of high intensities cannot be explained by the theory of scarring as no periodic orbits exist. They simply arise at values of  $\mathbf{x}$  when  $\cos(\mathbf{k}_i \cdot \mathbf{x} + \phi_i) \approx 1$  for most orientations of  $\mathbf{k}_i$ . The ridges appear to be a type of localization for a random system and this is contrary to the ergodic hypothesis.

Deviations from ergodicity has been observed in the localization of the wave functions as Anderson localization [8] in disordered systems, which is strongly exponential, and in a more weak form as scarring in chaotic systems. Anderson localization occurs in infinite, disordered systems when the intensities of the eigenfunctions are concentrated in a relatively small area of coordinate space. Scarring is observed in bounded chaotic systems where periodic orbits

exist. The connection between scars and periodic orbits was developed by Heller [5] through the use of strength functions and stability matrices. Heller found that most of eigenstates in the stadium billiard are scarred and, thus, associated with periodic orbits. A large value of the strength function indicates scarring, but a small value does not necessary mean that no scarring occurs. Since the strength function is state dependent, another state may yield a large value and thus indicate scarring. Other possible methods of localization are transport barriers in the form of broken separatrices [9], and cantori [10, 11], or diffusive motion [12]. These observations placed doubts on the ergodicity of the eigenstates of the stadium billiard or any classically chaotic system. The eigenstates of these systems were once thought to be entirely ergodic.

The deviations of ergodicity that we explore here arise out of the classical orbits of the system. A useful tool in the semiclassical calculations which we develop throughout the rest of this dissertation is the stability matrix,  $M$  [7]. The stability matrix relates nearby orbits to a reference trajectory. It is derived from a Taylor's expansion of the final positions and momenta in terms of the initial phase space coordinates. For a one-dimensional system we have

$$\begin{aligned}\delta p_f &= \frac{\partial p_f}{\partial p_i} \delta p_i + \frac{\partial p_f}{\partial q_i} \delta q_i = m_{11} \delta p_i + m_{12} \delta q_i \\ \delta q_f &= \frac{\partial q_f}{\partial p_i} \delta p_i + \frac{\partial q_f}{\partial q_i} \delta q_i = m_{21} \delta p_i + m_{22} \delta q_i\end{aligned}\tag{2.4}$$

where the  $m_{ij}$ 's are the elements of the stability matrix and  $\delta p_f$ ,  $\delta q_f$ ,  $\delta p_i$  and  $\delta q_i$  are the differences in the phase space coordinates between the orbit and the reference trajectory. The

subscripts  $f$  and  $i$  denote final and initial coordinates, respectively. This is more conveniently written in matrix form as

$$\begin{pmatrix} \delta p_f \\ \delta q_f \end{pmatrix} = \mathbf{M} \begin{pmatrix} \delta p_i \\ \delta q_i \end{pmatrix} \quad (2.5)$$

The determinant is always equal to unity by Liouville's Theorem. The trace determines whether the trajectory is stable or chaotic. If the absolute value of the trace is greater than two, then the eigenvalues are real and the trajectory is unstable and chaotic. The eigenvalues are given by  $\mu_{\pm} = \exp[\pm\lambda\tau]$  where  $\lambda > 0$  and is defined as the Lyapunov exponent. Conversely, stable trajectories result in complex eigenvalues and an absolute value of the trace less than two. These eigenvalues are given by  $\mu_{\pm} = \exp[\pm i\omega\tau]$ .

Another useful tool for studying chaotic systems in quantum mechanics which should obey the ergodic hypothesis is to use random matrix theory (RMT) [13]. A random matrix is an  $N \times N$  matrix whose elements are Gaussian random distributed according to a specific set of rules. A set of random matrices make up an ensemble. RMT is commonly used to simulate a Hamiltonian with complex interactions such as is found in chaotic systems. They were originally applied to nuclear spectra. It was shown [14] that there are only three possible types of Gaussian ensembles depending on the general symmetries of the system. For time-reversal symmetry the system is invariant under an orthogonal transformation and we have the Gaussian orthogonal ensemble (GOE). The system is invariant under a unitary transformation if time-reversal symmetry is broken and we have the Gaussian unitary ensemble (GUE). The Gaussian symplectic ensemble (GSE) is used when rotational invariance

is broken. When diagonalized, random matrices yield spectra and eigenstates for a generic quantum chaotic system. RMT predicts several statistical quantities for chaotic systems: the spacing distribution of the eigenvalues, the static correlation function, and the spectral rigidity [15].

The rest of this dissertation shows some examples of how quantum chaotic systems deviate from ergodicity. Allowing  $\hbar \rightarrow 0$  is analogous to letting the wavelength approach zero, i.e the system is becoming more classical. In this limit RMT and “ergodicity” are recovered. Expanding the quantities of interest in powers of  $\hbar$  yields that the zero order approximation is the RMT result. We will use this conjecture in the next several chapters to verify the validity of the derivations of some quantities that exhibit deviations from ergodicity.

## References

- [1] M. V. Berry, *J. Phys. A* **10**, 2083 (1977).
- [2] E. B. Stechel and E. J. Heller, *Ann. Rev. Phys. Chem.* **35**, 563 (1984).
- [3] M. Srednicki and F. Stiernelof, *J. Phys. A* **29**, 5817 (1996).
- [4] P. O'Connor, J. Gehlen and E. J. Heller, *Phys. Rev.* **58**, 1296 (1987).
- [5] E. J. Heller, *Phys. Rev. Lett.* **53**, 1515 (1984).
- [6] L. Kaplan and E. J. Heller, *Ann. Phys.* **264**, 171 (1998).
- [7] E. J. Heller, in *Les Houches LII, Chaos and Quantum Physics*, edited by M.-J. Giannoni, A. Voros, and J. Zinn-Justin (North-Holland, Amsterdam 1991).
- [8] P. W. Anderson, *Phys. Rev.* **109**, 1492 (1958).
- [9] O. Bohigas, S. Tomsovic and D. Ullmo, *Phys. Rep.* **223**, 43 (1993).
- [10] R. S. McKay and J. D. Meiss, *Phys. Rev. A* **37**, 4702 (1988).
- [11] R. Ketzmerick, G. Petschel and T. Geisel, *Phys. Rev. Lett.* **69**, 695 (1992).

- [12] S. Fishman, D. R. Grempel and R. E. Prange, *Phys. Rev. A* **36**, 289 (1987).
- [13] M. L. Mehta, *Random Matrices* (Academic Press, Boston, 1991).
- [14] F. J. Dyson, *J. Math. Phys.* **3**, 140 (1962); **3**, 157 (1962); **3**, 166 (1962); **3**, 1199 (1962).
- [15] O. Bohigas, in *Les Houches LII, Chaos and Quantum Physics*, edited by M.-J. Giannoni, A. Voros, and J. Zinn-Justin (North-Holland, Amsterdam 1991).

## Chapter 3

# Classical Diffusion of Quantum Level Velocities: Systematic Deviations from Random Matrix Theory

By Arul Lakshminarayan,<sup>1</sup> Nicholas R. Cerruti and Steven Tomsovic

Department of Physics, Washington State University,

Pullman, Washington 99164

Physical Review E **60**, 3992 (1999)

Copyright 1999 by the American Physical Society.

### 3.0 Abstract

We study the response of the quasi-energy levels in the context of quantized chaotic systems through the level velocity variance and relate them to classical diffusion coefficients using detailed semiclassical analysis. The systematic deviations from random matrix theory, assuming independence of eigenvectors from eigenvalues, is shown to be connected to classical higher order time correlations of the chaotic system. We study the standard map as a specific example, and thus the well known oscillatory behavior of the diffusion coefficient with respect to the parameter is reflected exactly in the oscillations of the variance of the level

---

<sup>1</sup>Permanent address: Physical Research Laboratory, Navrangpura, Ahmedabad 380 009, India



velocities. We study the case of mixed phase space dynamics as well and note a transition in the scaling properties of the variance that occurs along with the classical transition to chaos.

### 3.1 Introduction

The quantum spectrum is well known to reflect in several ways classical integrability or its lack thereof [1–3]. For a completely chaotic, quantized system the energy eigenvalues have characteristic, in fact, universal fluctuation properties that coincide with random matrix theory (RMT) universality classes and the eigenfunction components are also distributed as Gaussian random variables. However, there are important deviations from this dull uniformity imposed by the underlying (asymptotic) deterministic chaos. Classical periodic orbits, a dense set of measure zero unstable orbits, introduce characteristic deviations that are well documented, including the phenomenon of eigenfunction scarring [4]. The movement of energy levels with the variation of an external parameter, level dynamics, has also been studied by several authors with different motivations [5–10]. It is known that the motion of the energy levels as a function of the parameter, now a psuedo-time variable, is completely integrable whether the system is itself chaotic or not [11]. Nevertheless there are characteristic features that are introduced by chaos, for instance avoided crossings that may be characterized by the second derivative of the energy levels, *i.e.* the curvatures.

Here we study level “velocities”, and relate them directly to certain classical diffusion coefficients related to the diffusion of the variation of the action with the external parameter. Although we are using the term velocities, we are not discussing adiabatically changing a

system, just the slopes of the level curves as a function of a controllable parameter. It has been known for some time that these are Gaussian distributed with a variance that has been related to a classical “generalized conductance”, especially in the context of weakly disordered metallic grains. Methods employed were mostly field theoretic and RMT based, while numerical simulations of chaotic billiards led to the conjecture that the behavior of disordered systems could be extended to chaotic ones as well [8].

The variance has a significance beyond setting the scale of the Gaussian distribution of velocities. It enters as a normalization required to uncover possible universalities in parametric level correlations. It encodes the system specific characteristics of level motions as a function of an external parameter. Level correlations and velocities are experimentally accessible, for example in microwave cavities [12] or quantum dots, Although, universal parametric correlations are not well established experimentally, a recent experiment exploiting the similarity of elastomechanical wave equations of flexural modes of plates to the Schrodinger equation, seems to lend support to it [13].

In the case when the changing parameters are Aharanov-Bohm flux lines that do not lead to any classical dynamical changes, but do lead to important spectral modifications, correlation between level velocities were semiclassically considered in [14]. For a treatment of Hamiltonian flows see [15]. Recent closely related work, in the context of Hamiltonian flows, is also found in [16], where detailed results about the variance of level velocities are presented for billiards.

We make precise the connection between classical diffusion and the variance of the level

velocities in the simpler context of quantized maps or more generally time periodic systems where detailed semiclassical (and classical) analysis is possible. We evaluate the variance for the standard map as a function of the external kicking strength and show system specific correlations in the form of Bessel function oscillations. Since two-dimensional area preserving, or more generally symplectic maps, are Poincare sections of Hamiltonian flows, our analysis also reflects upon these systems and is consistent with results derived therein. On the other hand, due to the vastly simpler numerical and analytical work involved with maps, they lend themselves to more detailed and extensive work.

We relate our analysis to a semiclassical evaluation of expectation values of generic operators in the eigenbasis, as well as touch upon two parameter variations and their correlations. The case when the dynamics leads to a mixed phase space is generic and we find a Weyl type expansion in  $\hbar$  for the variance. The principal contribution in this regime is well predicted by a simple *classical* correlation, which vanishes as the system undergoes a transition to chaos. The different scaling behaviors in effective  $\hbar$  for mixed and chaotic systems can be experimentally observed. We will consider the standard map as an example. Others before us have used such systems to study level dynamics [9, 17].

## 3.2 The Standard Map and Random Matrix Theory

Here we define the model studied below and derive the RMT predictions for these. Let the classical Hamiltonian have the form

$$H = p^2/2 - \lambda V(q) \sum_{n=-\infty}^{\infty} \delta(t - n) \quad (3.1)$$

so that the Floquet operator connecting states just before kicks is given by

$$U = \exp(-ip^2/2\hbar) \exp(i\lambda V(q)/\hbar). \quad (3.2)$$

The time between kicks is taken to be unity, as there are two independent parameters already present, namely  $\lambda$  and  $N$ . Such systems, known as quantum maps, were first studied in [18, 19] and led to the uncovering of dynamical localization, akin to Anderson localization in disordered conductors [20]. We will typically consider the above to be the way the parameter of interest ( $\lambda$ ) enters the problem.

While this is a map on the plane (for one-degree-of-freedom systems), we consider their restriction to the torus  $[0, 1)^2$ . This is essential as we have in mind bounded Hamiltonian systems and not open scattering ones. Periodic boundary conditions are imposed in both  $p$  and  $q$  directions. We will assume that  $V(q)$  is a smooth function on  $[0, 1)$  with unit periodicity. Denote its average as

$$\bar{V} = \int_0^1 V(q) dq. \quad (3.3)$$

Let the quantum map be the  $N$  dimensional unitary matrix operator denoted by  $U$ . Maps, such as the standard map, restricted to a torus are quantized using standard canonical quantization [21]. Periodic boundary conditions in both canonical variables imposes a finite number of states which is the inverse effective Planck constant ( $\hbar = 1/N$ ). Thus the classical limit is approached in the large  $N$  limit. Various quantum maps on the torus have been studied and form an important part of the literature on quantum chaos due to their inherent simplicity [22–25]. The discrete spectra ( $N$  levels) obtained are then analyzed for various properties, in particular here the eigenangle velocities are obtained.

The classical standard map is given by the recursion

$$\begin{aligned} q_{i+1} &= (q_i + p_{i+1}) \bmod (1) \\ p_{i+1} &= (p_i - (k/2\pi) \sin(2\pi q_i)) \bmod (1), \end{aligned} \tag{3.4}$$

where  $i$  is the discrete time. This is the solution to the Hamiltonian equations of motion for the potential  $V(q) = \cos(2\pi q)$  and the Hamiltonian in Eq. (3.1). The dynamical variables are monitored just before the kicks, and  $\lambda = k/(2\pi)^2$ . The standard map is of central importance as many other maps are locally described by this and the potential may be considered to be the first term in the Fourier expansion of more general periodic potentials. The parameter  $k$  is of principal interest and it controls the degree of chaos in the map, a complete transition to ergodicity is attained above values of  $k \approx 5$ , while the last rotational KAM torus breaks around  $k \approx .971$  [26].

The quantum map in the discrete position basis is given by [27]

$$\langle n|U|n'\rangle = \frac{1}{\sqrt{iN}} \exp\left(i\pi(n-n')^2/N\right) \exp\left(i\frac{kN}{2\pi} \cos(2\pi(n+a)/N)\right). \quad (3.5)$$

The parameter to be varied will be the “kicking strength”  $k$ , while the phase  $a$  will be used to avoid exact quantum symmetries, and  $n, n' = 0, \dots, N-1$ . The eigenvalue problem of the unitary matrix is written as  $U|\psi_j\rangle = \exp(-i\phi_j)|\psi_j\rangle$ . The eigenangles  $\phi_j$  are real and their variation with the parameter  $k$  (level “velocities”) are given simply by the matrix elements

$$\frac{d\phi_j}{dk} = \frac{N}{2\pi} \langle \psi_j | V | \psi_j \rangle = \frac{N}{2\pi} \langle \psi_j | \cos(2\pi q) | \psi_j \rangle. \quad (3.6)$$

The  $2\pi$  factor is the result of choosing  $k$  as the relevant parameter and not  $k/2\pi$  and we retain this as this corresponds to the more conventional usage where the last KAM torus breaks when the parameter value is just under unity.

It is then clear that studying level velocities is equivalent to studying expectation values of operators in the eigenbasis. Thus if we require  $\langle \psi_i | A | \psi_i \rangle$  we would look at the modified unitary operator (assuming  $A$  is Hermitian)

$$U = U_0 \exp(-i\lambda A/\hbar) \quad (3.7)$$

where  $U_0$  is the quantum system under study. Then the expectation values are simply the corresponding level velocities evaluated at  $\lambda = 0$ , multiplied by  $\hbar$ . If one may identify the

classical canonical transformation generated by  $A$ , we could study a modified classical map, as well. However since  $\lambda = 0$ , it is the properties of the original classical map that will be relevant. The work [28] already discussed the general problem of semiclassical evaluation of matrix elements and our following work may be viewed in this context as well.

From the Gaussian distribution of eigenfunctions for a quantum chaotic system we expect the level velocities be similarly distributed. We will concentrate on the variance of these velocities, namely the sum:

$$\sigma^2(k, N) = \frac{1}{N} \sum_{j=1}^N \left( \frac{d\phi_j}{dk} \right)^2 - \left( \frac{1}{N} \sum_{j=1}^N \left( \frac{d\phi_j}{dk} \right) \right)^2, \quad (3.8)$$

We will assume, as is the case with the standard map example, that the average vanishes, *i.e.*  $\bar{V} = 0$ . Later we will generalize to the case of a non-vanishing average, or expectation values of operators with non-zero traces. Figure 3.1 shows a scaled  $\sigma^2$  as a function of the parameter  $k$ . At about  $k \approx 5$  the variance settles down to a near constant, this value coincides with the disappearance of major islands of stability in the classical phase space. What interests us primarily here however is the clear oscillations that persist as a function of  $k$  right into regions of large chaos as shown in the inset.

First we study the value around which the oscillations occur, as this is provided by assuming RMT models. Using Eq. (3.6) we get

$$\sigma_{\text{RMT}}^2 = \frac{N}{4\pi^2} \sum_{m=0}^{N-1} \left( \sum_{n=0}^{N-1} |\langle \psi_m | n \rangle|^2 V((n+a)/N) \right)^2$$

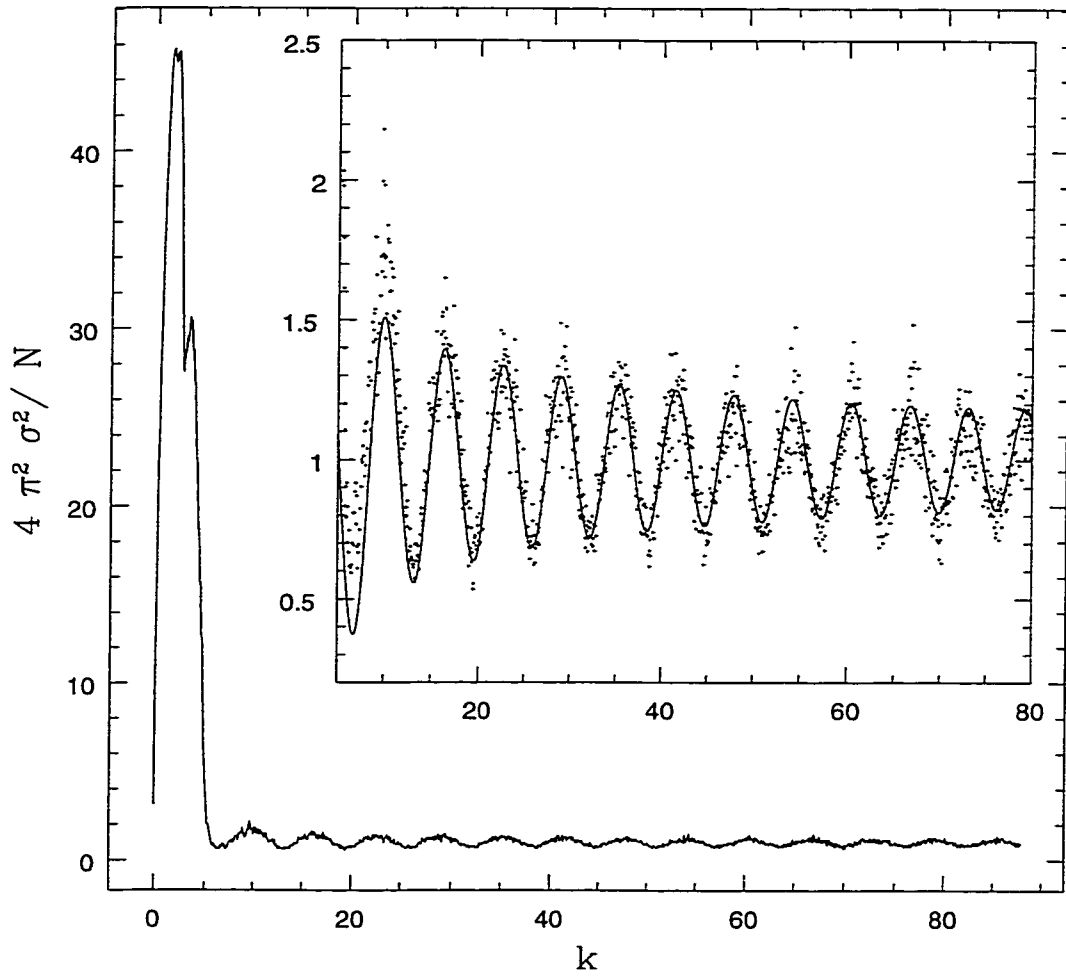


Figure 3.1: Scaled variance as a function of the parameter  $k$ ,  $N=300$ ,  $a=0.35$ . The inset shows a part of the plot magnified, the points are numerical data while the smooth line is the twice the diffusion coefficient. Quantities plotted are dimensionless.



$$\begin{aligned}
&= \frac{N}{4\pi^2} \sum_{m=0}^{N-1} \left( \sum_{n=0}^{N-1} |\langle \psi_m | n \rangle|^4 (V((n+a)/N))^2 + \right. \\
&\quad \left. \sum_{n \neq n'} |\langle \psi_m | n \rangle|^2 |\langle \psi_m | n' \rangle|^2 V((n+a)/N) V((n'+a)/N) \right). \tag{3.9}
\end{aligned}$$

The eigenfunctions have been expanded in a basis that diagonalizes the perturbation  $V$ , which we have taken to be the position basis. Since we assume a zero centered or trace-less perturbation

$$\sum_{n=0}^{N-1} V((n+a)/N) = 0.$$

We use the square of this relation in Eq. (3.9) while replacing eigenfunction components by their ensemble averages (denoted by angular brackets) to derive that

$$\sigma_{\text{RMT}}^2 = \frac{N^3}{4\pi^2} \overline{V^2} \left( \langle |\langle \psi_m | n \rangle|^4 \rangle - \langle |\langle \psi_m | n \rangle|^2 |\langle \psi_m | n' \rangle|^2 \rangle \right). \tag{3.10}$$

A crucial step in writing down the above is to assume the independence of the eigenfunction components from any specific position eigenvalues. While this is a reasonable statistical assumption we will see below that it misses important correlations that are incorporated naturally in semiclassical treatments. This is the origin of the non-universality of level dynamics, as this implies system dependent correlation effects. The same perturbations ( $V$ ) applied to different chaotic systems will result in different statistical responses, unlike the predictions of RMT.

We use standard results from RMT relevant to the Gaussian Orthogonal Ensemble (GOE), which is applicable here as well as the relevant Circular ensembles, [29]. In par-

ticular

$$\begin{aligned}\langle |\langle \psi_m | n \rangle|^4 \rangle &= \frac{3}{N(N+2)} \sim \frac{3}{N^2}, \\ \langle |\langle \psi_m | n \rangle|^2 |\langle \psi_m | n' \rangle|^2 \rangle &= \frac{1}{N(N+2)} \sim \frac{1}{N^2}.\end{aligned}$$

We finally get

$$\sigma_{\text{RMT}}^2 = \frac{N}{2\pi^2} \overline{V^2}. \quad (3.11)$$

As a special case for the standard map  $\overline{V^2} = 1/2$  and we get  $\sigma_{\text{RMT}}^2 = N/4\pi^2$ . This last result explains the value about which the oscillations occur in Fig. 3.1. This implies that the response of the system as measured by the movement of the energy levels is essentially the intensity of the perturbation. For chaotic systems then the response is independent of the system's detailed dynamical properties. We must also point out that when time reversal symmetry is broken the response is half as large. We now turn to the systematic oscillations that are not readily predicted by random matrix theory and are manifestly system dependent.

## 3.3 Semiclassical Theory

### 3.3.1 The chaotic phase space

We first develop in some generality expressions for the variance of the level velocities in which semiclassical methods can be easily applied. We write a gaussian smoothed density

of states [30] as

$$\rho_M(\phi) = \sum_{n=-\infty}^{\infty} F_M(n) \exp(in\phi) \text{Tr} U^n, \quad (3.12)$$

where  $F_M(n) = \exp(-n^2/2M^2)/(2\pi)$  is introduced to avoid divergences. The exact spiked density of states is obtained in the limit  $M \rightarrow \infty$  although almost all levels will be resolved at  $M = N$ , as the mean level spacing is  $2\pi/N$ . The smoothed step function,  $N_M(\phi)$  is the integral of the level density with respect to  $\phi$ . We derive then that

$$\int_0^{2\pi} \left( \frac{dN_M(\phi)}{dk} \right)^2 d\phi = \frac{MN\sigma^2(k, N)}{2\sqrt{\pi}} = 2\pi \sum_{n=-\infty}^{\infty} \frac{F_M^2(n)}{n^2} \left| \frac{d}{dk} \text{Tr}(U^n) \right|^2. \quad (3.13)$$

The term  $n = 0$  does not belong in the sum, and it is understood that the first equality is an approximation that becomes exact as  $M \rightarrow \infty$ . From this expression it follows that it is the long time traces of the propagator, and therefore semiclassically, long periodic orbits that are important.

Another very similar route is through the identity

$$\text{Tr}(U^n V) = \sum_{j=0}^{N-1} \langle \psi_j | V | \psi_j \rangle \exp(-i\phi_j n) \quad (3.14)$$

thus implying that

$$\sigma^2(k, N) = \frac{N}{4\pi^2} \left\langle |\text{Tr}(U^n V)|^2 \right\rangle_n, \quad (3.15)$$

where the angular brackets indicate averaging over time  $n$  in the neighborhood of large  $n$ . We assume as is relevant for chaotic systems that there are no degeneracies. To make

connections with the standard map above we would take  $V = \cos(2\pi q)$ .

Now we make use of the semiclassical approximation of the trace of the propagator as a sum over periodic orbits [1, 31] which is

$$\text{Tr}(U^n) \sim n \sum_p A_p^{(n)} \exp\left(2\pi i N S_p^{(n)} - i\pi\nu_p/2\right), \quad (3.16)$$

where  $A_p^{(n)} = 1/(2 \sinh(\lambda_p n/2))$ , and the sum is over periodic orbits of period  $n$  which labelled by  $p$  and have a Lyapunov exponent  $\lambda_p$ . The actions of these orbits are denoted by  $S_p^{(n)}$  and are calculated from the generating function of the classical map. The phases  $\nu_p$  are Maslov like indices and will not concern us here.

There is also a generalization of the above, which is particularly easy to derive when the perturbation is diagonal in the position (or momentum) basis.

$$\text{Tr}(U^n V) \sim \sum_p A_p^{(n)} \exp\left(2\pi i N S_p^{(n)} - i\pi\nu_p/2\right) \sum_{j=1}^n V(x_j^p). \quad (3.17)$$

Here  $V(x_j^p)$  is the value of a phase space representation of the operator  $V$  that is evaluated along the periodic orbit labelled  $p$  and at the point labelled  $j$ . An appropriate generalization in the energy domain for continuous time systems is found in [28]. The sum around the periodic orbit of the function  $V$  is essentially the derivative of the action with the parameter, and we may use either the first trace formula in conjunction with Eq. (3.13) or the second with Eq. (3.15).

We take the second route as we connect with the first subsequently. Taking the modulus

of the second trace formula gives

$$|\mathrm{Tr}(U^n V)|^2 \sim \sum_p A_p^{(n)2} \left( \sum_{j=1}^n V(q_j^p) \right)^2 + \sum_{p \neq p'} A_p^{(n)} A_{p'}^{(n)} \left( \sum_{j=1}^n V(q_j^p) \right) \left( \sum_{j=1}^n V(q_j^{p'}) \right) \exp(2\pi i N(S_p - S_{p'})). \quad (3.18)$$

As is usual, we have separated the diagonal contribution from the “off-diagonal”, which corresponds to distinct pairs of orbits, with distinct actions. We have also assumed for simplicity, as is the case with the specific parameter variation chosen above in the standard map, that  $V(x)$  is only position dependent; this does not alter the results below. We have also included the phases into the actions.

Since we expect that long periodic orbits are important, the diagonal approximation, which relies on random phases may be violated due to subtle correlations among their actions. The time at which we may expect action differences of the order of  $\hbar$  is the so called log-time, or Ehrenfest time. We argue that action differences are of the order of the orbit separation, and since areas of the order of  $\hbar$  (for two-dimensional maps) would be populated with multiple periodic orbits beyond the log-time, their action differences would also be comparable with  $\hbar$ . However long periodic orbit actions are randomly distributed and will acquire correlations only around the Heisenberg time. At this time the off-diagonal terms will dominate the sum, as happens if we simply consider  $\langle |\mathrm{Tr}(U^n)|^2 \rangle_n$ , which is asymptotically  $N$ , while the diagonal term is linearly increasing in time.

However the off-diagonal term vanishes due to the sums of  $V(q)$  over very long periodic

orbits. We may write for two distinct orbits  $p$  and  $p'$  after assuming uniform measure and replacing time averages over the periodic orbit, by the phase space average that

$$\left(\sum_{j=1}^n V(q_j^p)\right)\left(\sum_{j=1}^n V(q_j^{p'})\right) \sim n \bar{V}^2 \quad (3.19)$$

From our initial assumption that  $\bar{V} = 0$ , the off-diagonal term vanishes. The diagonal term is non-vanishing as we once again treat periodic orbits as ordinary long chaotic trajectories and derive that

$$\frac{1}{n}\left(\sum_{j=1}^n V(q_j^p)\right)^2 \equiv D(k) = C(0) + 2 \sum_{l=1}^n C(l) \quad (3.20)$$

where the time correlations are replaced by classical phase space averages due to ergodicity.

$$C(l) = \langle V(q_0)V(q_l) \rangle = \frac{1}{\mathcal{A}} \int_{\mathcal{A}} dq_0 dp_0 V(q_0)V(f^l(q_0, p_0)), \quad (3.21)$$

where  $f^l(q_0, p_0) = q_l$ ,  $f^l$  is the integrated dynamics in time  $l$ , and  $\mathcal{A}$  denotes both the phase space and its area (in the cases considered this is unity). We assume that these exist, and are decreasing with  $l$ , typically exponentially for chaotic systems and that a few terms may be sufficient. This is not established in generality and complications may arise due to marginally stable orbits leading to non-exponential behaviors. For the standard map, coefficients upto  $C(2)$  are dominant and sufficient to see the essential behaviour. We have dropped the index  $p$  as now we will treat such long periodic orbits as generic non-periodic orbits. Indeed by using the ergodic theorem we have already abandoned any particularities that may arise due to the orbit being periodic. Later, we remark on a case when we may not neglect off-diagonal

terms.

The alternative route is to take the derivative of the first trace formula and use Eq. (3.13). Again we neglect the off-diagonal terms for reasons given above. We will assume that the derivatives of the actions with the parameter (“action velocities”), for a given period or period interval, are such that their average is zero while their variance is proportional to the time period. This assumption is equivalent to the vanishing of the phase space average of  $V(q)$  and the presence of ergodicity. This was noted for general Hamiltonian systems in [32], and we will see below in the context of maps how this simply arises. We replace then for each time  $n$  the individual action velocities (squared) by the variance,

$$\left\langle \left( \frac{dS_p^{(n)}}{dk} \right)^2 \right\rangle_p = D(k) n, \quad (3.22)$$

where the angular brackets indicate the average over periodic orbits of period  $n$ .

In either approach, the uniformity principle [33] is applied in the form that there are  $e^{hn}/n$  orbits each with a Lyapunov exponent approximately  $\lambda$  per unit time. Then  $|A_p^{(n)}|^2 \approx e^{-\lambda n}$ , and assuming near equality of the topological entropy  $h$  and  $\lambda$ , we derive from Eq. (3.18) that

$$|\text{Tr}(U^n V)|^2 \sim g D(k). \quad (3.23)$$

Similarly from the other approach

$$\frac{1}{n^2} \left| \frac{d}{dk} \text{Tr} U^n \right|^2 \sim g \frac{N^2}{4\pi^2} D(k). \quad (3.24)$$

The tilde sign in the above equations implies that the L.H.S can be expected to be the R.H.S in an average sense. The spread in time  $n$  will also reflect the spread in the average action velocity diffusion coefficient  $D(k)$  with period. Results not shown here indicate that in the chaotic regime this is an exponential distribution. The factor  $g$  inserted above is due the fact that symmetries can impose distinct orbits to have identical actions. This factor must be determined from classical and quantal symmetries, and includes phase space symmetries. We finally get then from either approach the response in terms of the variance of the level velocities:

$$\sigma^2(k, N) = g \frac{N}{4\pi^2} D(k). \quad (3.25)$$

Thus the variance of the level velocities is proportional to a classical diffusion coefficient that determines the diffusion of action velocities of periodic orbits. More explicit expressions for this coefficient are now derived. Area preserving maps, such as the standard map, have a generating function  $L(q_{i+1}, q_i; k)$  from which the map may be derived as  $\partial L/\partial q_i = -p_i$  and  $\partial L/\partial q_{i+1} = p_{i+1}$  (I. C. Percival in [2]). The total action of a periodic orbit is equal to  $S_p^{(n)} = \sum_i L(q_{i+1}, q_i; k)$ , where the sum is over the  $n$  periodic points of the orbit  $p$ . Thus we derive, after assuming that the orbit is not at a point of bifurcation, that for a periodic orbit:

$$\frac{dS_p^{(n)}}{dk} = \frac{\partial S_p^{(n)}}{\partial k}. \quad (3.26)$$

We have not used the partial derivative sign in defining the level velocities although we assume that only one parameter is varied. This is due to the subsequent fact that when the



classical action derivative is written, it is a total derivative, in as much as the periodic orbit itself changes with the parameter. These two, however, are shown to be equal in the case of periodic orbits.

The variance is given by

$$\left\langle \left( \frac{dS_p^{(n)}}{dk} \right)^2 \right\rangle_p = \left\langle \sum_{i,j=1}^n \cos(2\pi q_i) \cos(2\pi q_j) \right\rangle_p \sim \frac{n}{2} (1 + 2J_2(k)) \quad (3.27)$$

In the equality the sum is over different times along a given periodic orbit and then averaged over all periodic orbits of period  $n$ , while the approximation arises from a replacement of the average by the usual ensemble average and retaining up to the second order time correlation. More precisely  $C(0) = 1/2$ ,  $C(1) = 0$ ,  $C(2) = J_2(k)/2$ , where  $J_2(k)$  is a Bessel function. These are derived from:

$$\begin{aligned} C(0) &= \frac{1}{n} \sum_{i=1}^n \cos^2(2\pi q_i) \sim \int_0^1 \int_0^1 \cos^2(2\pi q) dq dp = 1/2, \\ C(1) &= \frac{1}{n} \sum_{i=1}^n \cos(2\pi q_i) \cos(2\pi q_{i+1}) \\ &\sim \int_0^1 \int_0^1 \cos(2\pi q) \cos(2\pi(q + p - (k/2\pi) \sin(2\pi q))) dq dp = 0, \\ C(2) &= \frac{1}{n} \sum_{i=1}^n \cos(2\pi q_{i-1}) \cos(2\pi q_{i+1}) \\ &\sim \int_0^1 \int_0^1 \cos(2\pi(q - p)) \cos(2\pi(q + p - (k/2\pi) \sin(2\pi q))) dq dp = J_2(k)/2. \end{aligned} \quad (3.28)$$

The symmetry factor is  $g = 2$ , for the standard map, if we assume time-reversal invariance

alone. This is the case for the data presented in Fig. 3.1 as we have intentionally broken the phase space symmetry in the quantum system by assuming  $a = .35$ , (generic value) rather than  $a = .5$ , which will lead to twice the variance. Periodic orbits are either self-symmetric or more generically have symmetric partners with identical actions. The Bessel functions are characteristic of the diffusion coefficient in the standard map; the above simple derivation was proposed in the context of deterministic diffusion in [34]. However we note that the diffusion relevant for level velocities is the diffusion in the action-velocities and not the momentum, which is the usual quantity in which diffusion is studied [35].

The linear time dependence is a consequence of ergodicity, whereby time averages are replaced by phase space averages, and the coefficient is also easy to find and is the scaling of the parameter introduced to uncover possible universalities in level dynamics. These then are the oscillations observed in the figure. The bold line in the inset is  $2D(k) = (1 + 2J_2(k))$ . The significant deviation around the first minimum in the inset ( $k \approx 6.5$ ) from theory could be due to the presence of small stable islands, which are the accelerator modes and are known to lead to anomalous transport in the standard map (B. V. Chirikov in [2]).

### 3.3.2 The mixed phase space

The regime where there is a mixed phase space consisting of large stable regions is generic, and in this case the analysis above fails: the assumptions about the trace formula and the uniformity principle operate only under conditions of complete hyperbolicity. While in the completely chaotic regime the variance scales as  $N$ , in the mixed phase space regime it

(principally) scales as  $N^2$ . This relates to the large hump in Fig. 3.1, to which we now turn our attention. One way of relating the variance to classical quantities is to recognize that

$$\sigma^2(k, N) = \frac{N}{4\pi^2} \left\langle \text{Tr}(U^{-n} V U^n V) \right\rangle_n, \quad (3.29)$$

where the average is once more the time average. Thus the variance of the quantum level velocities is directly the time average of operator auto-correlations. We consider the case when the average level velocity is zero, as the generalization is evident. Replacing operators by the corresponding classical observables, we expect to get the variance in the mixed phase regime. This is particularly successful as we are dealing with averages over the entire quantum spectrum. Thus we replace the trace operation divided by  $N$  with the classical phase space average to get

$$\sigma^2(k, N)_{cl} = \frac{N^2}{4\pi^2} \int_0^1 dp_0 \int_0^1 dq_0 V(q_0) \left\langle V(q^{(n)}(q_0, p_0)) \right\rangle_n, \quad (3.30)$$

where  $q^{(n)}(q_0, p_0)$  is the position after  $n$  iterations starting from the initial condition  $(q_0, p_0)$ . For the case in Fig. 3.1,  $V(q) = \cos(2\pi q)$  and Fig. 3.2 compares in the mixed phase space regime the exact quantum calculation with a purely classical simulation corresponding to  $\sigma^2(k, N)_{cl}$ . We see that a simple classical simulation reproduces the curve extremely well, including the secondary hump, till around  $k \approx 2\pi$ . It is quite remarkable that the classical curve continues to pick out the initial Bessel function oscillations in the deeply chaotic regime. In the figure the time average is done over an ensemble for the first hundred iterations, and

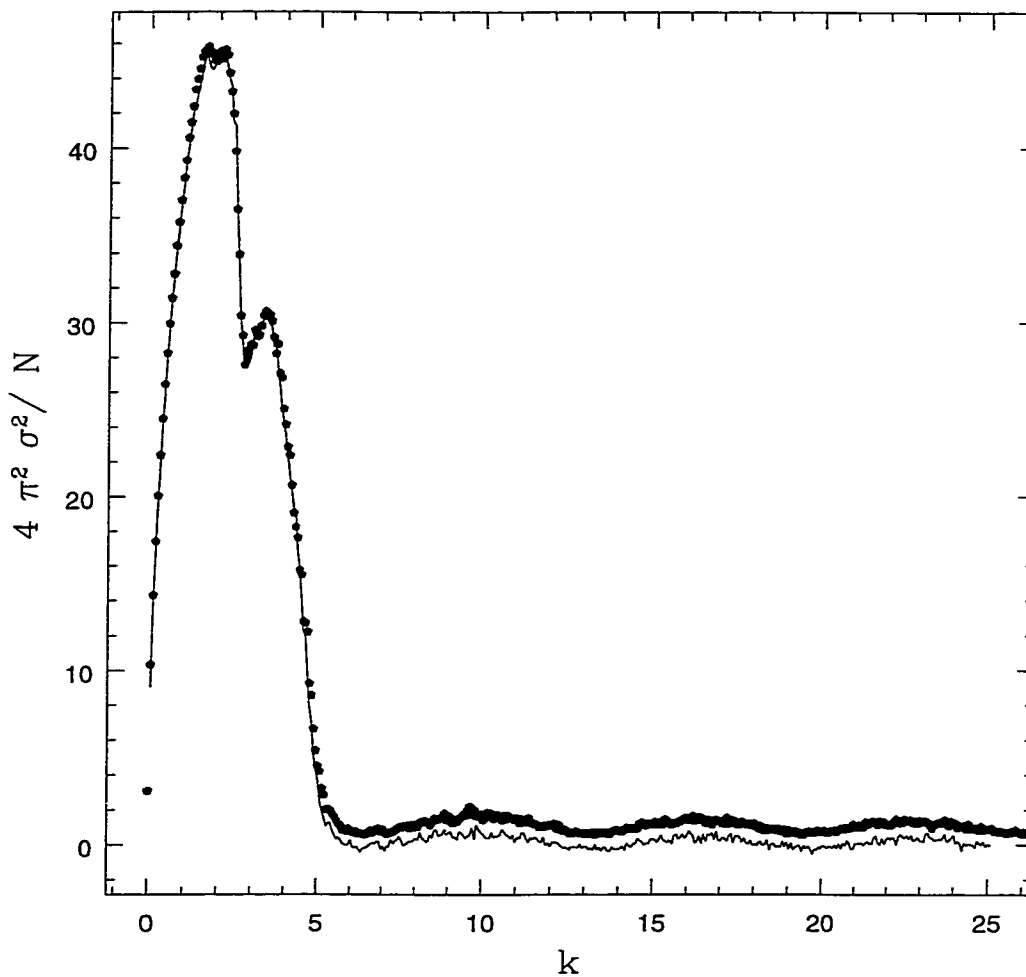


Figure 3.2: Same as Fig. 3.1, comparing, mainly in the mixed phase space regime, the exact variance (dots) with the classical estimate (the line). The classical estimate is after averaging over a hundred time steps. Quantities plotted are dimensionless.

the oscillations indicate short time correlations that will strictly disappear with increasing time.

The transition to classical chaos is accompanied then by a transition of the variance of the level velocities from a quadratic to a linear  $N$  dependence. Based on this observation we may write a general expression for the variance of the level velocities as a Weyl series with principal terms

$$\sigma^2(k, N) = c_1(k) N + c_2(k) N^2, \quad (3.31)$$

where  $c_1(k)$  and  $c_2(k)$  are system dependent and we have given above their expressions assuming only one of them is appreciable. Note that we have not evaluated  $c_1(k)$  in the mixed phase space regime, and that this will not in general vanish. On the other hand we expect that  $c_2(k)$  vanishes as a classical transition to chaos occurs. This is illustrated in Fig. 3.3, where  $c_2(k)$  is evaluated based on a best fitting curve using five  $N$  values, equally spaced, between 100 and 500. The curve is fitted by assuming a third-order polynomial in  $N$  for which the co-efficient of  $N^3$  returned by the fit was always of the order of  $10^{-6}$  or less.

In general the RMT result derived earlier Eq. (3.11) will be correct under the assumption that  $C(l) = C(0)\delta_{0,l}$ , implying delta correlated processes. Thus the departures from universality is related to higher order time correlations. The response of the system is not only dependent on the strength of the perturbation, but also on the dynamical correlations inherent to the system.

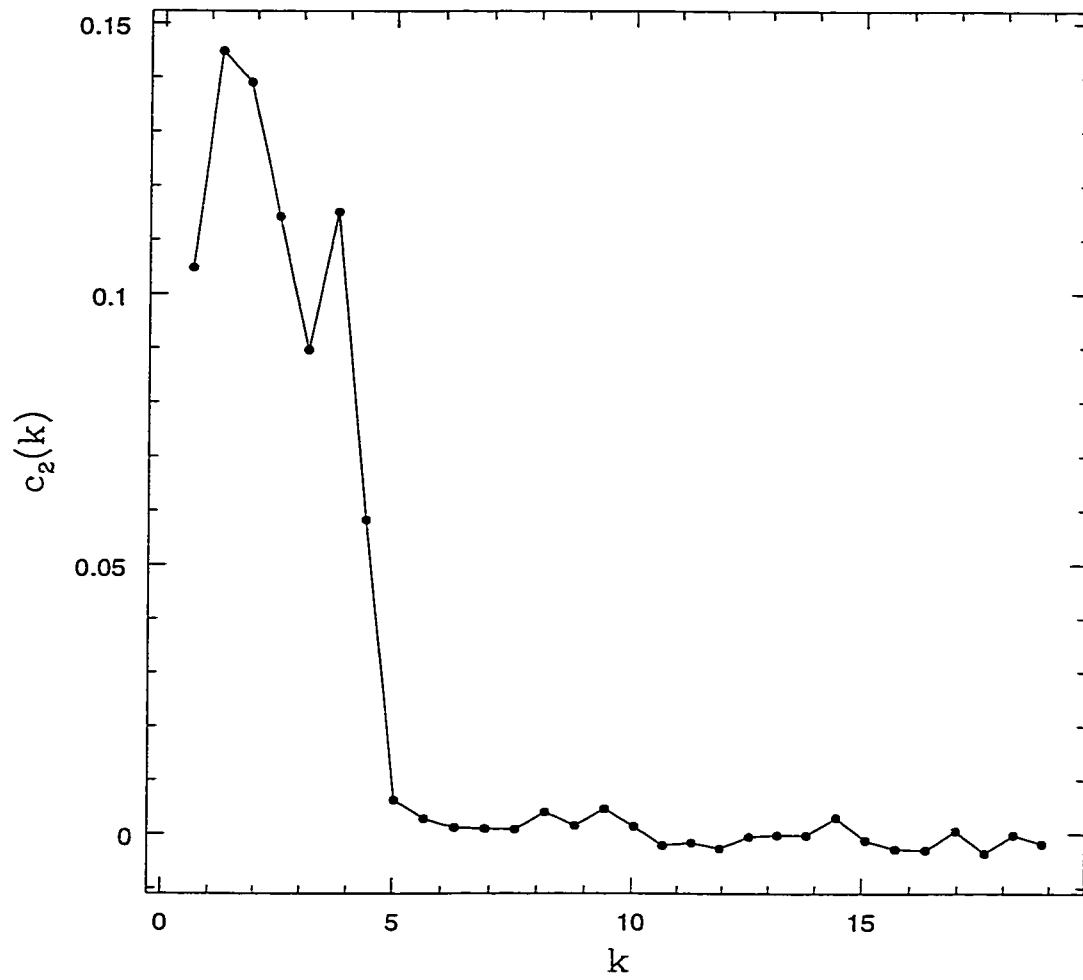


Figure 3.3: The coefficient  $c_2(k)$  as a function of the parameter; note that it reflects the classical transition to chaos. Quantities plotted are dimensionless.

### 3.3.3 Generalizations

We remark now on the general case  $\overline{V} \neq 0$ . This implies an overall drift to the energy levels due to changing phase space volumes. The drift may be removed by subtracting the phase space average,  $\overline{V}$ , from  $V$  before making use of the relations previous to this point in the text. It is understood as being performed for the remainder of the text. Using Eq. (3.19) and adding and subtracting  $n\overline{V}^2$  from the diagonal part of Eq. (3.18), we get after using  $\langle |\text{Tr}(U^n)|^2 \rangle_n = N$ ,

$$\sigma^2(k, N) = \frac{N}{4\pi^2} g(D(k) - \overline{V}^2). \quad (3.32)$$

The large chaos limit of this is

$$\sigma^2(\infty, N) = \frac{N}{4\pi^2} g(\overline{V^2} - \overline{V}^2), \quad (3.33)$$

and is the RMT result.

Variations of two independent parameters is an important problem, considering that many novel effects, including geometric phases may be observed. Here we will consider, in a generalization of the above, correlations between independent parameter variations. We assume that the Level velocities are given by the matrix elements:

$$\frac{\partial \phi_j}{\partial \lambda_i} = \frac{N}{2\pi} \langle \psi_j | V_i | \psi_j \rangle, \quad (3.34)$$

$i = 1, 2$ , and  $\lambda_i$  are two independent parameters while  $V_i$  are two Hermitian operators. Thus

the correlations considered below are also correlations between diagonal matrix elements of two arbitrary Hermitian operators.

We derive then that

$$\frac{1}{N} \sum_{j=1}^N \frac{\partial \phi_j}{\partial \lambda_1} \frac{\partial \phi_j}{\partial \lambda_2} = \frac{N}{4\pi^2} \left\langle \text{Tr}(U^n V_1) \text{Tr}(U^{-n} V_2) \right\rangle_n. \quad (3.35)$$

Using methods as outlined above the correlation function is semiclassically evaluated and we get

$$\sigma(\lambda_1, \lambda_2) \equiv \frac{1}{(\sigma_1 \sigma_2)} \left( \left\langle \frac{\partial \phi_j}{\partial \lambda_1} \frac{\partial \phi_j}{\partial \lambda_2} \right\rangle_j - \left\langle \frac{\partial \phi_j}{\partial \lambda_1} \right\rangle_j \left\langle \frac{\partial \phi_j}{\partial \lambda_2} \right\rangle_j \right) \sim \frac{(D(\lambda_1, \lambda_2) - \bar{V}_1 \bar{V}_2)}{\sqrt{(D_1 - \bar{V}_1^2)(D_2 - \bar{V}_2^2)}} \quad (3.36)$$

The function  $D$  is a generalization of Eq. (3.20) involving the dynamical correlation between the functions  $V_1$  and  $V_2$ :

$$D(\lambda_1, \lambda_2) = \frac{1}{\mathcal{A}} \left( \sum_{l=-\infty}^{\infty} \int_{\mathcal{A}} V_1(q_0, p_0) V_2(q_l, p_l) dq_0 dp_0 \right), \quad (3.37)$$

the dynamical variables after a time  $l$  integrated from  $(q_0, p_0)$  is denoted  $(q_l, p_l)$ . While  $D_{1,2}$  refer to the correlations appropriate to them individually and defined earlier in Eq. (3.20). Note that the backward and forward correlations ( $l < 0, l > 0$ ) are not in general equal. We remark that our derivations have assumed time-reversal symmetry, and that the factor  $g$  is responsible also for phase space symmetries. It may be generalized to include the factors that come due to breakdown of time-reversal, or inclusion of spin.



We finally consider the situation where not only the averages  $\overline{V}_i$  vanish, but also there is no tangible correlation between them, *i.e.*,  $D(\lambda_1, \lambda_2) = 0$ . Then the semiclassical expressions above give zero and are incapable of capturing the small albeit finite and rapid oscillations (with parameter). This limitation is of course evident all along, including Fig. 3.1, where the Bessel function captures the low frequency oscillations only.

In Fig. 3.4, is one such example, where we have considered  $V_1 = \cos(2\pi q)$  and  $V_2 = \cos(4\pi q)$ . The parameter  $\lambda_2$  is set as zero so that the relevant classical system is still the standard map, while the other parameter is  $k$  above. The correlation is seen as a function of this last parameter, the average actually vanishing. We see that this measure too captures the transition from mixed phase space to chaotic phase space, but that after the transition there are only extremely rapid oscillations about zero, although there are quite frequently fairly large correlations. In fact the frequency of the oscillations are so rapid that they seem to have self-similar properties as a random fractal. We may estimate the order of magnitude of the frequency if we assume that these arise from the off-diagonal part of the semiclassical sums. The magnitude of the parameter change needed to change a typical orbit action by  $\hbar$  or  $(1/N)$  is needed. From the fact that action changes have a variance proportional to the period, we get  $|\Delta S| \sim \sqrt{n}|\Delta\lambda|$ , and therefore  $|\Delta\lambda| \sim N^{-3/2}$ , if we take as the period  $n = N$ , which is the Heisenberg time and represents the time by which the spectrum is practically resolved.

In conclusion then, we have studied variances of level velocities and their generalizations in the chaotic as well as mixed phase space regimes. Noting that the transition to chaos

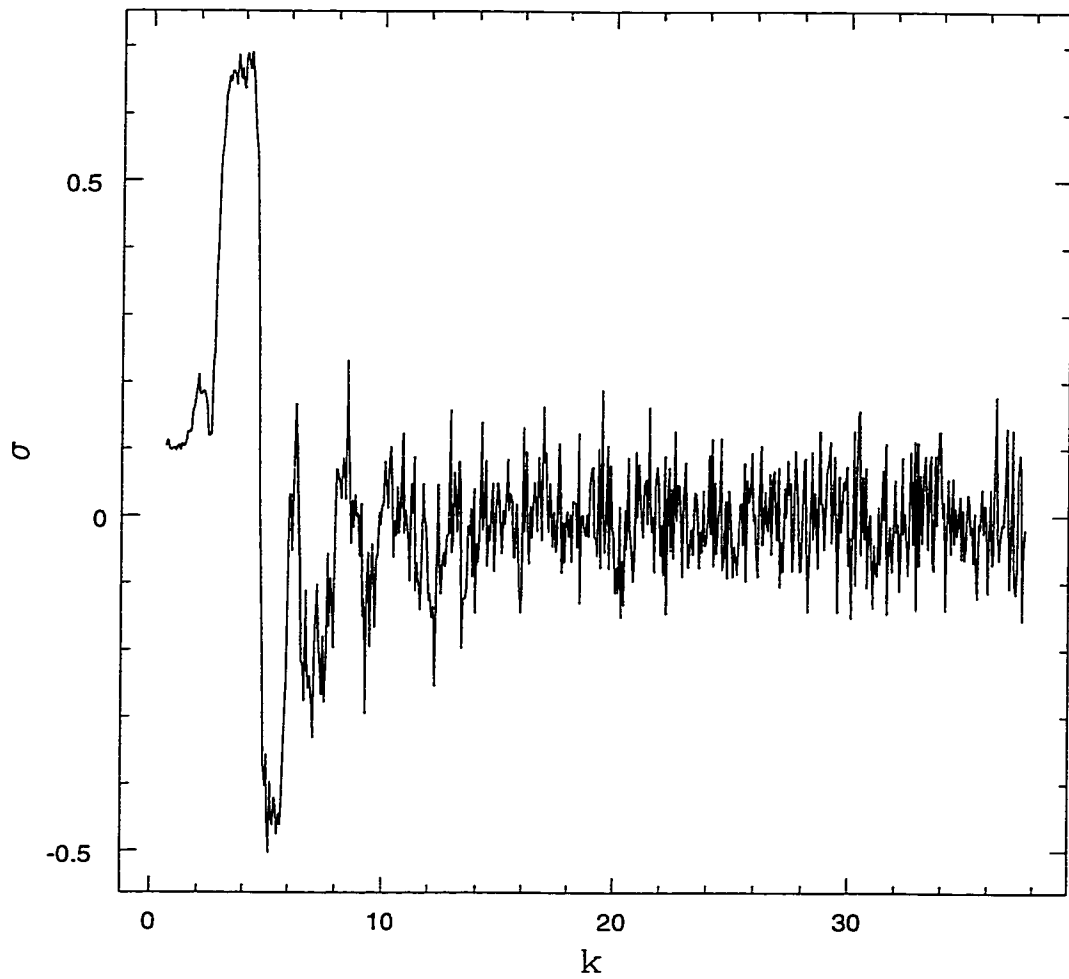


Figure 3.4: The quantum correlation between the matrix elements of the two operators  $\cos(2\pi q)$  and  $\cos(4\pi q)$  whose classical correlation vanishes in the chaotic regime. Quantities plotted are dimensionless.

is perfectly reflected in this measure, we derived detailed formulae for them, in terms of classical correlation coefficients and illustrated this with the help of the standard map. The mixed phase space regime was surprisingly well captured by a simple classical estimate. The observations of oscillations or variations in the level velocity variances due to classical correlations, as well as using them to distinguish mixed from chaotic phase space are both experimentally accessible.

The possibility of using the level velocity in conjunction with wavefunction intensities in a measure of phase space localization has been proposed [36], and it is hoped that this detailed understanding of the level velocities will help in this as well. In particular this measure is a special case of the correlation between two operators discussed above, with an important complication being that the Wigner transform of the relevant operator, a projector in phase space, varies over scales of order  $\hbar$ . We have also noted that the RMT results, after assuming independence of eigenvalues and eigenfunctions is capable of predicting the level velocities only in the limit of extremely large chaos, or equivalently ignoring all higher order time correlations other than the zeroth.

This work was supported by NSF-PHY-9800106 and the ONR grant N00014-98-1-0079.

## References

- [1] M. C. Gutzwiller, *Chaos in Classical and Quantum Mechanics*, ( Springer, New York, 1990).
- [2] Lectures in *Les Houches LII, Chaos and Quantum Physics*, edited by M.-J. Giannoni, A. Voros, and J. Zinn-Justin (North-Holland, Amsterdam 1991).
- [3] A. M. Ozorio de Almeida, *Hamiltonian Systems: Chaos and Quantization* (Cambridge University Press, Cambridge, 1988).
- [4] E. J. Heller, *Phys. Rev. Lett.* **53**, 1515 (1984).
- [5] P. Gaspard, S. A. Rice, and K. Nakamura, *Phys. Rev. Lett.* **63**, 930 (1989); P. Gaspard, S. A. Rice, H. J. Mikesaka, and K. Nakamura, *Phys. Rev. A* **42**, 4015 (1990).
- [6] T. Takami and H. Hasegawa, *Phys. Rev. Lett.* **68**, 419 (1992).
- [7] J. Zakrzewski and D. Delande, *Phys. Rev. E* **47**, 1650 (1993).
- [8] B. D. Simons and B. L. Altshuler, *Phys. Rev. Lett.* **70**, 4063 (1993); *Phys. Rev. B.* **48**, 5422 (1993).

- [9] M. M. Sano, Phys. Rev. E **54**, 3591 (1996).
- [10] P. Kunstman, K. Zyczkowski, and J. Zakrzewski, Phys. Rev. E **55**, 2446 (1997).
- [11] K. Nakamura and M. Lakshmanan, Phys. Rev. Lett. **57**, 1661 (1986).
- [12] S. Sridhar and A. Kudrolli, Phys. Rev. Lett. **72**, 2175 (1994).
- [13] K. Schaadt and A. Kudrolli, Preprint (1999).
- [14] M. V. Berry and J. P. Keating, J. Phys. A **27**, 6167 (1994).
- [15] N. R. Cerruti, A. Lakshminarayan, J. H. Lefebvre, and S. Tomsovic, Preprint (1999).
- [16] P. Lebouef and M. Sieber, Preprint (1999); cond-mat/9905015.
- [17] D. Saher, F. Haake, and P. Gaspard, Phys. Rev. A **44**, 7841 (1991).
- [18] G. Casati, B. V. Chirikov, F. M. Izrailev, and J. Ford, in *Stochastic Behaviour in Classical and Hamiltonian Systems*, Lecture notes in physics, **93**, edited by G. Casati and J. Ford ( Springer-Verlag, Berlin, 1979).
- [19] M. V. Berry, N. L. Balazs, M. Tabor, and A. Voros, Ann. Phys. (N.Y.) **122**, 26 (1979).
- [20] D. R. Grempel, R. E. Prange, and S. Fishman, Phys. Rev. A **29**, 1639 (1984).
- [21] F. M. Izrailev, Phys. Rep. **196**, 299 (1990).
- [22] A. Voros in *Nonlinear Dynamics and Computational Physics*, edited by V. B. Sheorey (Narosa, New Delhi, 1999).

- [23] N. L. Balazs and A. Voros, *Ann. Phys. (N. Y.)* **190**, 1 (1989).
- [24] S.J. Chang, and K. J. Shi, *Phys. Rev. Lett.* **55**, 269 (1985).
- [25] J. H. Hannay, and M. V. Berry, *Physica* **D1**, 267 (1980).
- [26] L. E. Reichl, *The Transition to Chaos*, (Springer-Verlag, New York, 1992).
- [27] A. Lakshminarayan, *Pramana* **48**, 517 (1997).
- [28] B. Eckhardt, S. Fishman, K. Muller, and D. Wintgen, *Phys. Rev. A* **45**, 3531 (1992).
- [29] T. A. Brody, J. Flores, J. B. French, P. A. Mello, A. Pandey, and S.S.M. Wong, *Rev. Mod. Phys.* **53**, 385 (1983).
- [30] A. M. Ozorio de Almeida, and M. Saraceno, *Ann. Phys. (N. Y.)* **210**, 1 (1991).
- [31] M. Tabor, *Physica* **D6**, 195 (1983).
- [32] O. Bohigas, M. J. Giannoni, A. M. Ozorio de Almeida, and C. Schmit, *Nonlinearity* **8**, 203 (1995).
- [33] J. H. Hannay and A. M. Ozorio de Almeida, *J. Phys. A* **17**, 3429 (1984).
- [34] B. V. Chirikov, *Reviews of Plasma Physics*, Vol. 13, 1, ed., B. B. Kadomtsev (Consultants Bureau, New York, 1987).
- [35] The difference between the two diffusion coefficients results in the absence of the  $k^2$  factor in Eq. (3.27). The momentum is proportional to  $k$ , while the change in the

action with the parameter (action-velocity) is not. Also there is a minor difference in the momentum being a sum of the sines of the position variable at intermediate times, while it is the cosines for the action-velocity.

[36] S. Tomsovic, Phys. Rev. Lett. **77**, 4158 (1996).

## Chapter 4

# Exploring Phase Space Localization of Chaotic Eigenstates via Parametric Variations

By Nicholas R. Cerruti, Arul Lakshminarayan,<sup>1</sup> Julie H. Lefebvre,<sup>2</sup>

and Steven Tomsovic

Department of Physics, Washington State University,

Pullman, Washington 99164-2814

Physical Review E **63** (2001) (to be published)

Copyright 2001 by the American Physical Society.

### 4.0 Abstract

In a previous Letter [Phys. Rev. Lett. **77**, 4158 (1996)], a new correlation measure was introduced that sensitively probes phase space localization properties of eigenstates. It is based on a system's response to varying an external parameter. The measure correlates level velocities with overlap intensities between the eigenstates and some localized state of interest. Random matrix theory predicts the absence of such correlations in chaotic systems whereas in the stadium billiard, a paradigm of chaos, strong correlations were observed.

---

<sup>1</sup>Permanent address: Physical Research Laboratory, Navrangpura, Ahmedabad 380 009, India.

<sup>2</sup>Current address: Defence Research Establishment Ottawa, Ottawa, Ontario, K1A 0Z4, Canada



Here, we develop further the theoretical basis of that work, extend the stadium results to the full phase space, study the  $\hbar$ -dependence, and demonstrate the agreement between this measure and a semiclassical theory based on homoclinic orbits.

## 4.1 Introduction

The two general motivations for our investigation are understanding better the nature of eigenstates of bounded quantum systems possessing ‘simple’ classical analogs, and exploring new features of such systems’ behavior as a system parameter is smoothly varied. Simple in this context refers to few degrees of freedom and a compact Hamiltonian. Nevertheless, the classical dynamics may display a rich variety of features from regular to strongly chaotic motion. We focus on the strongly chaotic limit for which semiclassical quantization of individual chaotic eigenstates does not hold, and the correspondence principle is less well understood [1]. Even though there has been some recent progress [2], it turns out that with a detailed understanding of chaotic systems a statistical theory provides a well-developed, alternative approach to these difficulties. Twenty years ago, Berry [3] conjectured and Voros [4] discussed that in this case as  $\hbar \rightarrow 0$  the eigenstates should respect the ergodic hypothesis in phase space,  $\delta(E - H(\mathbf{p}, \mathbf{q}))$ , as it applies to wavefunctions. In essence, the eigenmodes should appear as Gaussian random wavefunctions locally in configuration space with their wavevector constrained by the ergodic measure of the energy surface. Discussion of the properties of random waves and recent supporting numerical evidence can be found in refs. [5, 6].

The second general motivation relates to a long recognized class of problems, i.e. a system's response to parametric variation. Our interest here is restricted to external, controllable parameters such as electro-magnetic fields, temperatures, applied stresses, changing boundary conditions, etc..., through whose variation one can extract new information about a system not available by other means. A multitude of examples can be found in the literature [7]. A recent concern has been universalities in the response of chaotic or disordered systems and statistical approaches to measuring the response [8]. Universal parametric correlations have been derived via field theoretic or random matrix methods for quantities involving level slopes (loosely termed velocities in this paper), level curvatures, and eigenfunction amplitudes [9, 10]. In contrast, our motivation is not the universal features per se for they cannot tell us anything specific about the system other than it is, in fact, chaotic and/or symmetry is present. Rather we are interested in what system specific information can be extracted in the case that the system's response deviates from universal statistical laws. The specific application discussed in this paper shows how one can decipher phase space localization features of the eigenstates. The theory naturally divides into a two-step process. One must first understand any implied limiting universal response of chaotic systems. Next, one must develop a theory which gives a correct interpretation of any deviations seen from the universal response. The necessarily close interplay between theory and observation required to deduce new information forms part of the attractiveness of investigating parametric response.

Taking up the first step of understanding universal response, an expected but rarely dis-

cussed property is the independence of eigenvalue and eigenfunction fluctuation measures [11] which is found in the random matrix theories anticipated to describe the statistical properties of quantum systems with chaotic classical analogs [12, 13]. Coupled with Berry's conjecture mentioned above, these properties imply a 'democratic' response to parametric variation for an ergodically behaving quantum system. The perturbation connects one state to all other states locally with equal probability. The variation of any one eigenstate or eigenvalue over a large enough parameter range will be statistically equivalent to their respective neighboring states or levels.

In a pioneering work on the ergodic hypothesis using the stadium billiard, now a paradigm of chaos studies, McDonald noticed larger than average intensities of the eigenstates in certain regions [14]. In his thesis he states that "a small class of modes (bouncing ball, whispering gallery, etc.) seem to correspond naively to a definite set of 'special' ray orbits." Heller initiated a theory concerning these large intensities when he modified the random wavefunction picture with his prediction and numerical observations of eigenstate scarring [15]. He derived a criterion for eigenstate intensity in excess of the ergodic predictions along the shorter, less unstable periodic orbits. Scarring is thus one possible phase space 'localization' property of a chaotic eigenstate. Other possibilities result from time scales not related directly to the Lyapunov instability such as transport barriers in the form of broken separatrices [16], and cantori [17, 18], or diffusive motion [19]. In the context of this paper, we take localization to mean some deviation from the ergodic expectation beyond the inherent quantum fluctuations, and it creates the possibility of a non-democratic response to parametric variation.

A perturbation could preferentially connect certain states or classes of states, thus leading to additional short-range avoided crossings or like level movements within a particular class, etc.

Debate ensued Heller's work on eigenstate scarring, in part, because of the difficulty in quantitatively characterizing and predicting its extent in either a particular eigenstate or even collective groups of eigenstates. Judging from the earlier literature, it was easier to graph eigenstates in order to see the scarring by eye than define precisely what it means or what its physical significance is. Furthermore, he linearized the semiclassical theory which was insufficient for a full description of scarring. We remark that recent work suggests the opposite, i.e. the linearized theory is sufficient assuming  $\hbar$  is smaller than some system specific value which is 'small enough' [20]. However, many of the experimental and numerical investigations are far from this regime and the nonlinear dynamical contributions are essential for understanding most of the work being done. The theory incorporating nonlinear dynamical contributions [2, 21] was developed much later than Heller's introduction of scarring. It is based on heteroclinic orbit expansions for wave packet propagation and strength functions. Ahead, we make extensive use of these forms to derive a semiclassical theory applicable to problems involving parametric variation.

In a previous Letter [22], one of us (ST) introduced a measure that very sensitively probes phase space localization for systems having continuously tunable parameters in their Hamiltonians. It correlates level motions under perturbation with overlap intensities between eigenstates and optimally localized wave packet states. The basic idea is that the wave packet

overlap intensities select eigenstates that potentially have excess support in the neighborhood of the phase point at the wave packet's position and momentum centroids. The perturbation will push these levels somewhat in the same direction depending on how it is distorting the energy surface near that particular phase point. If the level velocities associated with those states have similar enough values, then significant non-zero correlations will result that reveal the localization. The measure can be used in a forward or reverse direction. If phase space localization is present in a system of interest, then it predicts experimentally verifiable manifestations of that localization. Conversely, one can first experimentally determine the level velocity - overlap intensity measure in that system for the purpose of inferring the existence and extent of localization.

Our purpose in this paper is to give a complete account of that Letter, develop further the semiclassical theory, and explore the full phase space and  $\hbar$  behavior of the stadium billiard, a continuous time system. In a companion paper immediately following this one, we give the theory for quantized maps (discretized time) [23]. The next section introduces strength functions and a new class of correlation coefficients. Section 4.3 utilizes ergodicity and random wave properties to motivate the introduction of random matrix ensembles. The ensembles describe the statistical properties of chaotic systems in the  $\hbar \rightarrow 0$  limit. The correlation measures vanish for these ensembles indicating the absence of localization and universal response to perturbation (i.e. parameter variation). Section 4.4 gives the semiclassical theories of level velocities, strength functions, and overlap intensity-level velocity correlation coefficients. We finish with a full treatment of the stadium billiard and concluding

remarks.

## 4.2 Preliminaries

Consider a quantum system governed by a smoothly parameter-dependent Hamiltonian,  $\hat{H}(\lambda)$  with classical analog  $H(\mathbf{p}, \mathbf{q}; \lambda)$ . We suppose that the dynamics are chaotic for all values of the  $\lambda$  range of interest, and suppose the absence of symmetry breaking. Then the expectation is that all statistical properties are stationary with respect to  $\lambda$ . Without loss of generality, we also assume the phase space volume of the energy surface is constant as a function of  $\lambda$ . This ensures that the eigenvalues do not collectively drift in some direction in energy, but rather wander locally. We use the same strength function Heller employed in his prediction of scarring [15] except slightly generalized to include parametric behavior;

$$\begin{aligned}
S_\alpha(E, \lambda) &= \frac{1}{2\pi\hbar} \int_{-\infty}^{\infty} dt e^{iEt/\hbar} \langle \alpha | e^{-i\hat{H}(\lambda)t/\hbar} | \alpha \rangle \\
&= \text{Tr}[\hat{p}_\alpha \delta(E - \hat{H}(\lambda))] \\
&= \sum_n p_{\alpha n}(\lambda) \delta(E - E_n(\lambda)); \quad p_{\alpha n}(\lambda) = |\langle \alpha | E_n(\lambda) \rangle|^2 \quad (4.1)
\end{aligned}$$

where  $\hat{p}_\alpha = |\alpha\rangle\langle\alpha|$ .  $S_\alpha(E, \lambda)$  is the Fourier transform of the autocorrelation function of a special initial state  $|\alpha\rangle$  of interest. Ahead  $\bar{S}_\alpha(E, \lambda)$  will denote the smooth part resulting from the Fourier transform of just the extremely rapid initial decay due to the shortest time scale of the dynamics (zero-length trajectories). We will take  $|\alpha\rangle$  to be a Gaussian wave packet because of its ability to probe “quantum phase space,” but other choices are possible.

Say momentum space localization were the main interest, the natural choice would be a momentum eigenstate.  $|\alpha\rangle$  can be associated with a phase space image  $\rho_\alpha(\mathbf{p}, \mathbf{q})$  of Gaussian functional form using Wigner transforms or related techniques.  $\rho_\alpha(\mathbf{p}, \mathbf{q})$  turns out to be positive definite and maximally localized in phase space, i.e. it occupies a volume of  $h^d$ .

For a fixed value of the parameter, an example strength function is shown in Fig. (4.1). If the wave packet is centered somewhere on a short periodic orbit, large amplitudes necessarily indicate significant wave intensity all along the orbit as seen in the inset eigenstates. This behavior cannot, a priori, be stated to be obviously in violation of the quantum statistical fluctuation laws even if it appears so. That remains to be determined. With the inclusion of parametric variation, the eigenvalues of a chaotic system are supposed to move along smoothly varying curves of the type shown in the upper square of Fig. (4.2). Many of the previous studies of parametric variation focussed on the properties of such level curves. A great deal is known about the distribution of level velocities [24, 25], the decay of correlations in parametric statistics [10, 26], the distribution of level curvatures [27–29], and the statistics of the occurrences of avoided crossings [30, 31].

We now superpose the strength function overlap intensity information on Fig. (4.2) in the lower square as vertical lines centered on the levels; the lengths are scaled by the intensities (3-D versions of this figure turned out not to be very helpful). By considering the full strength function and not just the level curves (i.e. density of states), the eigenstate properties can be more directly probed. A new class of statistical measures can be defined that cross correlate intensities with levels. The most evident examples are the four correlation co-

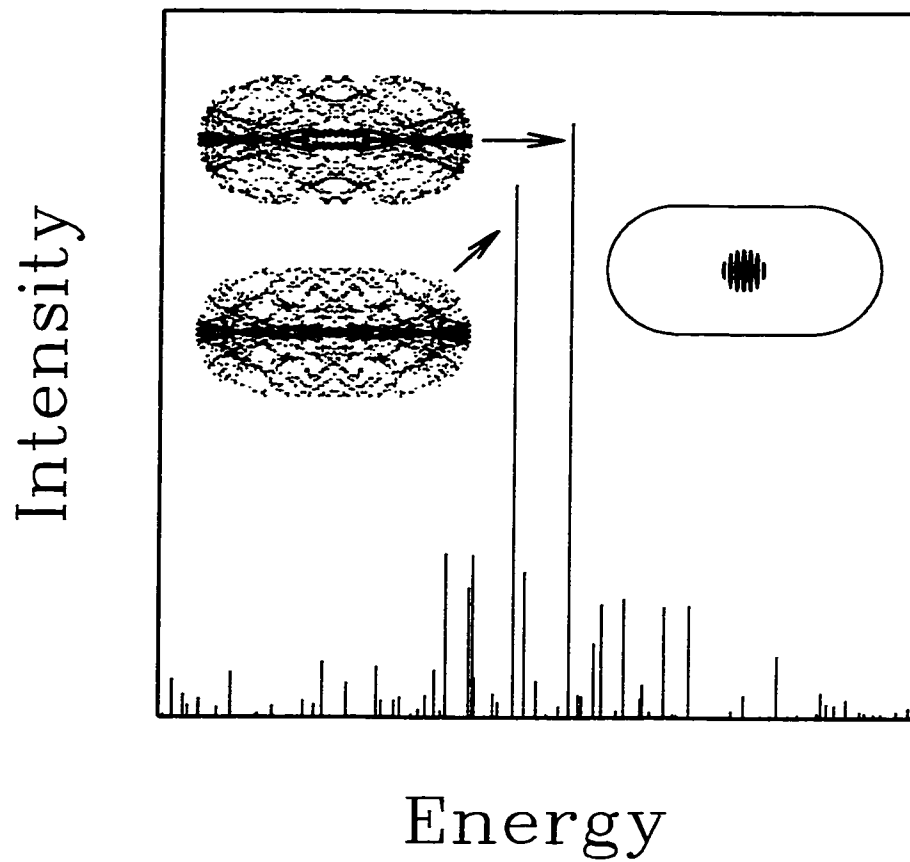


Figure 4.1: Strength function for the stadium billiard. The Gaussian wave packet is centered in the stadium with momentum directed towards the end cap. The large intensities are where the scarring occurs.



efficients involving both level curves and eigenstate amplitudes that can be defined from the following quantities: (i) the level velocities,  $\partial E_n(\lambda)/\partial\lambda$ , (ii) level curvatures,  $\partial^2 E_n(\lambda)/\partial\lambda^2$ , (iii) overlaps,  $p_{\alpha n}$ , and (iv) overlap changes,  $\partial p_{\alpha n}/\partial\lambda$ . The most important is the overlap intensity-level velocity correlation coefficient,  $C_\alpha(\lambda)$ , which is defined as

$$C_\alpha(\lambda) = \frac{\left\langle p_{\alpha n} \frac{\partial E_n(\lambda)}{\partial\lambda} \right\rangle_E}{\sigma_\alpha \sigma_E} \quad (4.2)$$

where  $\sigma_\alpha^2$  and  $\sigma_E^2$  are the local variances of the overlaps and level velocities, respectively. The brackets denote a local energy average in the neighborhood of  $E$ . It weights most the level velocities whose associated eigenstates possibly share common localization characteristics and measures the tendency of these levels to move in a common direction. In this expression, the phase space volume remains constant so that the level velocities are zero-centered (otherwise the mean must be subtracted), and  $C_\alpha(\lambda)$  is rescaled to a unitless quantity with unit variance making it a true correlation coefficient. The set of states included in the local energy averaging can be left flexible except for a few constraints. Only energies where  $\bar{S}_\alpha(E, \lambda)$  is roughly constant can be used or some intensity unfolding must be applied. Also, the energy range must be small so that the classical dynamics are essentially the same throughout the range, but it must also be broad enough to include several eigenstates.

$C_\alpha(\lambda)$  thus has a simple form and the additional advantage of involving quantities of direct physical interest. Level velocities (curvatures also) arise in thermodynamic properties of mesoscopic systems [32], and overlap intensities often arise in the manner used to couple into the system [33]. It is the most sensitive measure of the four possible combinations, the

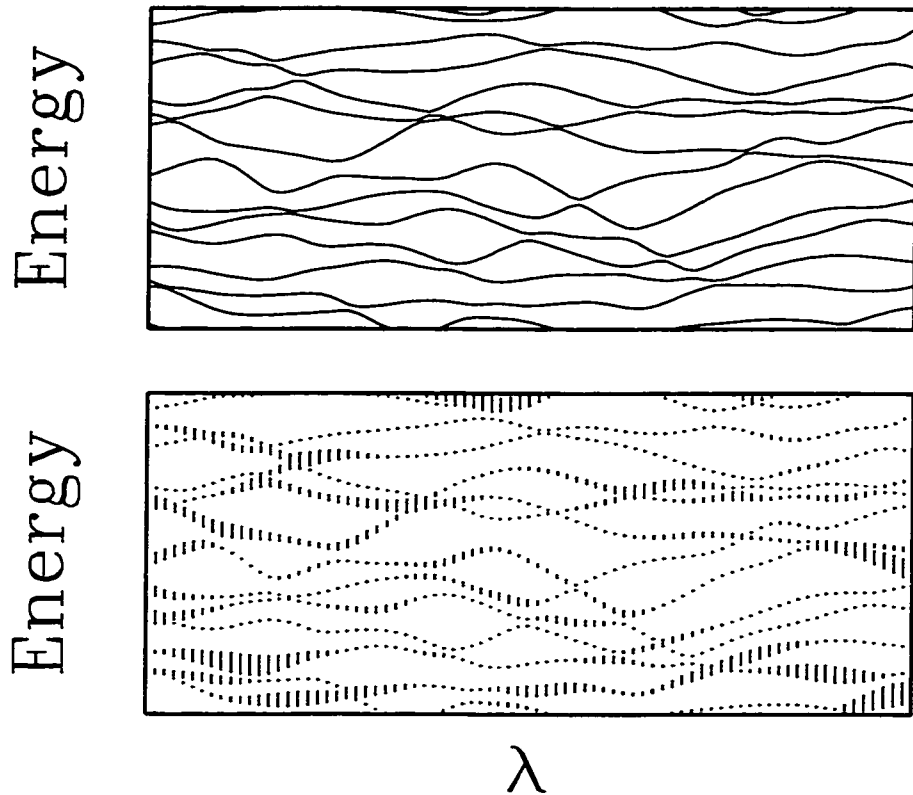


Figure 4.2: Illustration of ergodic behavior. The upper square shows how the energy eigenvalues move as a function of  $\lambda$ . The lower square is a graphical representation of  $S_\alpha(E, \lambda)$ . Each small line segment is centered on an eigenvalue and its lambda value. The heights are proportional to the overlap intensity with a wavepacket. The level velocities and overlap intensities were produced using a Gaussian orthogonal ensemble.

others being the intensity-curvature, intensity change - curvature and intensity change - level velocity correlation coefficients. The first two are far less sensitive measures of eigenstate localization effects, even though curvature distributions are affected by localization because of the relative rareness of being near avoided crossings where curvatures are large. The last shows no effect since intensities will change whether the level is moving up or down. These three measures will not be considered further in this paper, but we did calculate them to verify their lack of sensitivity.

### 4.3 Ergodicity, Random Waves, and Random Matrix Theory

Semiclassical expressions for wavefunctions have the form

$$\Psi(\mathbf{x}) = \sum_n A_n(\mathbf{x}) \exp(iS_n(\mathbf{x})/\hbar - i\nu_n\pi/2) \quad (4.3)$$

where  $S_n(\mathbf{x})$  is a classical action,  $\nu_n$  is a phase index, and  $A_n(\mathbf{x})$  is a slowly varying function given by the square root of a classical probability. The classical trajectory underlying each term arrives at the point  $\mathbf{x}$  with momentum,  $\mathbf{p}_n = \nabla S_n(\mathbf{x})$ . For a chaotic system, a complete theory leading to an equation of the form of Eq. (4.3) does not exist [1]. Nevertheless, Berry [3] conjectured that for the purposes of understanding the statistical properties of chaotic eigenfunctions, the ergodic hypothesis implies that the true eigenfunction will appear statistically equivalent to a large sum of these terms each arriving with a random

phase (since each wave contribution extends over a complicated, chaotic path). For systems whose Hamiltonian is a sum of kinetic and potential energies, the energy surface constraint  $\delta(E - H(\mathbf{p}, \mathbf{q}))$  fixes only the magnitude of the wavevector. The eigenfunctions therefore appear locally as a sum of randomly phased plane waves pointing in arbitrary directions with fixed wavevector  $k$ . The central limit theorem asserts such waves are Gaussian random. An example is shown in Fig. (4.3) for a two-degree-of-freedom system where the spatial correlations fall off as a Bessel function,  $J_0(kr)$ .

If the eigenstates truly possessed these characteristics, then a perturbation of the Hamiltonian would have matrix elements that behaved as Gaussian random variables whose variance depended only on the energy separation of the two eigenstates, i.e. an energy-ordered, banded random matrix. The energy ordering separates the weakly interacting states, and therefore only the local structure is of importance here. The range of the averaging carried out in the correlation function is taken to be much less than the bandwidth of such a random matrix. The ultimate statistical expression of this structure is embodied in one of the standard Gaussian ensembles (GE). We construct a parametrically varying ensemble  $\{\hat{H}(\lambda)\}$  as

$$\hat{H}(\lambda) = \hat{H}_0 + \lambda \hat{H}_1 \tag{4.4}$$

where  $\hat{H}_0$  and  $\hat{H}_1$  are independently chosen GE matrices. Note that the sum of two GE matrices is also a GE matrix which thus satisfies our desire to consider stationary statistical properties as  $\lambda$  varies.

It is unnecessary to specify the abstract vector space of  $\{\hat{H}(\lambda)\}$  (only the dimensionality

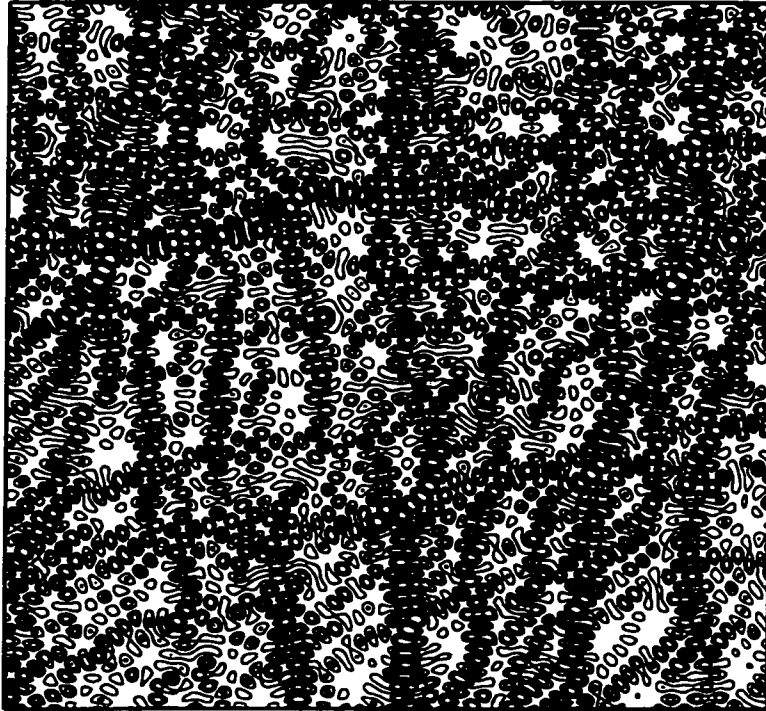


Figure 4.3: Realization of random wavefunctions in two degrees of freedom. A superposition of 30 plane waves with random direction and phase shift, but fixed magnitude of the wavevector is shown.

of the space) in the definition of the ensemble. However,  $|\alpha\rangle$  has to be overlapped with the eigenstates, and thus a localized wave packet seemingly must be specified. In fact, the specific choice is completely irrelevant because the GEs are invariant under the set of transformations that diagonalize them.  $|\alpha\rangle$  can be taken as any fixed vector in the space by invariance. The overlaps and level velocities turn out to be independent over the ensemble since diagonalizing  $\{\hat{H}_0\}$  leaves  $\{\hat{H}_1\}$  invariant and the level velocities are equal to the diagonal matrix elements of  $\hat{H}_1$ . With the overbar denoting ensemble averaging,

$$\overline{C_\alpha(\lambda)} = \frac{\overline{\langle p_{\alpha n} \frac{\partial E_n}{\partial \lambda} \rangle_E}}{\sigma_\alpha \sigma_E} = \frac{\overline{\langle p_{\alpha n} \rangle_E} \overline{\langle \frac{\partial E_n}{\partial \lambda} \rangle_E}}{\sigma_\alpha \sigma_E} = 0 \quad (4.5)$$

In fact, it is essential to keep in mind that *every* choice of  $|\alpha\rangle$  gives zero correlations within the random matrix framework. The existence of even a single  $|\alpha\rangle$  in a particular system that leads to nonzero correlations violates ergodicity.

It is straightforward to go further and consider the mean square fluctuations of  $C_\alpha(\lambda)$ ,

$$\begin{aligned} \overline{C_\alpha(\lambda)^2} &= \frac{\overline{\left( \langle p_{\alpha i} \frac{\partial E_i}{\partial \lambda} \rangle_E \right)^2}}{(\sigma_\alpha \sigma_E)^2} \\ &= \frac{1}{(N\sigma_\alpha \sigma_E)^2} \sum_i^N \sum_j^N \overline{p_{\alpha i} \frac{\partial E_i}{\partial \lambda} p_{\alpha j} \frac{\partial E_j}{\partial \lambda}} \\ &= \frac{1}{(N\sigma_\alpha \sigma_E)^2} \sum_i^N \sum_j^N \overline{p_{\alpha i} p_{\alpha j} \frac{\partial E_i(\lambda)}{\partial \lambda} \frac{\partial E_j(\lambda)}{\partial \lambda}} \\ &= \frac{1}{(N\sigma_\alpha \sigma_E)^2} \sum_i^N \overline{p_{\alpha i}^2} \overline{\left( \frac{\partial E_i(\lambda)}{\partial \lambda} \right)^2} = \frac{1}{N} \end{aligned} \quad (4.6)$$

where  $N$  is the effective number of states used in the energy averaging. Again the level

velocities are independent of the eigenvector components. The  $\partial E_j(\lambda)/\partial\lambda = \langle j|\hat{H}_1|j\rangle$  and thus the  $i \neq j$  terms vanish due to the independence of the diagonal elements of the perturbation leaving only the diagonal terms that involve the quantities that respectively enter the variance of the eigenvector components and the mean square level velocity. The final result reflects the equivalence of ensemble and spectral averaging in the large- $N$  limit. Therefore, in ergodically behaving systems,  $C_\alpha(\lambda) = 0 \pm N^{-1/2}$  for every choice of  $|\alpha\rangle$ . Fig. (4.2) was made using the orthogonal GE. It illustrates a manifestation of ergodicity, i.e. universal response of the quantum levels with respect to  $\lambda$  and democratic behavior of the overlap intensities.

## 4.4 Semiclassical Dynamics

We develop a theory based upon semiclassical dynamics which explains how nonzero overlap correlation coefficients arise out of the localization properties of the system. The theory simply reflects the quantum manifestations of finite time correlations in the classical dynamics. In a chaotic system, the classical propagation of  $\rho_\alpha(\mathbf{p}, \mathbf{q})$  will relax to an ergodic long time average. However, wave packet revivals in the corresponding quantum system earlier than this relaxation time can occur [34]. In Heller's original treatment of scars [15], he uses arguments based upon these recurrences which occur at finite times to infer localization in the eigenstates.

In the correlation function, the intensities,  $p_{\alpha n}$ , weight most heavily the level motions of the group of eigenstates localized near  $\rho_\alpha(\mathbf{p}, \mathbf{q})$ , if indeed such eigenstates exist. If we construct the Hamiltonian as in Eq. (4.4) where  $\hat{H}_0$  is the unperturbed part, then by first-

order perturbation theory, the level velocities are the diagonal matrix elements of  $\hat{H}_1$  just as in random matrix theory. We showed in the previous section that in random matrix theory these elements weighted with the intensities are zero centered. For a general quantum system the equivalent expectation would be fluctuations about the corresponding classical average of the perturbation over the microcanonical energy surface,  $\delta(E - H(\mathbf{p}, \mathbf{q}))$ . In this case,  $C_\alpha(\lambda) \approx 0$  for all  $|\alpha\rangle$ . On the other hand, the quantum system will fluctuate differently if there is localization in the eigenstates. Note that this means some choices of  $|\alpha\rangle$  will still lead to zero correlations. It only takes one statistically significant nonzero result to demonstrate localization conclusively, but to obtain a complete picture, it is necessary to consider many  $|\alpha\rangle$  covering the full energy surface.

We begin by examining the individual components of the overlap correlation coefficient, the level velocities and intensities. Their  $\hbar$ -dependences are derived and also they are shown to be consistent with random matrix theory as  $\hbar \rightarrow 0$ . Finally, the weighted level velocities are discussed. We give an estimate based upon a semiclassical theory involving homoclinic orbits for the slope of the large intensities.

#### 4.4.1 Level velocities

In random matrix theory (RMT) level velocities are Gaussian distributed as would also be expected of a highly chaotic system in the small  $\hbar$  limit. Thus, the mean and variance,  $\sigma_E^2$ , give a complete statistical description in the limiting case and are the most important quantities more generally. Since the purpose of this section is to derive their scaling properties, it



is better to work with dimensionless quantities. Thus, the dimensionless variance is defined as  $\bar{\sigma}_E^2 \equiv \bar{d}^2(E, \lambda) \sigma_E^2$  where  $\bar{d}(E, \lambda)$  is the mean level density which is the reciprocal of the mean level spacing.

We begin by following arguments originally employed by Berry and Keating [35] in which they investigated the level velocities normalized by the mean level spacing for classically chaotic systems with the topology of a ring threaded by quantum flux. In order to make the discussion self contained we will summarize their basic ideas using their notation and then extend their results to include level velocities for any classically chaotic system. More recently, Leboeuf and Sieber [36] studied the non-universal scaling of the level velocities using a similar semiclassical theory. The  $\hbar$ -dependence of the average and root mean square level velocities for an arbitrary parameter change is derived and is consistent with the previous works.

The smoothed spectral staircase is

$$N_\epsilon(E, \lambda) = \sum_n \theta_\epsilon(E - E_n(\lambda)) \quad (4.7)$$

and taking the derivative with respect to the parameter, we obtain

$$\frac{\partial N_\epsilon(E, \lambda)}{\partial \lambda} = \sum_n \delta_\epsilon(E - E_n(\lambda)) \frac{\partial E_n(\lambda)}{\partial \lambda} \quad (4.8)$$

The quantity  $\epsilon$  is an energy smoothing term which will be taken smaller than the mean level

spacing. Our calculations will use Lorentzian smoothing where

$$\delta_\epsilon(x) = \frac{\epsilon}{\pi(x^2 + \epsilon^2)} \quad (4.9)$$

The energy averaging of Eq. (4.8) yields

$$\left\langle \frac{\partial N_\epsilon(E, \lambda)}{\partial \lambda} \right\rangle_E = \bar{d}(E, \lambda) \left\langle \frac{\partial E_n(\lambda)}{\partial \lambda} \right\rangle_n \quad (4.10)$$

Thus, in order to obtain information about the level velocities, we will evaluate the spectral staircase.

The semiclassical construction of the spectral staircase is broken into an average part and an oscillating part

$$N_\epsilon(E, \lambda) = \bar{N}(E, \lambda) + \sum_p B_p(E, \lambda) \exp \left\{ i \left[ \frac{S_p(E, \lambda)}{\hbar} \right] \right\} \exp \left\{ \frac{-\epsilon T_p(E, \lambda)}{\hbar} \right\} \quad (4.11)$$

The average staircase  $\bar{N}(E, \lambda)$  is the Weyl term and to leading order in  $\hbar$  is given by

$$\bar{N}(E, \lambda) = \frac{1}{h^d} \int \int \theta(E - H(\mathbf{p}, \mathbf{q}; \lambda)) d\mathbf{p} d\mathbf{q} \quad (4.12)$$

This simply states that each energy level occupies a volume  $h^d$  in phase space. A change in the phase space volume will produce level velocities due to the rescaling. We wish to study level velocities created by a change in the dynamics, not the rescaling. Hence, without loss of generality we will require the phase space volume to remain unchanged, so  $\partial \bar{N}(E, \lambda) / \partial \lambda = 0$ .

The oscillating part of the spectral staircase is a sum over periodic orbits. In general, a perturbation will alter the value of the classical actions,  $S_p$ , the periods,  $T_p$ , and the amplitudes,

$$B_p = \frac{\exp(i\nu_p)}{2\pi\sqrt{\det(M_p - 1)}} \quad (4.13)$$

where  $M_p$  is the stability matrix and  $\nu_p$  is the Maslov phase index. The summation is most sensitive to the changing actions and periods because of the associated rapidly oscillating phases, i.e. the division by  $\hbar$  in the exponential. Since the energy smoothing term,  $\epsilon$ , is taken smaller than a mean level spacing, it scales at least by  $\hbar^d$  and the derivatives of the period vanish as  $\hbar \rightarrow 0$ . Thus, only the derivatives of the actions are considered, and the oscillating part of the staircase yields

$$\left\langle \frac{\partial N_{osc}(E, \lambda)}{\partial \lambda} \right\rangle_E = \left\langle \sum_p B_p \left[ \frac{i}{\hbar} \frac{\partial S_p(E, \lambda)}{\partial \lambda} \right] \exp \left\{ i \left[ \frac{S_p(E, \lambda)}{\hbar} \right] \right\} \exp \left\{ \frac{-\epsilon T_p(E, \lambda)}{\hbar} \right\} \right\rangle_E \quad (4.14)$$

It has been shown [37] that the change in the action for a periodic orbit is

$$\frac{\partial S_p}{\partial \lambda} = - \int_0^{T_p} \frac{\partial H(\mathbf{p}, \mathbf{q}; \lambda)}{\partial \lambda} dt \quad (4.15)$$

The above integral is over the path of the unperturbed orbit and the Hamiltonian can have the form of Eq. (4.4) where  $H_0$  is the unperturbed part. Eq. (4.14) can be solved without the explicit knowledge of the periodic orbits in the  $\hbar \rightarrow 0$  limit. The quantity  $\partial S_p / \partial \lambda$  is replaced by its average. By the principle of uniformity [38], the collection of every periodic orbit covers all of phase space with a uniform distribution. Thus, the time integral can be

replaced by an integral over phase space upon taking the average,

$$\lim_{T \rightarrow \infty} \frac{1}{T} \left\langle \frac{\partial S_p}{\partial \lambda} \right\rangle_p = \frac{-1}{V} \int \frac{\partial H(\mathbf{p}, \mathbf{q}; \lambda)}{\partial \lambda} \delta(E - H(\mathbf{p}, \mathbf{q}; \lambda)) d\mathbf{p} d\mathbf{q} \quad (4.16)$$

where  $V$  is the phase space volume of the energy surface. The above treatment of the average is only valid for the long orbits, but we may ignore the finite set of short orbits in the sum for small enough  $\hbar$ .  $\partial H(\mathbf{p}, \mathbf{q}; \lambda)/\partial \lambda$  is the perturbation of the system that distorts the energy surface. Since the phase space is assumed to remain constant, then the average change in the actions of the periodic orbits is zero in the limit of summing over all the orbits. If only a finite number of orbits are considered, corresponding to a finite  $\hbar$ , then there might be some residual effect of the oscillating part which will cause a deviation from RMT.

Continuing to follow Berry and Keating, the mean square of the counting function derivatives can be expressed in terms of the level velocities

$$\left\langle \left( \frac{\partial N_\epsilon}{\partial \lambda}(E, \lambda) \right)^2 \right\rangle_E = \left\langle \sum_n \sum_m \frac{\partial E_n}{\partial \lambda}(\lambda) \frac{\partial E_m}{\partial \lambda}(\lambda) \delta_\epsilon(E - E_n(\lambda)) \delta_\epsilon(E - E_m(\lambda)) \right\rangle_E \quad (4.17)$$

For a non-degenerate spectrum, the summation is non-zero only if  $n = m$  because of the product of the two delta functions. Since Lorentzian smoothing is applied, then

$$\delta_\epsilon^2(x) \approx \frac{1}{2\pi\epsilon} \delta_{\epsilon/2}(x) \quad (4.18)$$

for  $\epsilon \ll \bar{d}^{-1}$ . Thus we have

$$\left\langle \left( \frac{\partial N_\epsilon}{\partial \lambda}(E, \lambda) \right)^2 \right\rangle_E = \frac{\bar{d}}{2\pi\epsilon} \left\langle \left( \frac{\partial E_n}{\partial \lambda}(\lambda) \right)^2 \right\rangle_n \quad (4.19)$$

The final result will be independent of  $\epsilon$  and the type of smoothing, i.e. Lorentzian or Gaussian. Using the  $\lambda$  derivative of Eq. (4.11), the dimensionless level velocities are

$$\tilde{\sigma}_E^2 = \frac{2\pi\epsilon\bar{d}}{\hbar^2} \left\langle \sum_p \sum_{p'} |B_p B_{p'}| \frac{\partial S_p}{\partial \lambda} \frac{\partial S_{p'}}{\partial \lambda} \exp \left\{ i \left[ \frac{S_p - S_{p'}}{\hbar} \right] \right\} \exp \left\{ \frac{-\epsilon}{\hbar} [T_p + T_{p'}] \right\} \right\rangle_E \quad (4.20)$$

The diagonal and off-diagonal contributions are separated, so

$$\tilde{\sigma}_E^2 = \tilde{\sigma}_{E,diag}^2 + \tilde{\sigma}_{E,off}^2 \quad (4.21)$$

As  $\hbar \rightarrow 0$ , the phase of the exponential oscillates rapidly and averages out to be zero unless  $S_p = S_{p'}$ . We will assume that this occurs rarely except when  $p = p'$ . The product  $(\partial S_p / \partial \lambda)(\partial S_{p'} / \partial \lambda)$  can take on both positive and negative values. This also helps to reduce the contributions of the off-diagonal terms. For a more complete discussion of the diagonal vs. off-diagonal terms see [39]. We will only present the results for the diagonal terms, since the correlations between the actions of different orbits is not known but should not alter the leading  $\hbar$ -dependence.

The diagonal contribution is

$$\tilde{\sigma}_{E,diag}^2 = \frac{2\pi\epsilon\bar{d}g}{\hbar^2} \left\langle \sum_p |B_p|^2 \left( \frac{\partial S_p}{\partial \lambda} \right)^2 \exp \left\{ \frac{-2\epsilon T_p}{\hbar} \right\} \right\rangle_E \quad (4.22)$$

The factor  $g$  depends on the symmetries of the system. For systems with time-reversal invariance  $g = 2$  and without time-reversal symmetry  $g = 1$ . The precise values of  $\partial S_p/\partial \lambda$  are specific to each periodic orbit rendering the sum difficult to evaluate precisely. A statistical approach is possible though which generates a relationship between the sum and certain correlation decays. Hence, the quantity  $(\partial S_p/\partial \lambda)^2$  in Eq. (4.22) is replaced by its average,

$$\begin{aligned} \left\langle \left( \frac{\partial S_p}{\partial \lambda} \right)^2 \right\rangle_p &= \int_0^T \int_0^T \left\langle \frac{\partial H(\mathbf{p}(t), \mathbf{q}(t); \lambda)}{\partial \lambda} \frac{\partial H(\mathbf{p}(t'), \mathbf{q}(t'); \lambda)}{\partial \lambda} \right\rangle_p dt' dt \\ &= 2 \int_0^T \int_t^T \left\langle \frac{\partial H(\mathbf{p}(t), \mathbf{q}(t); \lambda)}{\partial \lambda} \frac{\partial H(\mathbf{p}(t'+t), \mathbf{q}(t'+t); \lambda)}{\partial \lambda} \right\rangle_p dt' dt \end{aligned} \quad (4.23)$$

Long orbits increasingly explore the available phase space on an ever finer scale. As the time between two points in a chaotic system goes to infinity, then they become uncorrelated from each other. This is a consequence of the mixing property,

$$\langle f(0)f(t) \rangle_p \rightarrow 0 \quad (4.24)$$

This property is independent of the placement of the two points, i.e. the two points can lie on the same orbit as long as the time between the points increases to infinity. Thus, by the central limit theorem,  $\partial S_p/\partial \lambda$  will be Gaussian distributed for the sufficiently long

periodic orbits. The time dependence of Eq. (4.23) is approximated by a method discussed by Bohigas *et al.* [40]. They define

$$K(E) = \int_0^\infty \left\langle \frac{\partial H(\mathbf{p}(0), \mathbf{q}(0); \lambda)}{\partial \lambda} \frac{\partial H(\mathbf{p}(t), \mathbf{q}(t); \lambda)}{\partial \lambda} \right\rangle_p dt \quad (4.25)$$

which can be evaluated in terms of properties of the perturbation. The variance of the actions in the limit of long periods becomes

$$\left\langle \left( \frac{\partial S_p}{\partial \lambda} \right)^2 \right\rangle_p \approx 2K(E)T \quad (4.26)$$

Applying the Hannay and Ozorio de Almeida sum rule [38], the following substitution is made

$$\sum_p |B_p|^2 \dots \rightarrow \frac{1}{2\pi^2} \int_0^\infty \frac{dT}{T} \dots \quad (4.27)$$

Hence, the diagonal contribution is

$$\begin{aligned} \tilde{\sigma}_{E,diag}^2 &\approx \frac{\epsilon \bar{d} g}{\pi \hbar^2} \int_0^\infty \frac{1}{T} (2K(E)T) \exp \left\{ \frac{-2\epsilon T}{\hbar} \right\} dT \\ &\approx \frac{gK(E)\bar{d}}{\pi \hbar} \\ &\propto \hbar^{-(d+1)} \end{aligned} \quad (4.28)$$

The variance of the level velocities on the scale of a mean spacing grows  $\hbar^{-1}$  faster than the density of states as the semiclassical limit ( $\hbar \rightarrow 0$ ) is approached; see numerical tests performed on the stadium in the next section.

The exact level velocities are perturbation dependent and cannot be determined without specific knowledge of the system (i.e. the evaluation of  $K(E)$ ).  $K(E)$  is a classical quantity that contains dynamical information about the periodic orbits. It should scale as the reciprocal of the Lyapunov exponent [41]. Leboeuf and Sieber derived  $K(E)$  for billiards where the perturbation is a moving boundary. In this case  $K(E)$  depends upon the autocorrelation function and the fluctuations of the number of bounces. For maps  $K(E)$  is an action velocity diffusion coefficient [42].  $\{\partial S_p/\partial\lambda\}$  being Gaussian distributed is linked to the level velocities being Gaussian distributed as in RMT. If the  $\{\partial S_p/\partial\lambda\}$  are not Gaussian distributed by the Heisenberg time, then one should not expect the level velocities to be consistent with RMT; again see the stadium results ahead.

#### 4.4.2 Overlap intensities

Now we investigate the overlap intensities and derive a semiclassical expression for the  $\hbar$ -scaling of the root mean square. Eckhardt *et al.* [43] developed a semiclassical theory based on periodic orbits to obtain the matrix elements of a sufficiently smooth operator. However, the projection operator of interest here,  $|\alpha\rangle\langle\alpha|$ , is not smooth on the scale of  $\hbar$  for Gaussian wave packets. Thus, their stationary phase approximations do not apply, in principle, to the oscillating part of the strength function. In Berry's work on scars [44], he used Gaussian smoothing of the Wigner transform of the eigenstates to obtain a semiclassical expression for the strength of the scars. His approach led to a sum over periodic orbits. We will use the energy Green's function similar to Tomsovic and Heller in [21] where they derived the



autocorrelation function using the time Green's function and gave results for the strength functions as well. This technique results in a connection between the overlap intensities and the return dynamics, namely the homoclinic orbits.

For completeness, we present the smooth part of the strength function which is easily obtained from the zero-length trajectories,

$$\overline{S}_\alpha(E, \lambda) = \frac{1}{h^d} \int A(\mathbf{q}, \mathbf{p}) \delta(E - H(\mathbf{q}, \mathbf{p})) d\mathbf{q} d\mathbf{p} \quad (4.29)$$

$A(\mathbf{q}, \mathbf{p})$  is the Wigner transform of the Gaussian wave packet and is given by

$$A(\mathbf{q}, \mathbf{p}) = 2^d \exp\{-(\mathbf{p} - \mathbf{p}_\alpha)^2 \sigma^2 / \hbar^2 - (\mathbf{q} - \mathbf{q}_\alpha)^2 / \sigma^2\} \quad (4.30)$$

The above results were previously used by Heller [45] in the derivation the envelope of the strength function and does not contain any information about the dynamics of the system.

The oscillating part of the strength function, on the other hand, includes dynamical information,

$$S_{\alpha,osc}(E, \lambda) = \frac{-1}{\pi} \text{Im} \int \langle \alpha | \mathbf{q} \rangle G(\mathbf{q}, \mathbf{q}'; E) \langle \mathbf{q}' | \alpha \rangle d\mathbf{q} d\mathbf{q}' \quad (4.31)$$

where

$$G(\mathbf{q}, \mathbf{q}'; E) = \frac{1}{i\hbar(2\pi i\hbar)^{(d-1)/2}} \sum_j |D_s|^{1/2} e^{i[S_j(\mathbf{q}, \mathbf{q}'; E) / \hbar - \nu_j' \pi / 2]} \quad (4.32)$$

is the semiclassical energy Green's function. The above sum is over all paths that connect  $\mathbf{q}$  to  $\mathbf{q}'$  on a given energy surface  $E$ . The action is quadratically expanded about each

reference trajectory; see Appendix 4.A for details. The initial and final points ( $\mathbf{q}_i$  and  $\mathbf{q}_f$ ) of the reference trajectories are obtained by considering the evolution of the wave packet. Nearby points will behave similarly for short times. Thus, the phase space can be partitioned into connecting areas. As the time is increased the number of partitions grow and the size of their area shrinks. The reference trajectories are the paths that connect the partitions. The autocorrelation function in [21] has the same form as Appendix 4.A where the paths that contribute to the saddle points are the orbits homoclinic to the centroid of the Gaussian wave packet so that  $\mathbf{q}_i$  and  $\mathbf{q}_f$  lie on the intersections of the stable and unstable manifolds. The result from Appendix 4.A is

$$S_{\alpha,osc}(E) = \frac{\sigma}{\pi^{1/2}\hbar} \text{Re} \sum_j \left( \frac{\det \tilde{\mathbf{A}}^{21}}{\det \mathbf{A}} \right)^{1/2} \left( \frac{1}{|\dot{q}^{(N)}| |\dot{q}'^{(N)}|} \right)^{1/2} f_j(\mathbf{q}_f, \mathbf{q}_i) e^{iS_j(\mathbf{q}_f, \mathbf{q}_i; E)/\hbar} \quad (4.33)$$

where

$$f_j(\mathbf{q}_f, \mathbf{q}_i) = \exp \left\{ \frac{1}{4} \mathbf{b} \cdot \mathbf{A}^{-1} \cdot \mathbf{b} - \frac{i}{\hbar} \mathbf{p}_\alpha \cdot (\mathbf{q}_f - \mathbf{q}_i) - \frac{(\mathbf{q}_f - \mathbf{q}_\alpha)^2}{2\sigma^2} - \frac{(\mathbf{q}_i - \mathbf{q}_\alpha)^2}{2\sigma^2} - \frac{i\nu'_j \pi}{2} \right\} \quad (4.34)$$

The function  $f_j(\mathbf{q}_f, \mathbf{q}_i)$  in the above equation is a damping term which depends on the end points of the homoclinic orbits. Only orbits which approach the center of the Gaussian wave packet in phase space will contribute to the sum. The time derivatives of the parallel coordinates are evaluated at the saddle points which are near the centroid of the Gaussian, so we may set  $|\dot{q}^{(N)}| \approx |\dot{q}'^{(N)}| \approx |p_\alpha|/m$ . The sum over homoclinic orbits used for the autocorrelation function in [21] converged well to the discrete quantum strength function

when only those orbits whose period did not exceed the Heisenberg time, ( $\tau_H = 2\pi\hbar\bar{d}(E, \lambda)$ ), were included. As happened with the periodic orbits and the level velocities, in order to evaluate Eq. (4.33) the homoclinic orbits and their stabilities must be computed rendering the sum tedious to evaluate precisely as done in [21].

By taking a statistical approach we can gain some insight into the workings of this summation. The variance of the intensities are obtained by a similar fashion as the level velocities. Using Eq. (4.1) and Eq. (4.18), we have

$$\langle S_{\alpha,osc}^2(E, \lambda) \rangle_E = \frac{\bar{d}}{2\pi\epsilon} \sigma_{\alpha}^2 \quad (4.35)$$

Since the square of the strength function is a product of two delta functions, an energy smoothing term is required. After making the diagonal approximation, we obtain

$$\sigma_{\alpha,diag}^2 = \frac{2\pi\epsilon g}{\bar{d}} \left\langle \sum_j \frac{m^2 \sigma^2}{\pi \hbar^2} \left| \frac{\det \tilde{\mathbf{A}}^{21}}{\det \mathbf{A}} \right| \frac{|f_j(\mathbf{q}_f, \mathbf{q}_i)|^2}{|p_{\alpha}|^2} e^{-2\epsilon T_j/\hbar} \right\rangle_E \quad (4.36)$$

A classical sum rule is applied to the above sum for special cases including two-dimensional systems; see Appendix 4.B for the details. Thus,

$$\begin{aligned} \sigma_{\alpha,diag}^2 &\approx \frac{2\epsilon g m^2 \sigma^2}{\hbar^2 \bar{d} |p_{\alpha}|^2} \int \exp\{-2\epsilon T/\hbar\} dT \\ &\approx \frac{g m^2 \sigma^2}{\hbar \bar{d} |p_{\alpha}|^2} \end{aligned} \quad (4.37)$$

Setting  $\sigma \propto \hbar^{1/2}$  which shrinks the momentum and position uncertainties similarly, the

$\hbar$ -scaling of  $\sigma_{\alpha,diag}^2$  is  $\hbar^d$ ; see numerical tests of the stadium in the next section.

Assuming that the amplitudes of the wavefunctions are Gaussian random, then the RMT result for strength functions is a Porter-Thomas distribution which has a variance that is proportional to the square of its average. The average strength function, Eq. (4.29), scales as  $(\sigma/\hbar)^d$  for Hamiltonians which can be locally expanded as a quadratic. Therefore, with  $\sigma \propto \hbar^{1/2}$  the variance of the strength function, Eq. (4.37), scales as the square of the average and is consistent with RMT.

### 4.4.3 Weighted level velocities

A semiclassical treatment of the overlap correlation coefficient defined in Eq. (4.2) is now developed. As stated in the introduction, the companion paper [23] presents the semiclassical theory for maps. We stress that in the preceding subsections and in what follows is for conservative Hamiltonian systems. Here, the  $\hbar$ -dependence of the average overlap correlation coefficient is established and a semiclassical argument for the existence of nonzero correlations is presented.

#### Actions of homoclinic orbits

To calculate the overlap correlation coefficient, the rate of change of the actions for homoclinic orbits will be necessary. As discussed earlier, this was accomplished for periodic orbits [37]. We extend these results to include the actions of homoclinic orbits. Homoclinic orbits have infinite periods causing their actions to become infinite. We are interested in the

limiting difference of the action,  $\mathcal{S}_j^{(p)}$ , between the  $j^{\text{th}}$  homoclinic orbit and repetitions of its corresponding periodic orbit  $p$ . The difference is finite and is equal to the area bounded by the stable and unstable manifolds with intersection at the  $j^{\text{th}}$  homoclinic point in a Poincaré map.  $\mathcal{S}_j^{(p)}$  provides information about the additional phase gathered by the homoclinic orbit. The action of the  $j^{\text{th}}$  homoclinic orbit as  $n \rightarrow \infty$  in the time interval  $(-nT_p, nT_p)$  is

$$\mathcal{S}_{n,j}^{(p)} \rightarrow 2nS_p + \mathcal{S}_j^{(p)} \quad (4.38)$$

where  $T_p$  and  $S_p$  are the period and action of the periodic orbit, respectively. As a consequence of the Birkhoff-Moser theorem [46], if the Poincaré map is invertible and analytic, then there exist infinite families of periodic orbits that accumulate on a homoclinic orbit. It is thus possible to estimate the action of the homoclinic orbit by these periodic orbits whose action is given by [47]

$$\alpha_{n,j}^{(p)} = nS_p + \mathcal{S}_j^{(p)} - s_{n,j}^{(p)} \quad (4.39)$$

where  $s_{n,j}^{(p)}$  is the difference in action between a path defined by  $\mathcal{S}_j^{(p)}$  along the stable and unstable manifolds and the path of the new periodic orbit in a Poincaré map.  $s_{n,j}^{(p)}$  depends exponentially on  $n$ , so as  $n \rightarrow \infty$ ,  $\alpha_{2n,j}^{(p)}$  approaches the action of the homoclinic orbit. Thus, in the limit of large  $n$ ,  $\mathcal{S}_j^{(p)}$  is approximated by the difference between two periodic orbits (i.e.  $\mathcal{S}_j^{(p)} \approx \alpha_{n,j}^{(p)} - nS_p$ ). Hence, the change in  $\mathcal{S}_j^{(p)}$  due to a small perturbation is calculated

as in [37],

$$\Delta S_j^{(p)} = -\Delta\lambda \int_{\alpha_{n,j}^{(p)}} \frac{\partial H(\mathbf{p}, \mathbf{q}; \lambda)}{\partial \lambda} dt + n\Delta\lambda \int_{s_p} \frac{\partial H(\mathbf{p}, \mathbf{q}; \lambda)}{\partial \lambda} dt + O(\lambda^2) \quad (4.40)$$

where the integrals are over the unperturbed periodic orbits. The differences,  $s_{n,j}^{(p)}$ , can be made smaller than the second order term in Eq. (4.40) by taking  $n$  large enough. Interchanging the order of integration and differentiation, the integrals reduce to the unperturbed energy times the derivative of the orbit period with respect to the parameter,

$$\Delta S_j^{(p)} \approx -\Delta\lambda E_p \frac{\partial}{\partial \lambda} \left( T_{\alpha_{n,j}^{(p)}} - nT_p \right) \quad (4.41)$$

The orbit period  $T$  can be expressed as  $\partial S/\partial E$ . Thus, the difference of the two periods as  $n \rightarrow \infty$  is

$$T_{\alpha_{n,j}^{(p)}} - nT_p = \frac{\partial \alpha_{n,j}^{(p)}}{\partial E} - n \frac{\partial S_p}{\partial E} \approx \frac{\partial S_j^{(p)}}{\partial E} \quad (4.42)$$

Hence,

$$\begin{aligned} \Delta S_j^{(p)} &\approx -\Delta\lambda \frac{\partial}{\partial \lambda} \left( E_p \frac{\partial S_j^{(p)}}{\partial E} \right) \\ &\approx -\Delta\lambda \int_{s_j^{(p)}} \frac{\partial H(\mathbf{p}, \mathbf{q}; \lambda)}{\partial \lambda} dt \end{aligned} \quad (4.43)$$

Note that the integral is over the unperturbed path along the stable and unstable manifolds.

For zero correlations,  $\Delta S_j^{(p)}$  must be “randomly” distributed about zero.

If enough time is allowed, then for ergodic systems the set of all homoclinic orbits for a

given energy will come arbitrarily close to any point in phase space on that energy surface. Thus, an integral over phase space on the original energy surface can be substituted for the time integral,

$$\lim_{T \rightarrow \infty} \frac{1}{T} \langle \Delta \mathcal{S}_j^{(p)} \rangle_j = \frac{-\Delta \lambda}{V} \int \delta(E - H(\mathbf{p}, \mathbf{q}; 0)) \frac{\partial H(\mathbf{p}, \mathbf{q}; \lambda)}{\partial \lambda} d\mathbf{p}d\mathbf{q} \quad (4.44)$$

Since the density of states are kept constant, the perturbations fluctuate about zero and the integral vanishes. Hence, the average change in the actions will be zero. The mean square fluctuations of the actions,

$$\langle (\Delta \mathcal{S}_j^{(p)})^2 \rangle_j = (\Delta \lambda)^2 \int_0^{\tau_H} \int_0^{\tau_H} \left\langle \frac{\partial H(\mathbf{p}, \mathbf{q}; \lambda)}{\partial \lambda} \frac{\partial H(\mathbf{p}', \mathbf{q}'; \lambda)}{\partial \lambda} \right\rangle_j dt dt' \quad (4.45)$$

approaches a Gaussian distribution by the central limit theorem via the same reasoning as that for periodic orbits. Again we can define  $K_{hom}(E)$  as in Eq. (4.25), except now the average is over homoclinic orbits and instead of integrating to infinity we only integrate to the Heisenberg time to be consistent with the range of the sum in Eq. (4.33). It is the short time dynamics that dominate. Long time correlations will average to zero by the mixing property (Eq. (4.24)). Thus, the variance of the actions becomes

$$\left\langle \left( \frac{\partial \mathcal{S}_j^{(p)}}{\partial \lambda} \right)^2 \right\rangle_j \approx 2K_{hom}(E)T \quad (4.46)$$

$K_{hom}(E)$  will approach  $K(E)$  in the semiclassical limit ( $\tau_H \rightarrow \infty$ ).

## Overlap intensity-level velocity correlation coefficient

In the previous two subsections, we have examined the pieces that constitute the overlap correlation coefficient. The semiclassical theories of the level velocities and the intensities are now combined to construct a semiclassical theory for the weighted level velocities. The numerator of the overlap correlation coefficient is proportional to the energy averaged product of the intensities and level velocities,

$$\begin{aligned}
 \left\langle S_\alpha(E, \lambda) \frac{\partial N(E, \lambda)}{\partial \lambda} \right\rangle_E &= \left\langle \sum_n \sum_m p_{\alpha n}(\lambda) \frac{\partial E_m}{\partial \lambda} \delta_\epsilon(E - E_n) \delta_\epsilon(E - E_m) \right\rangle_E \\
 &= \frac{\bar{d}}{2\pi\epsilon} \left\langle p_{\alpha n}(\lambda) \frac{\partial E_n}{\partial \lambda} \right\rangle_n \\
 &= \frac{\bar{d}}{2\pi\epsilon} \tilde{C}_\alpha(\lambda)
 \end{aligned} \tag{4.47}$$

Lorentzian smoothing was again employed, Eq. (4.18), and we've defined  $\tilde{C}_\alpha(\lambda)$  to be the numerator of the overlap correlation coefficient (without the division of the rms level velocities and intensities). By the definition of the overlap correlation coefficient only the oscillating part of the level velocities and the intensities are considered. Using the derivative with respect to lambda of Eq. (4.11) and Eq. (4.33) the numerator becomes

$$\tilde{C}_\alpha(\lambda) = \frac{2\pi\epsilon}{\bar{d}} \left\langle \text{Re} \sum_j \sum_p \frac{m\sigma B_p}{\pi\hbar^2} \left( \frac{\det \tilde{\mathbf{A}}^{21}}{\det \mathbf{A}} \right)^{1/2} \frac{f_j(\mathbf{q}_f, \mathbf{q}_i)}{|p_\alpha|} \left( \frac{\partial S_p}{\partial \lambda} \right) e^{i(S_j - S_p)/\hbar - \epsilon(T_j + T_p)/\hbar} \right\rangle_E \tag{4.48}$$

Because of the rapidly oscillating phases, the energy averaging will result in zero unless  $S_j \approx S_p$ . As stated earlier, for every homoclinic orbit there is a periodic orbit that comes



infinitesimally close to it. The same periodic orbit's action can be nearly equal to the actions of different segments of the same homoclinic orbit. Thus, a diagonal approximation is used for the homoclinic segments

$$\bar{c}_\alpha(\lambda) \approx \frac{2\pi\epsilon g}{\bar{d}} \left\langle \text{Re} \sum_j \frac{m\sigma B_j}{\pi\hbar^2} \left( \frac{\det \tilde{\mathbf{A}}^{21}}{\det \mathbf{A}} \right)^{1/2} e^{-2\epsilon T_j/\hbar} \left( \frac{\partial S_j}{\partial \lambda} \right) \frac{f_j(\mathbf{q}_f, \mathbf{q}_i)}{|p_\alpha|} \right\rangle_E \quad (4.49)$$

Upon applying the sum rule for two-dimensional systems and other special cases, Eq. (4.72), we have

$$\bar{c}_\alpha(\lambda) \approx \frac{\epsilon g m \sigma}{\pi \bar{d} |p_\alpha| \hbar^2} \int_0^\infty e^{-2\epsilon T/\hbar} \left\langle \left( \frac{\partial S_j}{\partial \lambda} \right) f_j(\mathbf{q}_f, \mathbf{q}_i) \right\rangle_j dT \quad (4.50)$$

The changes in action of the homoclinic excursions are now weighted by the  $f_j(\mathbf{q}_f, \mathbf{q}_i)$ 's. Without the additional weighting the average in the changes in the action would be zero for all positions of the Gaussian wave packet.

In [22], a heuristic argument for the direction of the weighted level velocities was given. The argument basically states that the energy surface changes with the parameter such that the action changes are minimized. Eq. (4.50) differs from [22] in that the proper weightings,  $f_j(\mathbf{q}_f, \mathbf{q}_i)$ , of the homoclinic orbits are derived here, and the action changes are not correlated with the inverse periods. Also, in [22] the homoclinic orbits were strictly cut-off at the Heisenberg time whereas here there is an exponential decay on the order of the Heisenberg time with the energy smoothing term,  $\epsilon$ , equal to  $\hbar/\tau_H$  [35]. One reason that [22] reported such good results is that since the number of homoclinic segments proliferate exponentially, most of the included segments occurred near the Heisenberg time and the expression in

Eq. (4.50) is divided by the Heisenberg time (i. e. multiplied by  $\epsilon$ ).

As  $\hbar \rightarrow 0$  ( $\tau_H \rightarrow \infty$ ), the integral in Eq. (4.50) would be dominated by the subset of  $\{\partial S_j/\partial\lambda\}$  associated with very long orbits and would decouple from the weightings. For small enough  $\hbar$ , as previously stated, the  $\partial S_j/\partial\lambda$  for these orbits would approach a zero-centered Gaussian density, and the integral would vanish. In other words, we could use arguments analogous to those underlying Eq. (4.16) to write

$$\bar{C}_\alpha(\lambda) \approx \frac{-gm\sigma}{\pi d|p_\alpha|} \int_0^\infty dT e^{-2T/\tau_H} \frac{T}{\tau_H} \frac{F}{V} \int d\mathbf{p}d\mathbf{q} \frac{\partial H(\mathbf{p}, \mathbf{q}; \lambda)}{\partial\lambda} \delta(E - H(\mathbf{p}, \mathbf{q}; \lambda)) \quad (4.51)$$

where  $F$  is the phase space average of the weightings. Note that the phase space average of  $\partial H(\mathbf{p}, \mathbf{q}; \lambda)/\partial\lambda$  vanishes excluding an irrelevant drift of levels, so the RMT prediction of  $\tilde{C}_\alpha(\lambda)$  is recovered for  $\hbar$  small enough.

The leading order in  $\hbar$  correction to this is more difficult to ascertain.  $\hbar$  enters into the exponential in the integral for the energy smoothing, but not for the classical decay of the action changes. Upon taking the integral, this yields two competing terms for the  $\hbar$ -scaling which may depend upon the region of phase space the correlation is taken in. The numerics also show a large fluctuation of the scaling in the stadium (see the next section).

## 4.5 Stadium Billiard

In this section the semiclassical theories just presented and the numerical results from the stadium billiard are compared. The stadium billiard, which was proven by Bunimovich [48]

to be classically chaotic, has become a paradigm for studies of quantum chaos. It is defined as a two-dimensional infinite well with the shape pictured in Fig. (4.4). We continuously vary the side length,  $2\lambda$ , while altering the radii of the endcaps,  $R$ , to keep the area of the stadium a constant. Throughout this section, the level velocities and intensities are evaluated for a stadium with  $\lambda = R = 1$ . For billiards the average number of states below a given energy,  $E$ , is approximately  $\overline{N}(E) \approx mAE/2\pi\hbar^2$  where  $A$  is the area of the billiard. This is the first term in an asymptotic series in powers of  $\hbar$ . The density of the states,  $d\overline{N}/dE$ , is then a constant not depending on  $\lambda$  to the lowest power of  $\hbar$  if the area remains the same.

We will examine three different energy regimes for the stadium. Since billiards are scaling systems, this will correspond to three different values of  $\hbar$ . The energy regimes are separated by a factor of four in energy or conversely a factor of one half in  $\hbar$ . Twice as many states are taken in each successive energy regime so that the averages will incorporate the same relative size interval in energy as  $\hbar$  is decreased. This corresponds to the increase in the density of states for varying  $\hbar$ .

The distributions of the level velocities for all three energy regimes are shown in Fig. (4.5) along with the random matrix theory prediction. The skewness occurs because of a class of marginally stable orbits in the stadium. These orbits are the bouncing ball orbits which only strike the straight edges. Their contribution do not seem to decrease as the semiclassical limit is approached though they should once  $\hbar$  is sufficiently small. There is no clear trend for the level velocity distribution to approach Gaussian behavior. The root mean square of the level velocities also deviates from our calculations of the  $\hbar$ -scaling in Section 4.4 (Fig. (4.6)).

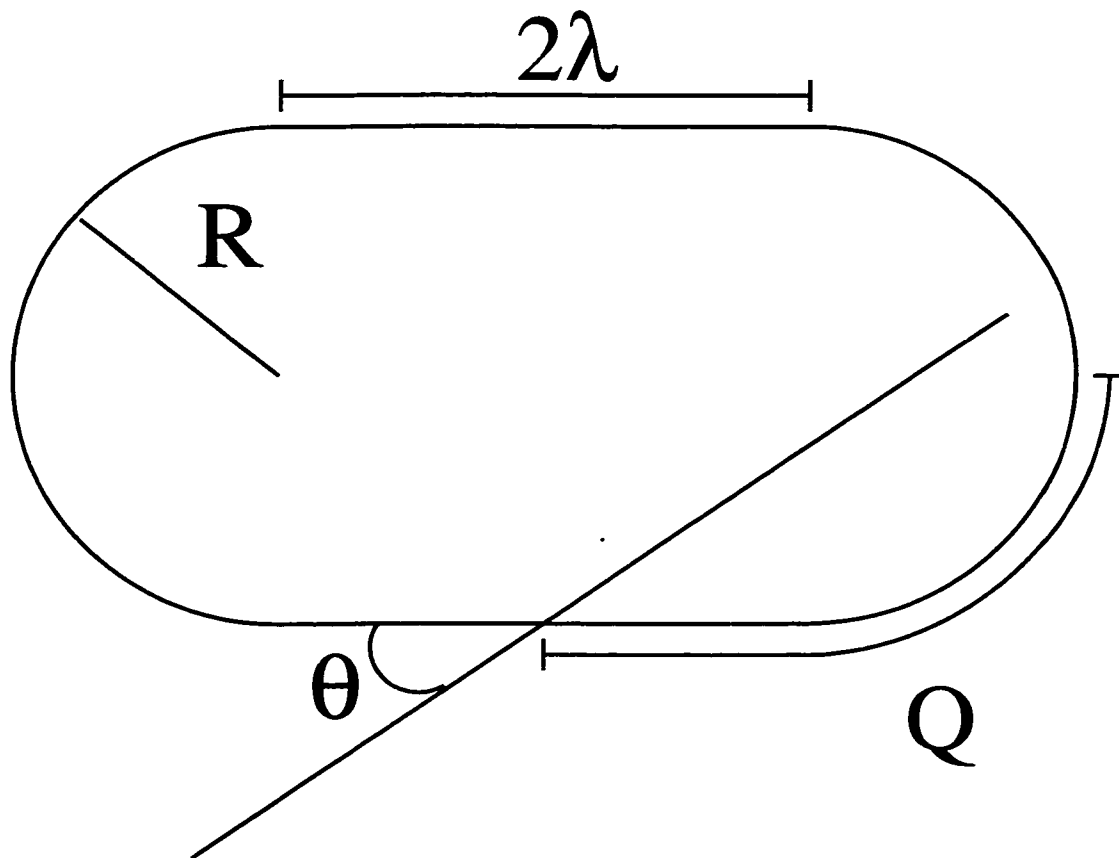


Figure 4.4: Birkhoff coordinates for the stadium billiard. The position coordinate can be taken to start anywhere along the perimeter. Here we have chosen the origin to be the middle of the right semicircle.

This is again explained by the bouncing ball orbits whose effects are missing from the trace formula. Quantizing only these orbits using WKB yields a dimensionless level velocity scaling of  $\hbar^{-2}$ , while the trace formula gives a scaling of  $\hbar^{-3/2}$ . The numerical results give a scaling of approximately  $\hbar^{-1.8}$  which lies in between the two suggesting that the marginally stable orbits significantly effect the level velocities.

To study the intensities, the eigenstates must first be constructed. Bogomolny's transfer operator method [49] was used to find the eigenstates. This method uses a  $(d - 1)$  dimensional surface of section. A convenient choice is the boundary of the stadium (Fig. (4.4)). The generation of a full phase space picture of the stadium would otherwise require four dimensions, two positions and two momenta. The position coordinate is measured along the perimeter and the momentum coordinate is defined by  $\cos \theta$ . The classical dynamics have a quantum analog that uses source points on the boundary. Thus, all of the eigenfunction's localization behavior can be explored using wave packets defined in these coordinates. A coherent state on the boundary is a one-dimensional Gaussian wave packet; see the lower figure in Fig. (4.7). The corresponding wave packet in the interior of the stadium can be generated by a Green's function and is shown in the upper figure of Fig. (4.7). For billiards the Green's function is proportional to a zero<sup>th</sup> order Hankel function of the first kind,  $H_0^{(1)}(kr)/2i\hbar^2$ . The centroid of the Gaussian wave packet is moved along the boundary and its momentum is changed according to the Birkhoff coordinate system. Thus, the entire phase space of the stadium is explored.

The results for the average and the standard deviation of the intensities using Birkhoff

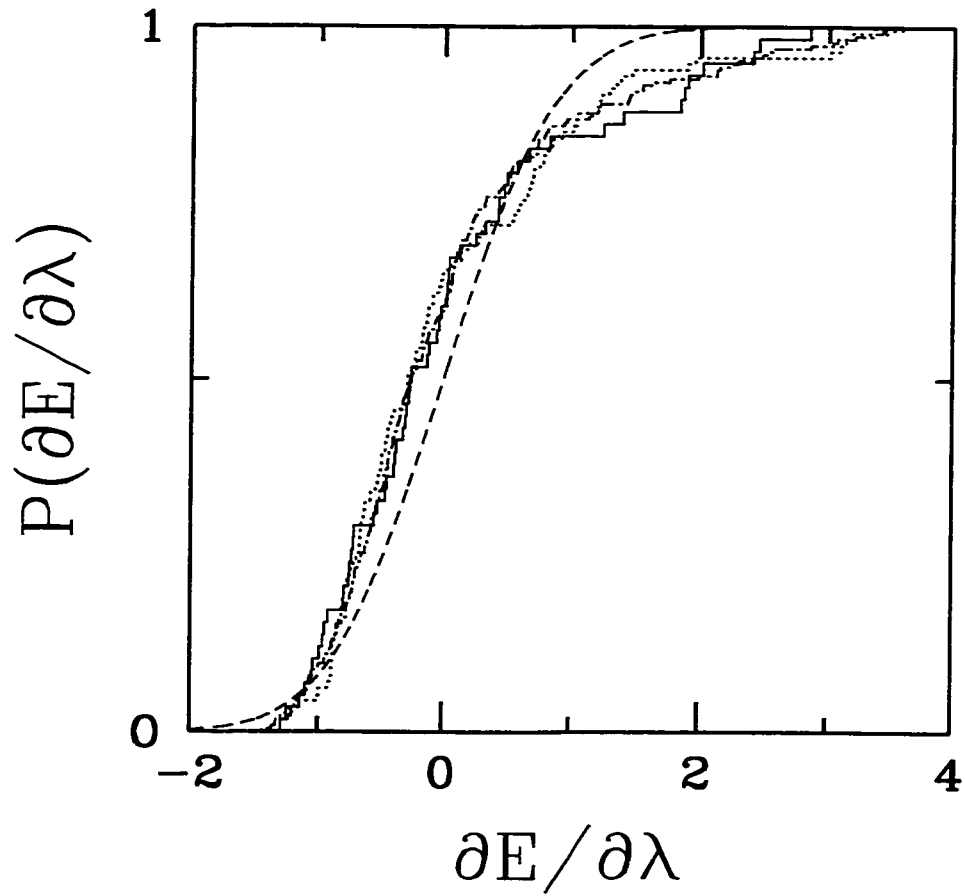


Figure 4.5: Distribution of the level velocities for a stadium billiard. The solid line is the lowest energy range, the dotted line is the middle energy range and the dash-dot line is the highest energy range. The RMT result is given by the dashed line. The level velocities have been rescaled to zero mean and unit variance.

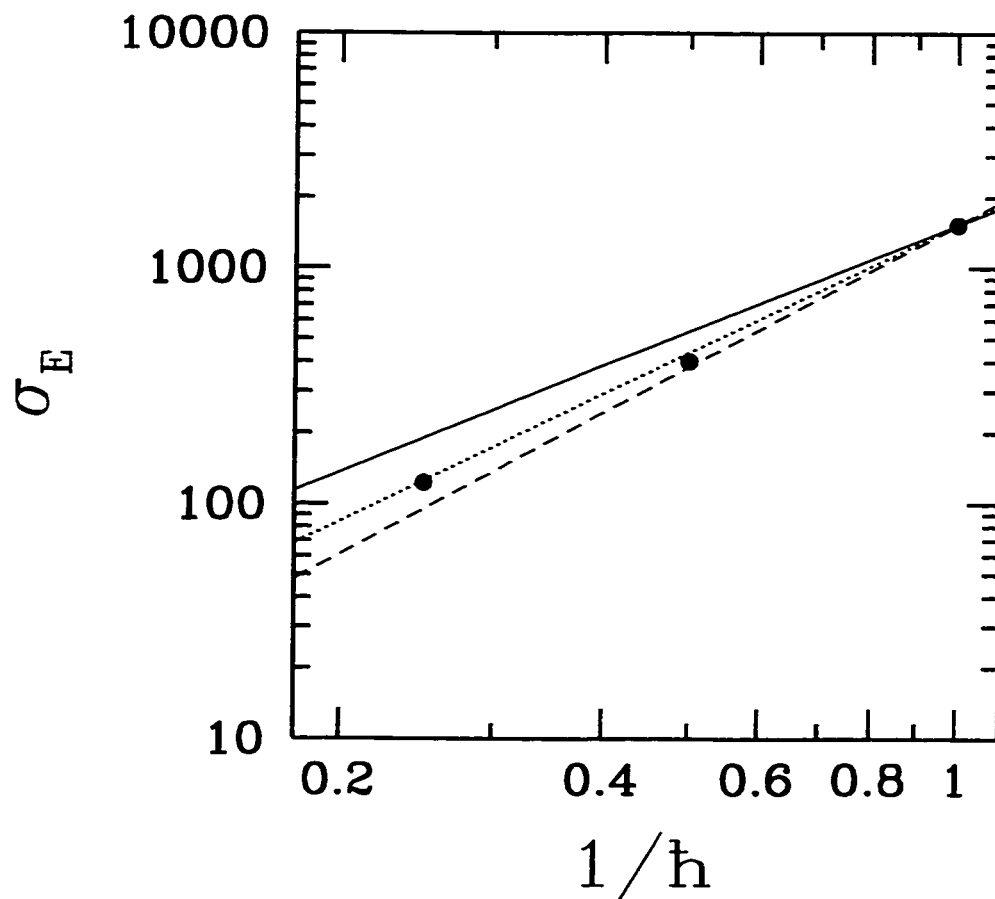


Figure 4.6: Root mean square of the level velocities as a function of  $1/\hbar$ . The solid line is the theoretical value from Section 4.4 and the dashed line is the WKB results for the bouncing ball motion. The best fit line through the stadium results is the dotted line.

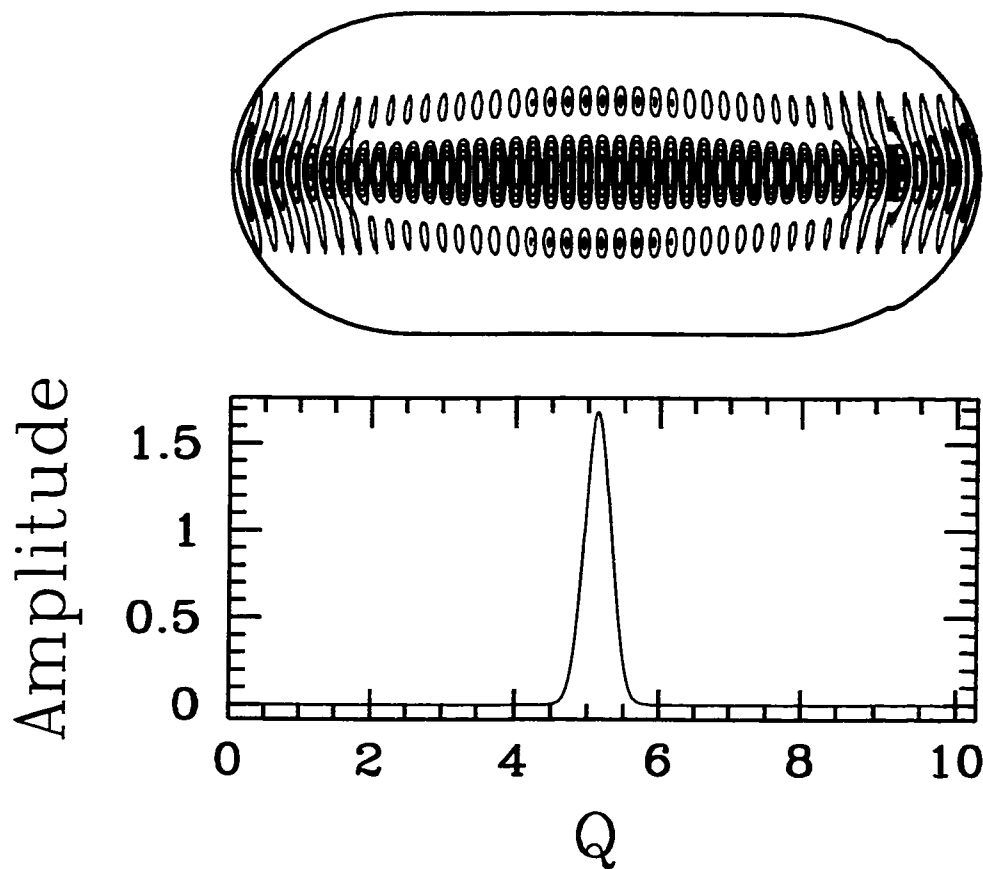


Figure 4.7: The lower figure is Gaussian wave packet on the boundary. The upper figure corresponds to the wave packet in the interior of the stadium.



coordinates are shown in Figs. (4.8) and (4.9), respectively. The average is flat except for peaks associated with the two symmetry lines of the stadium. The eigenstates used here were even-even states, so there is twice the intensity along the two symmetry lines that bisect the end caps and the straight edges. The standard deviation has two large peaks centered around the bouncing ball orbits. The rest of the figure is relatively flat with a few small bumps. Random matrix theory would predict this to be a flat figure with small oscillations. The marginal stability of the bouncing ball orbits can be seen but no other feature of the stadium, except for the horizontal bounce, is picked out by looking at the intensities. Fig. (4.10) shows the  $\hbar$ -scaling of the root mean square for the intensities where the wave packet is placed on various periodic orbits. The theory from Section 4.4 predicts a smaller scaling than the numerical results of the stadium.

The heights of the bouncing ball peaks can be approximated by quantizing the rectangular region of the stadium. The intensities obtained from this calculation are weighted by the ratio of the density of the bouncing ball states [50] to the total density of states. The Gaussian wave packet is placed in the center of the straight edge and the middle energy regime is used. The results of this approximation are 80.6 and 320.5 for the average intensity and rms intensity, respectively, compared to 80.7 and 386.3 for the numerical calculations of the stadium.

Random matrix theory suggests that the correlation coefficient for a generic chaotic system should result in zero. On the other hand, using the correlation coefficient for the stadium in Birkhoff coordinates, we found that some of the states gave nonzero correlations,

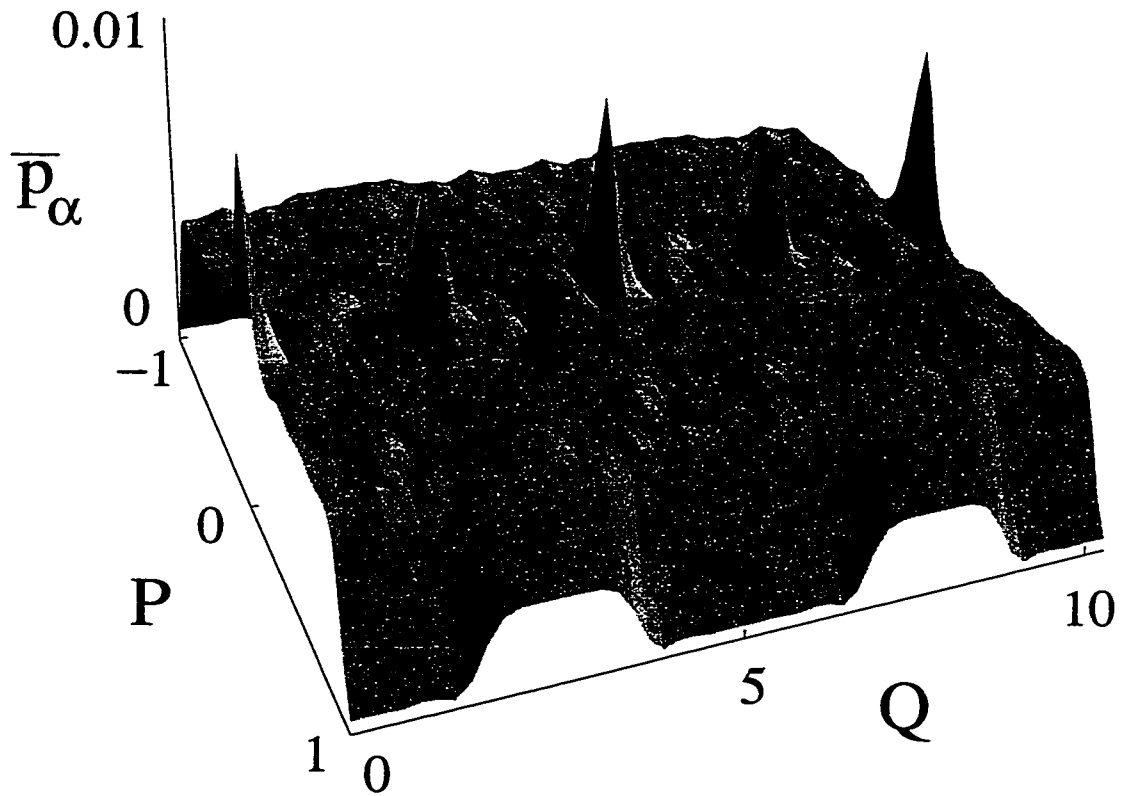


Figure 4.8: Average overlap intensity for a Gaussian wave packet defined in the Birkhoff coordinates of the stadium.

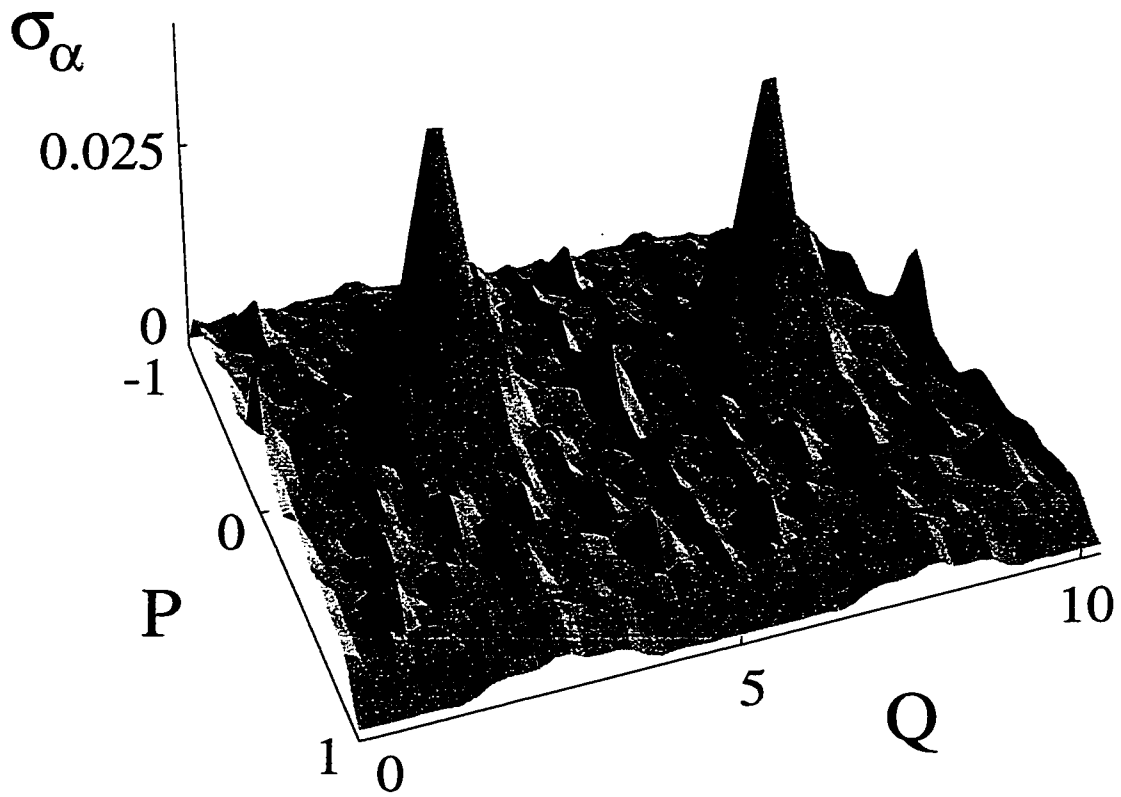


Figure 4.9: Root mean square of the overlap intensity for a Gaussian wave packet defined in the Birkhoff coordinates of the stadium.

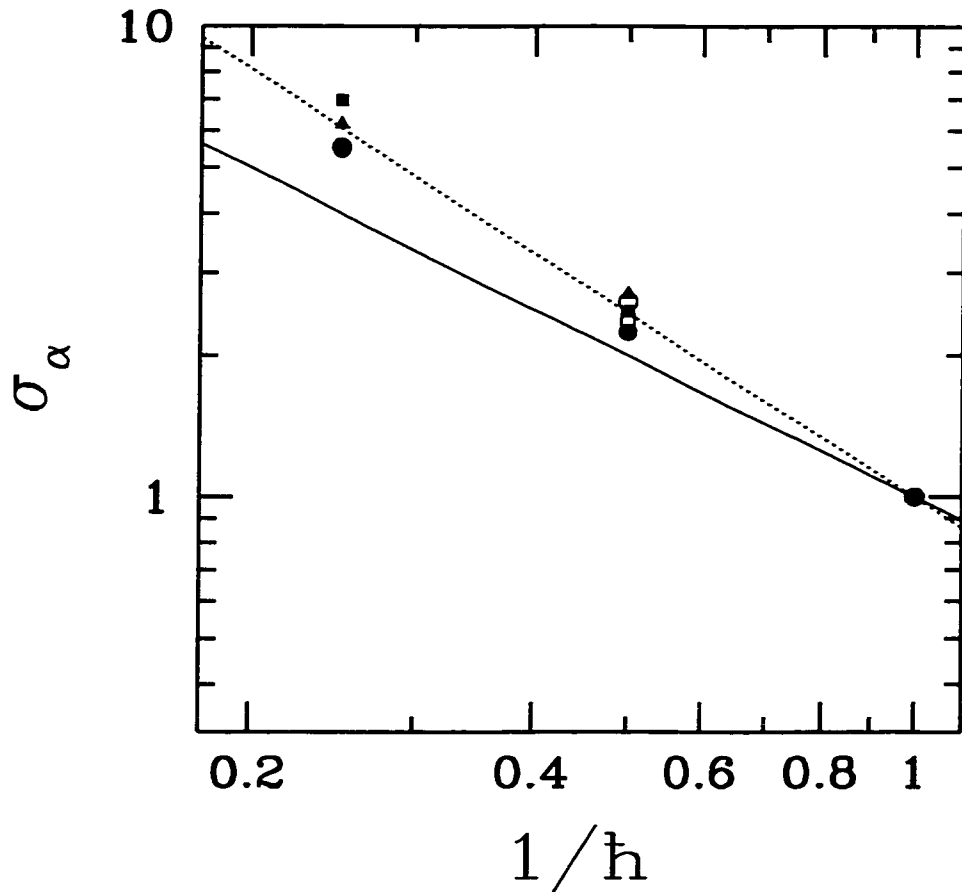


Figure 4.10: Root mean square of the overlap intensities as a function of  $1/\hbar$ . The wave packet was placed on the horizontal (solid circles), V (solid squares), diamond (solid triangles), rectangle (open circles) and bow tie (open squares) orbits. The solid line is the theoretical value of  $\hbar^{-1}$  from Section 4.4 and the dotted line is the best fit of the stadium results which is  $\hbar^{-1.3}$ . The intensities have been rescaled at  $\hbar = 1$  so that they occupy the same area of the plot.

Fig. (4.11). In fact, large correlations are found for nearly all the states in the stadium billiard which means that there exists phase space localization for most of the states. The large positive values of the correlation coefficient in the center of the figure again correspond to the bouncing ball states. Classically, this area of phase space is difficult to enter and leave. Hence, the localization is expected to be stronger for this area of phase space. The area beneath the peaks is several standard deviations ( $N^{-1/2} = (114)^{-1/2} \approx 0.09$ ) away from zero as predicted by random matrix theory. Thus, phase space localization is also occurring in this region. The point exactly in between the peaks is the point in phase space associated with the horizontal bounce. The series of smaller peaks leading up to the large peaks are the gateways into the vertical bouncing ball area. Fig. (4.12) is a plot of the orbits corresponding to these peaks. They are periodic orbits which only strike the endcaps twice and become almost vertical. Orbits must pass through these regions in order to enter or exit the vertical bounce states.

As the energy of the system is increased (i. e.  $\hbar$  is decreased), the results of the correlation function remain qualitatively the same, Fig. (4.13). All the peaks and valleys stay in the same place. The numerical results of the overlap correlation coefficient fluctuate depending upon the area of phase space being considered. This is consistent with the semiclassical theory in Section 4.4. More details of the system are explored as  $\hbar$  is decreased, since the phase space is divided into finer areas. Thus, more detailed information about the phase space localization of the system is observed in the overlap correlation coefficient at smaller values of  $\hbar$ .

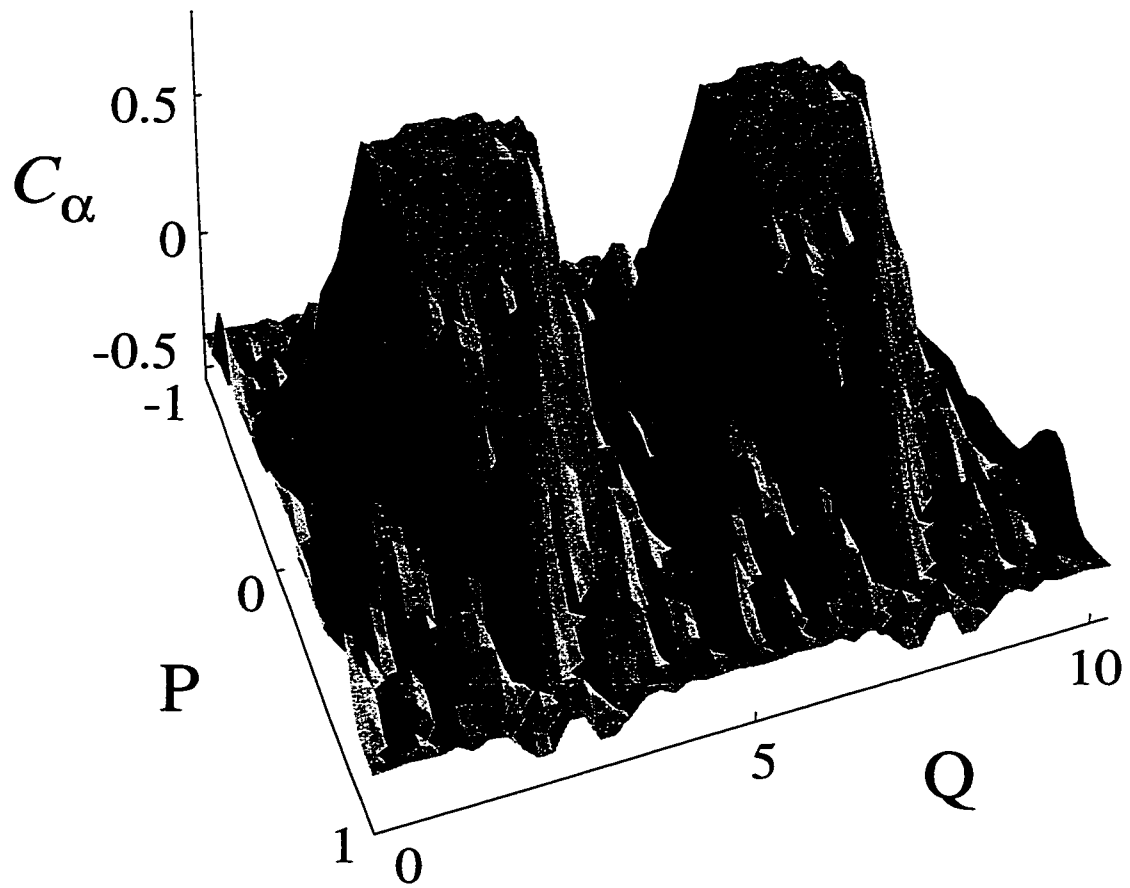


Figure 4.11: Overlap correlation coefficient for the stadium using Birkhoff coordinates. The energy range of the averaging is 2200-2600 where  $\hbar = m = 1$ .

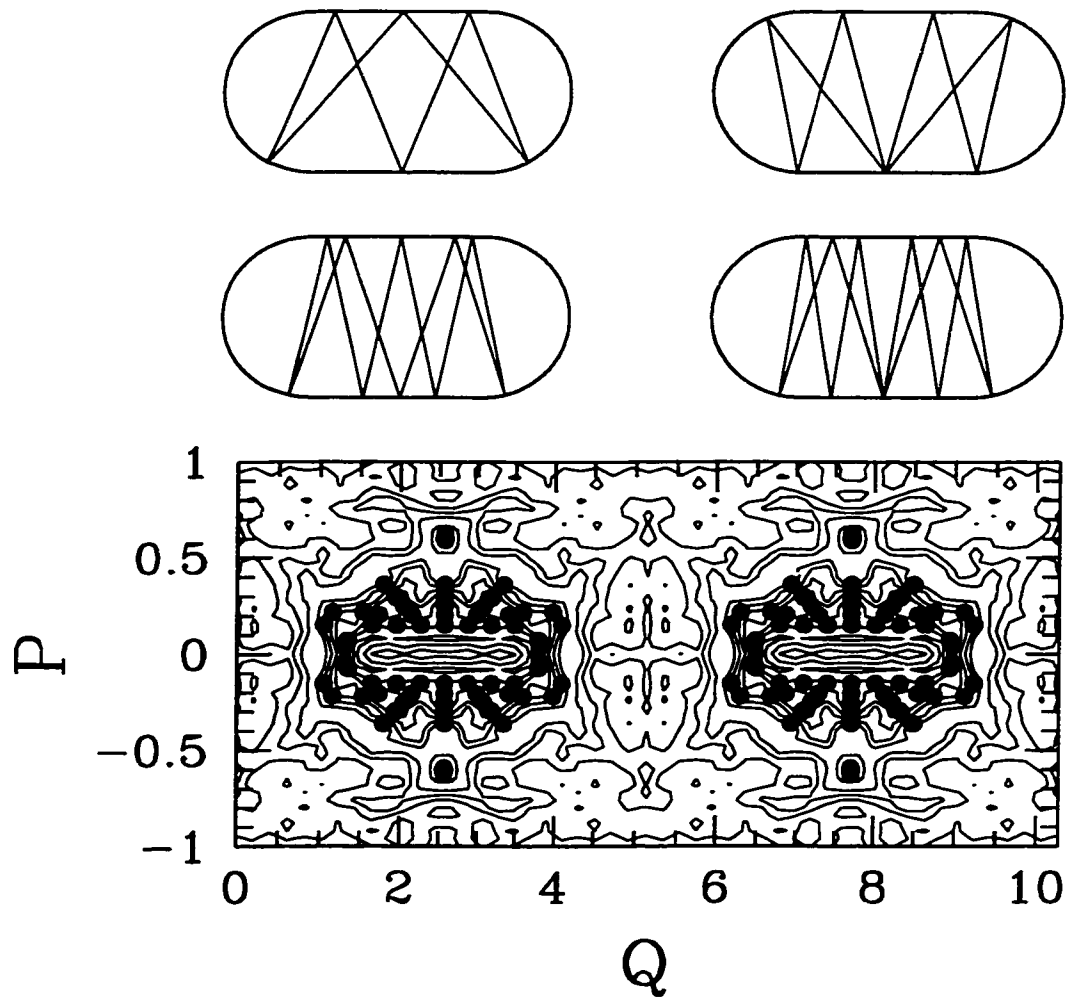


Figure 4.12: Trajectories corresponding to the peaks leading up to the bouncing ball orbits. The lower figure is a contour plot of Fig. (4.13). The solid circles correspond to the bounce points of the trajectories. Geometric and time-reversal symmetries were also included.

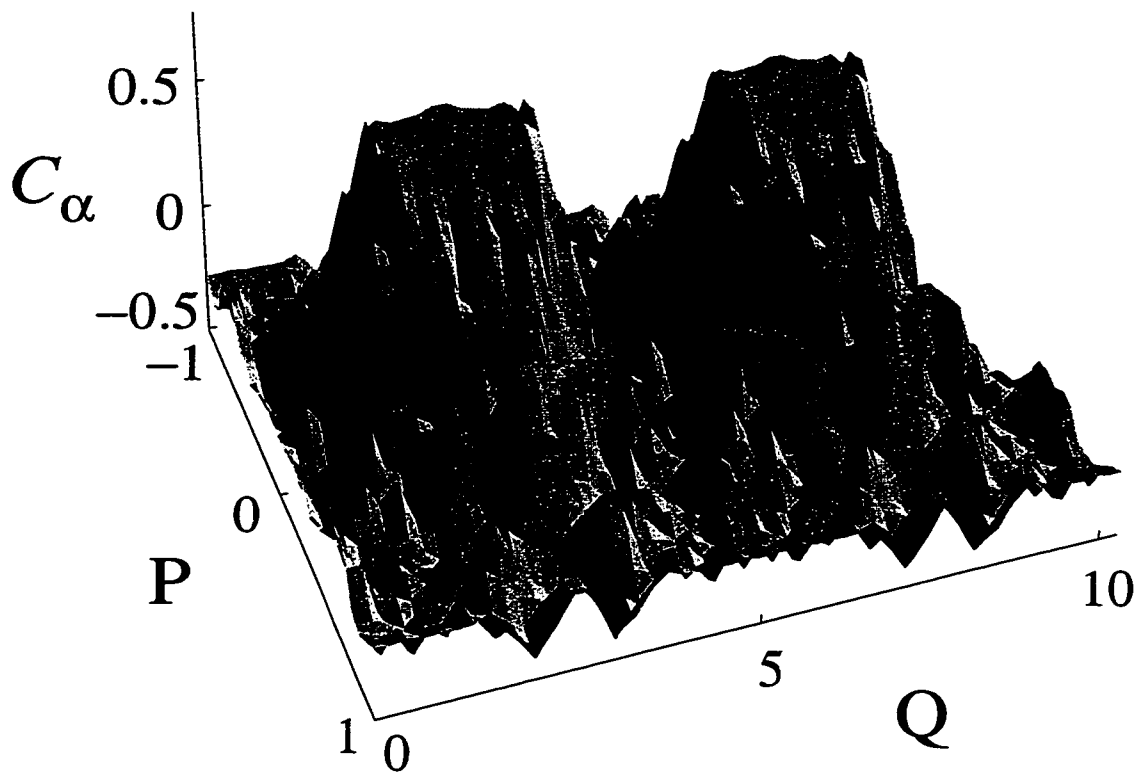


Figure 4.13: The same as Fig. (4.11) except for a higher energy range of 9200-10000 where  $\hbar = m = 1$ . Note the finer structure of the various peaks.



## 4.6 Conclusions

We have shown that intensity weighted level velocities are a good measure of the localization properties for chaotic systems. They are far more sensitive to localization than similarly weighted level curvatures (which are closely related to level statistics). Thus, a system can be RMT-like, yet the eigenstates are not behaving ergodically (as RMT predicts).

The stadium eigenstates show a great deal of localization. Not only are the vertical bouncing ball orbits predicted by the measure, but also other orbits. The overlap correlation coefficient is very parameter dependent. Choosing a different parameter to vary would highlight other sets of orbits depending on how strong the perturbation effects those orbits. The degree of localization can be predicted by the return dynamics. In a chaotic system, all the return dynamics can be organized by the homoclinic orbits. The manner in which a chaotic system's eigenstates approach ergodicity as  $\hbar \rightarrow 0$  will depend on a new time scale, i.e. that required for the homoclinic excursions to explore the available phase space fully.

Parametrically varied data exist that can be analyzed in this way. In the Coulomb-blockade conductance data to the extent that the resonance energy variations are related to a single particle level velocity (minus a constant charging energy and absent residual interaction effects) should show correlations. We mention also that the microwave cavity data can be studied with even more flexibility since they have measured the eigenstates and can therefore meticulously study a wide range of  $|\alpha\rangle$  to get a complete picture of the eigenstate localization properties.

Finally, this analysis could be applied in a very fruitful way to near-integrable and mixed

phase space systems. In these cases, standard random matrix theory would not give the zero<sup>th</sup> order statistical expectation, but the localization would still be determined by the return dynamics in the semiclassical approximation.

We gratefully acknowledge important discussions with B. Watkins and T. Nagano and support from the National Science Foundation under Grant No. NSF-PHY-9800106 and the Office of Naval Research under Grant No. N00014-98-1-0079.

## 4.A Gaussian Integration

Inserting Eq. (4.32) into Eq. (4.31), the strength function involves two  $N$ -dimensional integrals where  $N$  is the system's number of degrees of freedom,

$$S_{\alpha,osc}(E) = \frac{-1}{\pi} \text{Im} \frac{1}{i\hbar(2\pi i\hbar)^{(d-1)/2}} \left( \frac{1}{\pi\sigma^2} \right)^{d/2} \int \sum_j |D_s|^{1/2} \exp\{-i\mathbf{p}_\alpha \cdot (\mathbf{q} - \mathbf{q}')/\hbar - (\mathbf{q} - \mathbf{q}_\alpha)^2/2\sigma^2 - (\mathbf{q}' - \mathbf{q}_\alpha)^2/2\sigma^2 + iS_j(\mathbf{q}, \mathbf{q}'; E)/\hbar - i\nu'_j\pi/2\} d\mathbf{q}d\mathbf{q}' \quad (4.52)$$

To evaluate the integrals over  $\mathbf{q}$  and  $\mathbf{q}'$ , the action is quadratically expanded about the points  $\mathbf{q}_f$  and  $\mathbf{q}_i$ ,

$$\begin{aligned} S_j(\mathbf{q}, \mathbf{q}'; E) &= S_j(\mathbf{q}_f, \mathbf{q}_i; E) + \mathbf{p}_f \cdot (\mathbf{q} - \mathbf{q}_f) - \mathbf{p}_i \cdot (\mathbf{q}' - \mathbf{q}_i) \\ &\quad + \frac{1}{2} \sum_{i,k}^N \left[ \left( \frac{\partial p_f^{(i)}}{\partial q^{(k)}} \right)_{\mathbf{q}_f} (q^{(i)} - q_f^{(i)})(q^{(k)} - q_f^{(k)}) \right. \\ &\quad \left. - \left( \frac{\partial p_i^{(i)}}{\partial q'^{(k)}} \right)_{\mathbf{q}_i} (q'^{(i)} - q_i^{(i)})(q'^{(k)} - q_i^{(k)}) \right] \end{aligned}$$

$$+2 \left( \frac{\partial p_f^{(i)}}{\partial q'^{(k)}} \right)_{\mathbf{q}_i} (q^{(i)} - q_f^{(i)})(q'^{(k)} - q_i^{(k)}) \Big] \quad (4.53)$$

It is useful to define the vector

$$\mathbf{z} = (z_1, \dots, z_N, z'_1, \dots, z'_N) \quad (4.54)$$

where

$$\begin{aligned} z_i &= (q^{(i)} - q_f^{(i)})/\sigma \\ z'_i &= (q'^{(i)} - q_i^{(i)})/\sigma \end{aligned} \quad (4.55)$$

Thus, the integrals become

$$\begin{aligned} S_{\alpha,osc}(E) &= \frac{-1}{\pi} \text{Im} \frac{1}{i\hbar(2\pi i\hbar)^{(d-1)/2}} \left( \frac{1}{\pi\sigma^2} \right)^{d/2} \\ &\times \int \sum_j |D_s|^{1/2} \sigma^{2d} \exp\{-\mathbf{z} \cdot \mathbf{A} \cdot \mathbf{z} - \mathbf{b} \cdot \mathbf{z} + c\} d\mathbf{z} \end{aligned} \quad (4.56)$$

where  $\mathbf{A}$  is composed of four  $N$ -dimensional matrices

$$\mathbf{A} = \begin{pmatrix} \mathbf{A}^{11} & \mathbf{A}^{12} \\ \mathbf{A}^{21} & \mathbf{A}^{22} \end{pmatrix} \quad (4.57)$$

and

$$\mathbf{b} = \left( i\delta p_f^{(1)} - \delta q_f^{(1)}, \dots, i\delta p_f^{(N)} - \delta q_f^{(N)}, i\delta p_i^{(1)} - \delta q_i^{(1)}, \dots, i\delta p_i^{(N)} - \delta q_i^{(N)} \right) \quad (4.58)$$

with

$$\begin{aligned} \delta p_f^{(i)} &= (p_\alpha^{(i)} - p_f^{(i)})\sigma/\hbar \\ \delta p_i^{(i)} &= (p_\alpha^{(i)} - p_i^{(i)})\sigma/\hbar \\ \delta q_f^{(i)} &= (q_\alpha^{(i)} - q_f^{(i)})/\sigma \\ \delta q_i^{(i)} &= (q_\alpha^{(i)} - q_i^{(i)})/\sigma \end{aligned} \quad (4.59)$$

and

$$c = \frac{i}{\hbar} S_j(\mathbf{q}_f, \mathbf{q}_i; E) - \frac{i}{\hbar} \mathbf{p}_\alpha \cdot (\mathbf{q}_f - \mathbf{q}_i) - \frac{(\mathbf{q}_f - \mathbf{q}_\alpha)^2}{2\sigma^2} - \frac{(\mathbf{q}_i - \mathbf{q}_\alpha)^2}{2\sigma^2} - \frac{i\nu'_j\pi}{2} \quad (4.60)$$

The matrix  $\mathbf{A}$  can be expressed in terms of the stability matrix,  $\mathbf{M}$ , where  $\mathbf{M}$  has the same form as Eq. (4.57)

$$\begin{pmatrix} \mathbf{p} \\ \mathbf{q} \end{pmatrix} = \mathbf{M} \begin{pmatrix} \mathbf{p}' \\ \mathbf{q}' \end{pmatrix} \quad (4.61)$$

Thus,

$$\mathbf{A}_{ab}^{11} = \frac{\delta_{a,b}}{2} - \frac{i\sigma^2}{2\hbar} \left( \frac{\partial p_f^{(a)}}{\partial q^{(b)}} \right)_{\mathbf{q}_f} = \frac{\delta_{a,b}}{2} - \frac{i\sigma^2 \sum_i^N m_{a,i} \text{cof}(\mathbf{M}_{b,i}^{21})}{2\hbar \det \mathbf{M}^{21}} = \frac{\mathbf{I}}{2} - \frac{i\sigma^2}{2\hbar} \mathbf{M}^{11} (\mathbf{M}^{21})^{-1}$$

$$\begin{aligned}
\mathbf{A}_{ab}^{12} &= -\frac{i\sigma^2}{2\hbar} \left( \frac{\partial p_f^{(a)}}{\partial q'^{(b)}} \right)_{\mathbf{q}_i} = \frac{i\sigma^2 \operatorname{cof}(\mathbf{M}_{b,a}^{21})}{2\hbar \det \mathbf{M}^{21}} = \frac{i\sigma^2}{2\hbar} ((\mathbf{M}^{21})^{-1})^T \\
\mathbf{A}_{ab}^{21} &= \frac{i\sigma^2}{2\hbar} \left( \frac{\partial p_i^{(a)}}{\partial q^{(b)}} \right)_{\mathbf{q}_f} = \frac{i\sigma^2 \operatorname{cof}(\mathbf{M}_{a,b}^{21})}{2\hbar \det \mathbf{M}^{21}} = \frac{i\sigma^2}{2\hbar} (\mathbf{M}^{21})^{-1} \\
\mathbf{A}_{ab}^{22} &= \frac{\delta_{a,b}}{2} + \frac{i\sigma^2}{2\hbar} \left( \frac{\partial p_i^{(a)}}{\partial q'^{(b)}} \right)_{\mathbf{q}_i} = \frac{\delta_{a,b}}{2} - \frac{i\sigma^2 \sum_i^N m_{i+N,b+N} \operatorname{cof}(\mathbf{M}_{i,a}^{21})}{2\hbar \det \mathbf{M}^{21}} \\
&= \frac{\mathbf{I}}{2} - \frac{i\sigma^2}{2\hbar} (\mathbf{M}^{21})^{-1} \mathbf{M}^{22}
\end{aligned} \tag{4.62}$$

where  $m_{i,k}$  are elements of the stability matrix and  $\operatorname{cof}(\mathbf{M}_{ik}^{21})$  is the signed minor of  $\mathbf{M}_{ik}^{21}$ .

$D_s$  is a determinate involving second derivatives of the actions,

$$\begin{aligned}
D_s &= \begin{vmatrix} \frac{\partial^2 S}{\partial \mathbf{q} \partial \mathbf{q}'} & \frac{\partial^2 S}{\partial \mathbf{q} \partial E} \\ \frac{\partial^2 S}{\partial E \partial \mathbf{q}'} & \frac{\partial^2 S}{\partial E^2} \end{vmatrix} = \frac{1}{|\dot{q}^{(N)}| |\dot{q}'^{(N)}|} \left| \frac{-\partial^2 S}{\partial \bar{\mathbf{q}} \partial \bar{\mathbf{q}}'} \right| \\
&= \frac{1}{|\dot{q}^{(N)}| |\dot{q}'^{(N)}|} \left( \frac{2\hbar}{i\sigma^2} \right)^{(d-1)} |\tilde{\mathbf{A}}^{21}|
\end{aligned} \tag{4.63}$$

The tildes in the determinants in the above equation are used to exclude the  $N$ th coordinate.

To obtain the above result  $q^{(N)}$  and  $q'^{(N)}$  are chosen to be locally oriented along the trajectory where the dots indicate time derivatives. Since  $\mathbf{A}$  is a symmetric matrix, the result for a general Gaussian integral is used and, hence, the strength function becomes

$$\begin{aligned}
S_{\alpha,osc}(E) &= \frac{-1}{\pi} \operatorname{Im} \frac{1}{i\hbar (2\pi i\hbar)^{(d-1)/2}} \left( \frac{\sigma^2}{\pi} \right)^{d/2} \left( \frac{2\hbar}{i\sigma^2} \right)^{(d-1)/2} \sum_j \left( \frac{\pi^{2d}}{\det \mathbf{A}} \right)^{1/2} \\
&\quad \times \left( \frac{1}{|\dot{q}^{(N)}| |\dot{q}'^{(N)}|} \right)^{1/2} |\tilde{\mathbf{A}}^{21}|^{1/2} \exp \left\{ \frac{1}{4} \mathbf{b} \cdot \mathbf{A}^{-1} \cdot \mathbf{b} + c \right\}
\end{aligned}$$

$$= \frac{\sigma}{\pi^{1/2}\hbar} \text{Re} \sum_j \left( \frac{\det \tilde{\mathbf{A}}^{21}}{\det \mathbf{A}} \right)^{1/2} \left( \frac{1}{|\dot{q}^{(N)}| |\dot{q}'^{(N)}|} \right)^{1/2} \exp \left\{ \frac{1}{4} \mathbf{b} \cdot \mathbf{A}^{-1} \cdot \mathbf{b} + c \right\} \quad (4.64)$$

where the time derivatives are evaluated at the saddle points.

## 4.B Sum Rule for the Strength Function

The determinant of the  $(2N \times 2N)$  matrix  $\mathbf{A}$ ,

$$\det \mathbf{A} = \det \begin{pmatrix} \frac{1}{2} - \frac{i\sigma^2}{2\hbar} \mathbf{M}^{11} (\mathbf{M}^{21})^{-1} & \frac{i\sigma^2}{2\hbar} ((\mathbf{M}^{21})^{-1})^T \\ \frac{i\sigma^2}{2\hbar} (\mathbf{M}^{21})^{-1} & \frac{1}{2} - \frac{i\sigma^2}{2\hbar} (\mathbf{M}^{21})^{-1} \mathbf{M}^{22} \end{pmatrix} \quad (4.65)$$

can be reduced to determinants of  $(N \times N)$  matrices by using the relation  $((\mathbf{M}^{21})^{-1})^T = -\mathbf{M}^{12} + \mathbf{M}^{11} (\mathbf{M}^{21})^{-1} \mathbf{M}^{22}$  and some row and column manipulations [51], so that

$$\det \mathbf{A} = \det \left( \frac{-i\sigma^2}{4\hbar} \left[ \mathbf{M}^{11} + \mathbf{M}^{22} + i \left( \frac{\hbar}{\sigma^2} \mathbf{M}^{21} - \frac{\sigma^2}{\hbar} \mathbf{M}^{12} \right) \right] \right) / \det(\mathbf{M}^{21}) \quad (4.66)$$

The coordinates parallel to the trajectory do not mix with the transverse coordinates, since a point on an orbit will remain on that particular orbit. Thus, the  $N$ th rows and columns of the individual matrices in the above expression are zero except for the  $(N, N)$  elements.

It is convenient to re-express the submatrices of the stability matrix in terms of the Lyapunov exponents. Let  $\{\lambda_i\}$  be the set of Lyapunov exponents whose real part is positive ordered such that  $\lambda_1 > \lambda_2 > \dots > \lambda_{N-1}$ . The Lyapunov exponents along the parallel coordinate are zero and we will only work with the reduced  $(2(N-1) \times 2(N-1))$  stability

matrix in what follows. Let  $\Lambda$  be the diagonal matrix of the eigenvalues of the reduced stability matrix,

$$\Lambda = \begin{pmatrix} e^{\lambda_1 t} & \dots & 0 & 0 & \dots & 0 \\ \vdots & & \vdots & \vdots & & \vdots \\ 0 & \dots & e^{\lambda_{N-1} t} & 0 & \dots & 0 \\ 0 & \dots & 0 & e^{-\lambda_1 t} & \dots & 0 \\ \vdots & & \vdots & \vdots & & \vdots \\ 0 & \dots & 0 & 0 & \dots & e^{-\lambda_{N-1} t} \end{pmatrix} \quad (4.67)$$

Thus, by a similarity transform the reduced stability matrix can be written in terms of the Lyapunov exponents, i.e.

$$\mathbf{M} = \mathbf{L}\Lambda\mathbf{L}^{-1} \quad (4.68)$$

Hence, each of the elements of the stability matrix can be written as

$$m_{ij} = \sum_k^N a_{ij}^{(k)} e^{\lambda_k t} + b_{ij}^{(k)} e^{-\lambda_k t} \quad (4.69)$$

where  $a_{ij}^{(k)}$  and  $b_{ij}^{(k)}$  are linear combinations of the elements of the  $\mathbf{L}$  and  $\mathbf{L}^{-1}$  matrices. Because in general chaotic systems  $\lambda \gg 0$ , the  $b_{ij}^{(k)}$ 's may be omitted without seriously affecting the above sum. All the determinants including the numerator and denominator of  $\det \mathbf{A}$  as well as  $\det \tilde{\mathbf{A}}^{21}$ , thus, will involve products of Eq. (4.69). The homoclinic orbits in the sum begin and end at the intersections of the stable and unstable manifolds near the Gaussian centroid. Since neither manifolds may cross themselves, then in the vicinity of the

Gaussian centroid the branches of each manifold are nearly parallel to themselves. Thus, to an excellent approximation, the same similarity transformation will diagonalize the stability matrix for each individual orbit, regardless of the period. Consequently, the elements of  $\mathbf{L}$  and  $\mathbf{L}^{-1}$  are period independent.

Connections can be made between the determinants and the Kolmogorov-Sinai entropy. The Kolmogorov-Sinai entropy,  $h_{KS}$ , of a system can be expressed using Pesin's Theorem as the sum of the Lyapunov exponents with positive real part,

$$h_{KS} = \sum_i^{N-1} \lambda_i \quad (4.70)$$

If there is no mixing between the different coordinates, then the individual matrices  $\mathbf{M}^{11}$ ,  $\mathbf{M}^{12}$ ,  $\mathbf{M}^{21}$  and  $\mathbf{M}^{22}$  are diagonal. Thus, each matrix element depends only upon one Lyapunov exponent and the determinants are proportional to  $\exp(-h_{KS}t)$ . This is the case for two dimensional systems where the parallel and perpendicular coordinates in the stability matrix separate as mentioned above. Hence, we have

$$\left| \frac{\det \tilde{\mathbf{A}}^{21}}{\det \mathbf{A}} \right| \propto \exp(-h_{KS}t) \quad (4.71)$$

Unlike the periodic orbits, the homoclinic sum is over segments of the orbits. The number of homoclinic points will proliferate exponentially at the same rate as the fixed points in the neighborhood which is proportional to  $\exp(h_T T)$  where  $h_T$  is the topological entropy. This is demonstrated by examining the partitioning of the phase space mentioned in Sect. 4.4.2



which has exponential growth. The partitioning reflects the symbolic dynamics of the system. The symbolic code uniquely describes each orbit so that amount of code (partitions) cannot grow faster than the number of periodic points, since each code (partition) cannot represent more than one periodic point.

Finally, the sum rule is obtained by setting the topological entropy and Kolmogorov-Sinai entropy equal to each other. Then, for the special case of no mixing in the stability matrix as mentioned above the combination of the amplitudes and the number of orbits yields

$$\sum_j \left| \frac{\det \tilde{\mathbf{A}}^{21}}{\det \mathbf{A}} \right| \dots \rightarrow \int dT \dots \quad (4.72)$$

## References

- [1] A. Einstein, Verh. Deutsch. Phys. Ges. Berlin **19**, 82 (1917); English translation by C. Jaffe, JILA rep. No. 116.
- [2] S. Tomsovic and E. J. Heller, Phys. Rev. Lett. **70**, 1405 (1993).
- [3] M. V. Berry, J. Phys. A: Math. Gen. **10**, 2083 (1977).
- [4] A. Voros, in *Stochastic Behavior in Classical and Quantum Hamiltonian Systems*, eds. G. Casati and G. Ford, Lecture Notes in Physics **93**, (Springer, Berlin, 1979) p. 326.
- [5] P. O'Connor, J. Gehlen, and E. J. Heller, Phys. Rev. Lett. **58**, 1296 (1987).
- [6] S. Hortikar and M. Srednicki, Phys. Rev. Lett. **80**, 1646 (1998).
- [7] A. M. Chang, H. U. Baranger, L. N. Pfeiffer, and K. W. West, Phys. Rev. Lett. **73**, 2111 (1994); M. R. Haggerty, N. Spellmeyer, D. Kleppner, and J. B. Delos, Phys. Rev. Lett. **81**, 1592 (1998); C. M. Marcus, A. J. Rimberg, R. M. Westervelt, P. F. Hopkins, and A. C. Gossard, Phys. Rev. Lett. **69**, 506 (1992).
- [8] H. U. Baranger and P. A. Mello, Phys. Rev. Lett. **73**, 142 (1994); C. W. J. Beenakker, Rev. Mod. Phys. **69**, 731 (1997); A. M. Chang, H. U. Baranger, L. N. Pfeiffer,

- K. W. West, and T. Y. Chang, Phys. Rev. Lett. **76**, 1695 (1996); J. A. Folk, S. R. Patel, S. F. Godijn, A. G. Huibers, S. M. Cronenwett, C. M. Marcus, K. Campman, and A. C. Gossard, Phys. Rev. Lett. **76**, 1699 (1996).
- [9] B. D. Simons, P. A. Lee, and B. L. Altshuler, Phys. Rev. Lett. **70**, 4122 (1993).
- [10] Y. Alhassid and H. Attias, Phys. Rev. Lett. **74**, 4635 (1995).
- [11] M. L. Mehta, *Random Matrices*, 2<sup>nd</sup> ed., (Academic Press, Boston, 1991).
- [12] O. Bohigas, M.-J. Giannoni, and C. Schmit, Phys. Rev. Lett. **52**, 1 (1984); J. Physique Lett. **45**, 1015 (1984).
- [13] A. V. Andreev, O. Agam, B. D. Simons, and B. L. Altshuler, Phys. Rev. Lett. **76**, 3947 (1996).
- [14] S. W. McDonald, Ph. D. dissertation, University of California, Berkeley, Lawrence Berkeley Laboratory Report No. LBL-14837 (1983).
- [15] E. J. Heller, Phys. Rev. Lett. **53**, 1515 (1984).
- [16] O. Bohigas, S. Tomsovic, and D. Ullmo, Phys. Rep. **223**, 43 (1993).
- [17] R. S. McKay and J. D. Meiss, Phys. Rev. A **37**, 4702 (1988).
- [18] R. Ketzmerick, G. Petschel, and T. Geisel, Phys. Rev. Lett. **69**, 695 (1992).
- [19] S. Fishman, D. R. Grempel, and R. E. Prange, Phys. Rev. A **36**, 289 (1987).
- [20] L. Kaplan and E. J. Heller, Ann. Phys. **264**, 171 (1998).

- [21] S. Tomsovic and E. J. Heller, Phys. Rev. Lett. **67**, 664 (1991); Phys. Rev. E **47**, 282 (1993); Physics Today **46** (7), 38 (1993); P. W. O'Connor, S. Tomsovic and E. J. Heller, Physica D **55**, 340 (1992).
- [22] S. Tomsovic, Phys. Rev. Lett. **77**, 4158 (1996).
- [23] A. Lakshminarayan, N. R. Cerruti and S. Tomsovic, submitted to Phys. Rev. E.
- [24] B. D. Simons, A. Szafer, and B. L. Altshuler, JETP Lett. **57**, 277 (1993).
- [25] B. Mehlig and K. Muller, preprint.
- [26] B. D. Simons and B. L. Altshuler, Phys. Rev. B **48**, 5422 (1993).
- [27] P. Gaspard, S. A. Rice, H. J. Mikeska and K. Nakamura, Phys. Rev. A **42**, 4015 (1990).
- [28] J. Zakrzewski and D. Delande, Phys. Rev. E **47**, 1650 (1993).
- [29] F. von Oppen, Phys. Rev. E **51**, 2647 (1995); Phys. Rev. Lett. **73**, 798 (1994).
- [30] J. Zakrzewski, D. Delande, and M. Kus, Phys. Rev. E **47**, 1665 (1993).
- [31] M. Wilkinson, J. Phys. A **22**, 2795 (1989).
- [32] E. K. Riedel and F. von Oppen, Phys. Rev. B **47**, 15449 (1993).
- [33] A. M. Lane and R. G. Thomas, Rev. Mod. Phys. **30**, 257 (1958).
- [34] S. Tomsovic and J. H. Lefebvre, Phys. Rev. Lett. **79**, 3629 (1997).
- [35] M. V. Berry and J. P. Keating, J. Phys. A: Math. Gen. **27**, 6167 (1994).

- [36] P. Leboeuf and M. Sieber, *Phys. Rev. E* **60**, 3969 (1999).
- [37] A. M. Ozorio de Almeida, *Hamiltonian Systems: Chaos and Quantization*, Cambridge University Press, (1988).
- [38] J. H. Hannay and A. M. Ozorio de Almeida, *J. Phys. A: Math. Gen.* **17**, 3429 (1984).
- [39] Originally published by E. B. Bogomolny and J. P. Keating, *Phys. Rev. Lett.* **77**, 1472 (1996), but more details are given in A. M. Ozorio de Almeida, C. H. Lewenkopf and E. R. Mucciolo, *Phys. Rev. E* **58**, 5693 (1998).
- [40] O. Bohigas, M. J. Giannoni, A. M. Ozorio de Almeida and C. Schmit, *Nonlinearity* **8**, 203 (1995).
- [41] J. Goldberg, U. Smilansky, M. V. Berry, W. Scheizer, G. Wunner and G. Zeller, *Nonlinearity* **4**, 1 (1991).
- [42] A. Lakshminarayan, N. R. Cerruti and S. Tomsovic, *Phys. Rev. E* **60**, 3992 (1999).
- [43] B. Eckhardt, S. Fishman, K. Muller and D. Wintgen, *Phys. Rev. A* **45**, 3531 (1992).
- [44] M. V. Berry, *Proc. R. Soc. Lond. A* **423**, 219 (1989).
- [45] E. J. Heller, in *Chaos and Quantum Physics*, eds. M. J. Giannoni, A. Voros and J. Zinn-Justin (Elsevier, Amsterdam, 1991).
- [46] J. Moser, *Commun. Pure and Appl. Math* **IX**, 673 (1956); G. L. da Silva Ritter, A. M. Ozorio de Almeida and R. Douady, *Physica D* **29**, 181 (1987).

- [47] A. M. Ozorio de Almeida, *Nonlinearity* **2**, 519 (1989).
- [48] L. A. Bunimovich, *Funct. Anal. Appl.* **8**, 254 (1974); *Commun. Math. Phys.* **65**, 295 (1979).
- [49] E. B. Bogomolny, *Nonlinearity* **5**, 805 (1992).
- [50] M. Sieber, U. Smilansky, S. C. Creagh and R. G. Littlejohn, *J. Phys. A: Math. Gen.* **26**, 6217 (1993).
- [51] M. C. Gutzwiller, *J. Math. Phys.* **12**, 343 (1971).

## Chapter 5

# Phase Space Localization of Chaotic Eigenstates: Violating Ergodicity

By Arul Lakshminarayan,<sup>1,2</sup> Nicholas R. Cerruti<sup>1</sup> and Steven Tomsovic<sup>1</sup>

<sup>1</sup>Department of Physics, Washington State University,

Pullman, Washington 99164-2814

<sup>2</sup>Physical Research Laboratory, Navrangpura, Ahmedabad 380 009, India

Physical Review E **63** (2001) (to be published)

Copyright 2001 by the American Physical Society.

### 5.0 Abstract

The correlation between level velocities and eigenfunction intensities provides a new way of exploring phase space localization in quantized non-integrable systems. It can also serve as a measure of deviations from ergodicity due to quantum effects for typical observables. This paper relies on two well known paradigms of quantum chaos, the baker's map and the standard map, to study correlations in simple, yet chaotic, dynamical systems. The behaviors are dominated by the presence of several classical structures. These primarily include short periodic orbits and their homoclinic excursions. The dependences of the correlations deriving

from perturbations allow for eigenfunction features violating ergodicity to be selectively highlighted. A semiclassical theory based on periodic orbit sums leads to certain classical correlations that are super-exponentially cut off beyond a logarithmic time scale. The theory is seen to be quite successful in reproducing many of the quantum localization features.

## 5.1 Introduction

For a bounded, classically chaotic system, ergodicity is defined with respect to the energy surface, the only available invariant space of finite measure. In an extension developed just over twenty years ago, the consequences of ergodicity for the eigenstates of a corresponding quantum system were conjectured to give rise to a locally, Gaussian random behavior [1, 2]. Shortly thereafter, work ensued on defining the concept of eigenstate ergodicity within a more rigorous framework [3]. Some of the paradoxes and peculiarities have been recently explored as well [4]. One expression of eigenstate ergodicity is that a typical eigenstate would fluctuate over the energy surface, but otherwise be featureless, in an appropriate pseudo-phase-space representation such as the Wigner transform representation [5]. Any statistically significant deviation from ergodicity in individual eigenstates is termed phase space localization.

It came as a surprise when Heller discovered eigenstates were “scarred” by short, unstable periodic orbits [6, 7]. A great deal of theoretical and numerical research followed [8–13], and experiments also [14, 15]. In fact, scarring is just one of the means by which phase space localization can exist in the eigenstates of such systems. Another means would be localizing effects due to transport barriers such as cantori [16, 17] or broken separatrices [18].



Despite these studies and the semiclassical construction of an eigenstate [19], the properties of individual eigenstates remain somewhat a mystery.

Individual eigenfunctions may not be physically very relevant in many situations, especially those involving a high density of states. In this case, groups of states contribute towards localization in ways that may be understood with available semiclassical theories. One simple and important quantity where this could arise is the time average of an observable as this is a weighted sum of several (in principle all) eigenfunctions. In the Heisenberg picture, where the operator is evolving in time, the expectation value of the observable could be measured with any state. Phase space localization features would be especially evident if this state were chosen to be a wave packet well localized in such spaces.

In a system with a non-degenerate spectrum the time average of an observable  $\hat{A}$  in state  $|\alpha\rangle$  is

$$\langle \hat{A}(t) \rangle_t = \langle \langle \alpha | e^{i\hat{H}t/\hbar} \hat{A} e^{-i\hat{H}t/\hbar} | \alpha \rangle \rangle_t = \sum_n |\langle \alpha | \psi_n \rangle|^2 \langle \psi_n | \hat{A} | \psi_n \rangle, \quad (5.1)$$

where  $|\psi_n\rangle$  are the eigenstates of the Hamiltonian  $\hat{H}$ . Since experimental data exist, it is convenient to study systems that depend upon a parameter  $\lambda$  which varies continuously. The parameter may include electro-magnetic fields, temperatures, applied stresses, changing boundary conditions, etc. The Hamiltonian can be rewritten to first order as  $\hat{H}(\lambda) = \hat{H}_0 + \lambda \hat{A}$  where  $\hat{A} = \partial \hat{H}(\lambda) / \partial \lambda$ . Using the so called Hellmann-Feynman theorem (for instance [20]):

$$\langle \psi_n | \hat{A} | \psi_n \rangle = \langle \psi_n | \frac{\partial \hat{H}}{\partial \lambda} | \psi_n \rangle = \frac{\partial E_n}{\partial \lambda}. \quad (5.2)$$

$\partial E_n / \partial \lambda$  is defined as an energy level “velocity” for the  $n^{\text{th}}$  level (velocity is a bit of a misnomer for it is actually just a slope - we are not evolving the system parameter in time). Hence, for our specific choice of  $\hat{A}$  we are examining correlations between level velocities and wavefunction intensities, but Eq. (5.1) is applicable to more general observables.

One of us has already studied the correlation between level velocities and wavefunction intensities in connection with localization [21]. This can be directly connected to the issues raised above, and our treatment thus extends the previous work. The present paper is a companion to a study of similar problems in continuous Hamiltonian systems (as opposed to Hamiltonian maps, i.e. discrete time systems) and billiards [22]. The methods used in these two papers complement each other and the results in the present paper are detailed as the systems studied are much simpler. The companion paper contains a review of the general theories of the level velocities and wavefunction intensities and also gives relevant discussions pertaining to how these quantities demonstrate localization. It must be noted that while we call the operator average Eq. (5.1) a “correlation” it is not the true correlation that is obtained by dividing out the rms values of the wavefunction intensities and the operator expectation value (as defined in [21]). In other words we are going to study the covariance rather than the correlation. This is followed in this paper for two reasons; first, dividing out these quantities does not retain the meaning of the time average of an observable and second, the root mean square of the wavefunction intensities which is essentially the inverse participation ratio in phase space is itself a fairly complex quantity reflecting on phase-space localization.

Thus, the correlation introduced in [21] is:

$$C_A(\alpha) \equiv \langle \hat{A}(t) \rangle_t \quad (5.3)$$

with  $\hat{A} = \partial \hat{H} / \partial \lambda$ . The state  $|\alpha\rangle$  represents a wave packet that is well localized in the  $(q, p)$  coordinates [12, 23]. We will be interested in the quantum effects over and above the classical limit and we will require that the operator is traceless. Otherwise we will need to subtract the uncorrelated product of the averages of the eigenfunctions (unity) and the trace of the operator. This immediately also implies that the correlation according to Random Matrix Theory (RMT) [24] is zero as well. The ensemble average of  $C_A(\alpha)$  will wash out random oscillations that are a characteristic of the Gaussian distributed eigenfunctions of the random matrices. Specific localization properties that we will discuss are then not part of the RMT models of quantized chaotic systems. In the framework of level velocities, we are considering the situation where the average level velocity is zero, *i.e.*, there is no net drift of the levels.

A physically less transparent identity that is nevertheless useful in subsequent evaluations is:

$$C_A(\alpha) = \langle \langle \alpha | e^{-i\hat{H}t/\hbar} | \alpha \rangle \text{Tr} \left( \hat{A} e^{i\hat{H}t/\hbar} \right) \rangle_t \quad (5.4)$$

This may be written more symmetrically as

$$C_A(\alpha) = \langle \text{Tr} \left( |\alpha\rangle \langle \alpha| e^{-i\hat{H}t/\hbar} \right) \text{Tr} \left( \hat{A} e^{i\hat{H}t/\hbar} \right) \rangle_t \quad (5.5)$$

Thus, the correlation is a sort of time evolved average correlation between the two operators

$\hat{A}$  and  $|\alpha\rangle\langle\alpha|$ . The semiclassical expressions for these are however different as complications arise from the classical limit of  $|\alpha\rangle\langle\alpha|$  which would be varying over scales of  $\hbar$  that govern the validity of the stationary phase approximations. However, we may anticipate, based on the last form, that the semiclassical expression would be roughly the correlations of the classical limits of these two operators [25].

The classical dynamical systems that are investigated here are discrete maps on the dimensionless unit two-torus whose cyclical coordinates are denoted  $(q, p)$ . The first part of the paper explores the correlation in the bakers map, while the latter involves the standard map. The bakers map is the simpler of the two and a complete semiclassical evaluation of the correlation is given. This allows us to connect the observed localization with classical features of the map. On the other hand, the standard map is more complex. It has a continuous parameter whose variation takes the map through a transition from integrable to chaotic dynamics. Such a system is more typical and we are able to comment on some of the difficulties of such systems. Nevertheless, with some simple approximations the standard map demonstrates the same general features as the bakers map in its chaotic regime. We also compare quantum results with the semiclassical theory in its transitional regime.

## 5.2 The bakers map

### 5.2.1 Semiclassical Evaluation

The bakers map is a very attractive system to study the quantities discussed in the introduction. The classical dynamics is particularly simple (it is sometimes referred to as the “harmonic oscillator of chaos”). A simple quantization is due to Balazs and Voros [26] (where a discussion of the classical dynamics may also be found). As a model of quantum chaos it shows many generic features including the one central to this study namely scarring localization of eigenfunctions [12]. There are detailed semiclassical theories that have been verified substantially [23, 27–29]. We neglect certain anomalous features of the quantum bakers map [27, 29] that would eventually show up in the classical limit. This is reasonable in the range of scaled Planck constant values we have used in the following.

We use the second time averaged expression, Eq. (5.4), for the correlation. We do not repeat here details of the quantization of the bakers map or the semiclassical theories of this operator except note that we use the anti-periodic boundary conditions as stipulated by Saraceno [12] in order to retain fully the classical symmetries.

For the bakers map (and other maps as well), the quantum kinematics are set in a space of dimension  $N$  [26, 30, 31] where this is related to the scaled Planck constant as  $N = 1/h$ , and the classical limit is the large  $N$  limit. The quantum dynamics are specified by a unitary operator  $U$  (quantum map) that propagates states by one discrete time step. The quantum stationary states are the eigensolutions of this “propagator”. The  $N$  eigenfunctions and

eigenangles are denoted by  $\{|\psi_i\rangle, \phi_i; i = 0, \dots, N - 1\}$ . The eigenvalues lie on the unit circle and are members of the set  $\{\exp(-i\phi_i) i = 0, \dots, N - 1\}$ .

The semiclassical theory of the bakers map deals with the powers of the propagator. The trace of  $U^n$ , the time  $n$  propagator, has been written in the canonical form of a sum over classical hyperbolic periodic orbits with the phases being actions and the amplitudes relating to the linear stability of the orbits. The complications with Maslov phases is absent here [27, 28]. Also, the semiclassical expressions have been derived for matrix elements of the time  $n$  propagator in the wave packets basis [23]. The time domain dominates the study of the quantum maps, the Fourier transform to the spectrum being done exactly. Our approach to the correlation is then naturally built in the time domain. The situation is different in the case of Hamiltonian time independent flows where the energy domain is very useful.

We use the semiclassical expression for the propagator diagonal matrix elements derived in [23]:

$$\langle \alpha | U^n | \alpha \rangle \sim \sum_{\gamma} \frac{\exp(iS_{\gamma}/\hbar)}{\sqrt{\cosh(\lambda n)}} \sum_j \exp \left[ -\frac{\cosh(n\lambda) - 1}{2 \cosh(n\lambda) \hbar} (\delta q^2 + \delta p^2) - \frac{i\delta q \delta p}{\hbar} \tanh(n\lambda) \right]. \quad (5.6)$$

Here  $\gamma$  labels periodic orbits of period  $n$  including repetitions. The Lyapunov exponent is  $\lambda$  which is  $\ln(2)$  for the usual bakers map (corresponding to the  $(1/2, 1/2)$  partition and Bernoulli process). Also  $\hbar = h/(2\pi) = 1/(2\pi N)$ ,  $\delta q = q_j - q_{\alpha}$  and a similar relation for  $p$ . The position of  $j$ -th periodic point on the periodic orbit  $\gamma$  is  $(q_j, p_j)$ . The centroids of the wave packets, assumed circular Gaussians, are  $(q_{\alpha}, p_{\alpha})$ . The choice of type of wave packets is not crucial for the features we seek. We note that the simplicity of this expression for

the propagator derives from the simplicity of the classical bakers map, especially the fact that the stable and unstable manifolds are everywhere aligned with the  $(q, p)$  axes. That Eq. (5.6) happens to be a periodic orbit sum differs from the similar treatment for billiards as found in [32] where such sums are treated as homoclinic orbit sums. Note however, that the local linearity of the bakers map renders the two approaches (periodic orbit, homoclinic orbit) equivalent.

A generalization of the trace formula for the propagator is given below that is easily derived by the usual procedure employed for the propagator itself [28]. Such a formula was derived in [33] for the case of Hamiltonian flows in the energy domain. We make the simplifying assumption that the operator  $\hat{A}$  is diagonal in the position representation (we could treat the case of  $\hat{A}$  being diagonal in momentum alone as well). This avoids the problem of a Weyl-Wigner association of operators to functions on the torus. The quantum operator  $\hat{A}$  under this simplifying assumption has an obvious classical limit and associated function which is denoted by  $A(q)$ . The other major assumption used in deriving the formula below is that it does not vary on scales comparable to or smaller than  $\hbar$ .

Thus we derive:

$$\mathrm{Tr}(\hat{A}U^{-n}) \sim \sum_{\gamma} \frac{\exp(-iS_{\gamma}/\hbar)}{2 \sinh(n\lambda/2)} \sum_j A(q_j). \quad (5.7)$$

The index  $j$  again labels points along the periodic orbit  $\gamma$ . The sum over the periodic orbit is the analogue of the integral of the Weyl transform over a primitive periodic orbit in the Hamiltonian flow case [33]. The special case  $\hat{A} = I$  the identity corresponds to the usual trace formula [27, 28]. Note that we have written the sums above as being over periodic

orbits, while the trace formulas have been often written as sums over *fixed points*.

The first step is to multiply the two semiclassical periodic orbit sums in Eq. (5.6) and in Eq. (5.7). Since there is a time average,  $n$  is assumed large enough, but not too large (so that these expansions retain some accuracy). All hyperbolic functions are approximated by their dominant exponential dependences. The diagonal approximation and the uniformity principle [34] is used as well.

$$C_A(\alpha) = \left\langle \sum_{\gamma} \sqrt{2} \exp(-n\lambda) \sum_T \left( \sum_j F(q_j, p_j) \right) \left( \sum_j A(Tq_j, Tp_j) \right) \right\rangle_n \quad (5.8)$$

Here we have taken a more general dependence for  $A$  (including the possibility of momentum dependence).  $T$  represents elements of the symmetry group of the system including time-reversal symmetry and including, of course, unity. These symmetries imply in general, though not as a rule, distinct (for  $T \neq I$ ) orbits with identical actions. One assumes that the overwhelming number of action degeneracies are due to such symmetries.

The function  $F$  is the approximated Gaussian:

$$F(q_j, p_j) = \exp \left[ -\frac{1}{2\hbar} (\delta q^2 + \delta p^2) - \frac{i\delta q \delta p}{\hbar} \right] \quad (5.9)$$

Using  $\lambda = \ln(2)$  and the fact that there are approximately  $2^n/n$  orbits of period  $n$ , one finds

$$C_A(\alpha) = \sqrt{2} \sum_T \sum_{l=-M}^M \tilde{C}_T(l) \quad (5.10)$$



where  $\tilde{C}(l)$  is a classical  $l$ -step correlation:

$$\tilde{C}_T(l) = \frac{1}{n} \sum_{j=1}^n F(q_j, p_j) A(Tq_{j+l}, Tp_{j+l}). \quad (5.11)$$

The time average is taken over a *typical* orbit. We abandon any specific periodic orbit and appeal to ergodicity, taking  $n$  and also  $M$  as practically infinite. This is with the assumption that such correlations will decay with time  $l$ . In fact, below we calculate such correlations explicitly and display the decay. Note that  $\tilde{C}_T(l) \neq \tilde{C}_T(-l)$  in general. Although these are classical correlations, in the sense that  $q_j, p_j$  represent a classical orbit,  $\hbar$  appears as a parameter in them through  $F$ . Further, using the ergodic principle we can replace time averages in  $\tilde{C}_T(l)$  by appropriate phase space averages:

$$\tilde{C}_T(l) = \int dq \int dp F(q, p) A(Tf^l(q, p), Tg^l(q, p)) \quad (5.12)$$

where we have used the fact that the total phase space volume (area) is unity, and  $f^l(q, p) = q_l$ ,  $g^l(q, p) = p_l$  are the classical  $l$ -step integrated mappings.

## 5.2.2 Special case and verifications

We first consider the case that  $\hat{A} = A_0(\hat{T}_p + \hat{T}_p^\dagger)/2$ , where  $\hat{T}_p$  is the unitary single-step momentum translation operator that is diagonal in the position representation and  $A_0$  is a constant real number. This implies that the associated function is  $A(q) = A_0 \cos(2\pi q)$ . Below we consider  $A_0 = 1$  as the strength of the perturbation. The elements of  $T$ , apart

from the identity ( $I$ ), are time-reversal ( $TR$ ) symmetry and parity ( $P$ ). Time reversal in the bakers map is ( $T(q) = p, T(p) = q$ ) followed by backward iteration, while parity is the transformation ( $T(q) = 1 - q, T(p) = 1 - p$ ).

We begin with the evaluation of the forward correlation ( $l \geq 0$ ) corresponding to  $T = I$ .

$$\tilde{C}_I(l) = \int_{-\infty}^{\infty} dq dp F(q, p) \cos(2\pi 2^l q). \quad (5.13)$$

This follows from the equality:

$$f^l(q) = 2^l q \pmod{1} \quad (5.14)$$

for the bakers map. The limits of the integrals can be extended to the entire plane as long as the centroid of the weighting factor ( $q_\alpha, p_\alpha$ ) is far enough away from the edges of the unit phase space square that the Gaussian tails are small there. The integral is elementary, and using  $h = 1/N$  one gets:

$$\tilde{C}_I(l \geq 0) = \frac{1}{\sqrt{2N}} \exp(-2^{2l}\pi/(2N)) \cos(2\pi 2^l q_\alpha). \quad (5.15)$$

This explicit expression shows the super-exponential decrease with time  $l$  in the correlation coefficients. It is interesting to note that the logarithmic time scale which sets an important quantum-classical correspondence scale of divergence for chaotic systems, here  $\tau = 1/\lambda \ln(1/2\pi\hbar) = \ln(N)/\ln(2)$ , enters the correlation decay. In fact, the correlations are significant to precisely half the log-time. We anticipate this feature to hold in general, including autonomous Hamiltonian systems.

Since  $g^{-l}(p) = 2^l p \pmod{1}$ , for  $(l \geq 0)$ , the time-reversed backward correlation  $(l \leq 0)$  is

$$\tilde{C}_{TR}(l \leq 0) = \frac{1}{\sqrt{2N}} \exp(-2^{-2l} \pi / (2N)) \cos(2\pi 2^{-l} p_\alpha) \quad (5.16)$$

which also decays super-exponentially and is responsible for the  $(q \leftrightarrow p)$  symmetry in the final correlation.

Next we turn to the other, apparently more curious, correlations: the backward identity correlations and the forward time-reversed one. As an example of a backward  $(l \leq 0)$  identity correlation consider  $l = -1$ :

$$f^{-1}(q) = \begin{cases} q/2 & \text{for } p < 1/2 \\ (q+1)/2 & \text{for } p > 1/2 \end{cases}$$

Therefore

$$\tilde{C}_I(-1) = \int_0^1 dq \int_0^{1/2} dp F(q, p) \cos(\pi q) - \int_0^1 dq \int_{1/2}^1 dp F(q, p) \cos(\pi q) \quad (5.17)$$

In fact, since  $\cos(\pi q)$  vanishes at  $1/2$ , there is no discontinuity in the full integral, but it is more difficult to evaluate (and to approximate). If one were to take the upper limits of the  $p$  integrals to be infinity, there would be errors at  $p = 1/2$ . However, this is not terribly damaging, and tolerating a small discontinuity at this point due to this approximation leads to:

$$\tilde{C}_I(-1) = \pm \frac{1}{\sqrt{2N}} \exp(-\pi / (8N)) \cos(\pi q_\alpha) \quad (5.18)$$

the sign depending on if  $p_\alpha < 1/2$  or if  $p_\alpha > 1/2$  respectively. The time-reversed, forward correlation,  $\tilde{C}_{TR}(1)$ , is the same as this except for interchanging the roles of  $q_\alpha$  and  $p_\alpha$ .

The generalization of this to higher times is (take  $l > 0$  below):

$$\tilde{C}_I(-l) = \sum_{\nu=0}^{2^l-1} \int_0^1 dq \int_{\nu/2^l}^{(\nu+1)/2^l} dp F(q, p) \cos(2\pi(q + \bar{\nu})/2^l) \quad (5.19)$$

where  $\nu$  represents a partition of the bakers map at time  $l$ , and  $\bar{\nu}$  results from the bit-reversal of the binary expansion of  $\nu$ . The momentum gets exponentially partitioned with time, and it precludes going beyond the log-time here as well (like the forward correlation), although there is apparently no super-exponential decrease here. Indeed if we evaluate the above after neglecting finite limits in each of the  $p$  integrals above, so that we would have  $2^l$  discontinuities at time  $l$ , we get:

$$\tilde{C}_I(-l) = \frac{1}{\sqrt{2N}} \exp(-\pi/(2^{2l+1})N) \cos(2\pi(q_\alpha + \bar{\nu})/2^l) \quad (5.20)$$

depending on if  $p_\alpha$  lies in the interval  $(\nu/2^l, (\nu+1)/2^l)$ . So that for  $l$  large and  $N$  fixed, the exponential goes to unity; effectively, for large  $N$  and any  $l$ , the exponential can be replaced by unity. Even the  $q_\alpha$ -dependent part of the argument in the function (cos) itself is tending to vanish, so that the integral seems to give the area of the Gaussian ( $h$ ). The approximation of putting all  $p$  limits to infinity makes sense only if the Gaussian state is well within a zone of the partition and this is necessarily violated at half the log-time. So the approximate expression of Eq. (5.20) breaks down beyond  $\tau/2$ . This lack of a super-exponential cutoff

as seen with the previous correlations considered is due to two special conditions. First, the argument of the cosine has no  $p$ -dependence. Second, all the stable manifolds are perfectly parallel to the  $p$  axis. We would recover super-exponential decay in all the correlations if the operator,  $\hat{A}$ , being considered was a constant function along neither the stable nor the unstable manifold. In this sense, we have chosen a maximally difficult operator with which to test the semiclassical theory, though it simplifies the quantum calculations.

As before,  $\tilde{C}_{TR}(l)(q, p) = \tilde{C}_I(-l)(p, q)$ . Parity symmetry is benign and leads to an overall multiplication by a factor of 2. Thus, the final semiclassical expression for the full correlation for the quantum baker's map is:

$$C_A(\alpha) = \frac{2}{N} \left[ \sum_{l=0}^{T_1} \exp(-2^{2l}\pi/(2N)) \cos(2\pi 2^l q_\alpha) + \sum_{l=1}^{T_2} \exp(-\pi/(2^{2l+1}N)) \times \right. \quad (5.21)$$

$$\left. \sum_{\nu=0}^{2^l-1} \left( \cos(2\pi(q_\alpha + \bar{\nu})/2^l) \Theta(p_\alpha - \nu/2^l) \Theta((\nu+1)/2^l - p_\alpha) \right) \right] + (q_\alpha \leftrightarrow p_\alpha).$$

where  $T_1$  can be infinite but it is sufficient to stop just beyond half the log-time. As just discussed,  $T_2$ , is more problematic here, and we do not have an expression to use beyond  $\tau/2$ .  $\Theta$  is the Heavyside step function that is zero if the argument is negative and unity otherwise. The correlation is of the order  $1/N$  or  $\hbar$ . If one were to divide by the number of states in Eq. (5.3) so that it is a true average, this quantity would decrease as  $1/N^2$  or  $\hbar^2$ .

For the case of  $N = 100$ , we compare in Fig. (5.1) the full quantum correlation given by Eq. (5.3) with the final semiclassical evaluation given by Eq. (5.21). The absolute value of the correlation function is contoured and superposed on a grey scale. Figure (5.1a) shows

the quantum calculation for the full phase space. In other words, the intensity (value) of each point,  $(q, p)$ , on the plot represents the  $C_A(\alpha)$ -calculation for a wave packet centered at  $(q_\alpha = q, p_\alpha = p)$ . The first sum in Eq. (5.21) (over  $T_1$  terms) is a smooth function, and it also displays an additional symmetry about  $1/2$  in both canonical variables separately. This extra symmetry is broken by the second sum (over  $T_2$  terms). Figure 5.1(b) compares the semiclassical formula to the exact quantum calculation. We have taken eight “forward” correlations (excluding zero), i.e.  $T_1 = 8$ , while we have only taken two “backward” correlations, i.e.  $T_2 = 2$ . This is because it appears that the approximations that go into the latter expressions lead to non-uniformly converging quantities and it works better to stop at an earlier point in the series. The (artificial) discontinuities at  $1/2$  and  $1/4$  are seen prominently in the semiclassical results. Otherwise, it turns out that the semiclassical approximation captures many fine-scale features of the correlations, some of which will be discussed below. Figures (5.2a,b) are for specific one dimensional sections of the same quantities. The agreement is very good.

### 5.2.3 Classical features in the correlation

A strong (positive) correlation is indicated at the classical fixed points  $(0, 0)$  and  $(1, 1)$ , with the rest of the significant correlations being negative. They are dominated by several classical structures as illustrated in Fig. (5.3). Here the  $N$  value used is 200, and superposed on the significant contour features are the following classical orbits:

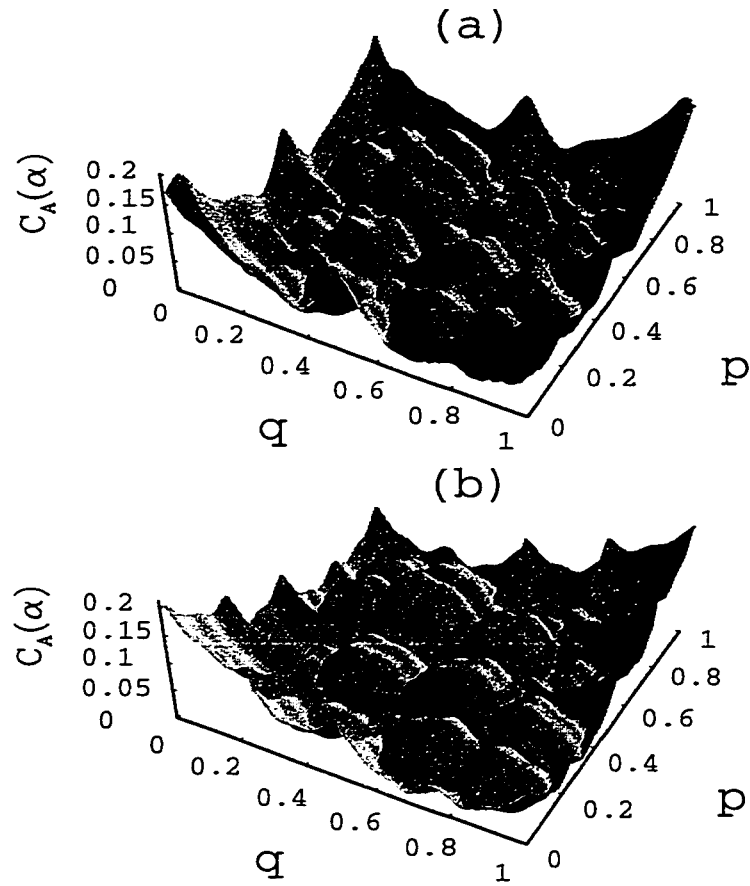


Figure 5.1: (a) The absolute value of the quantum correlation with the  $\cos(2\pi q)$  operator for  $N = 100$  whereas (b) corresponds to a semiclassical evaluation of the same.

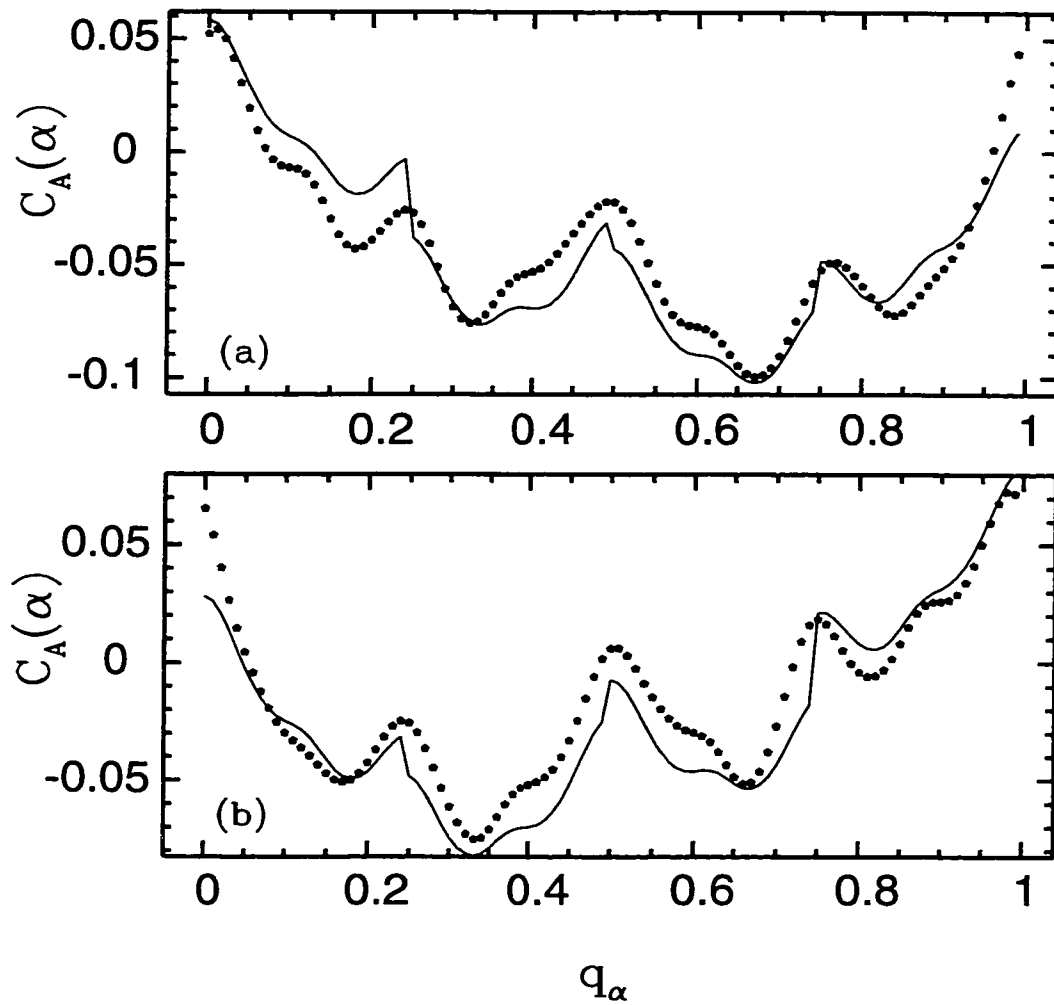


Figure 5.2: Sections of the correlation for  $N = 100$ . (a)  $p_\alpha = .33$  section, (b)  $p_\alpha = .72$  section. The points are the quantum calculation while the solid lines are semiclassical evaluations.



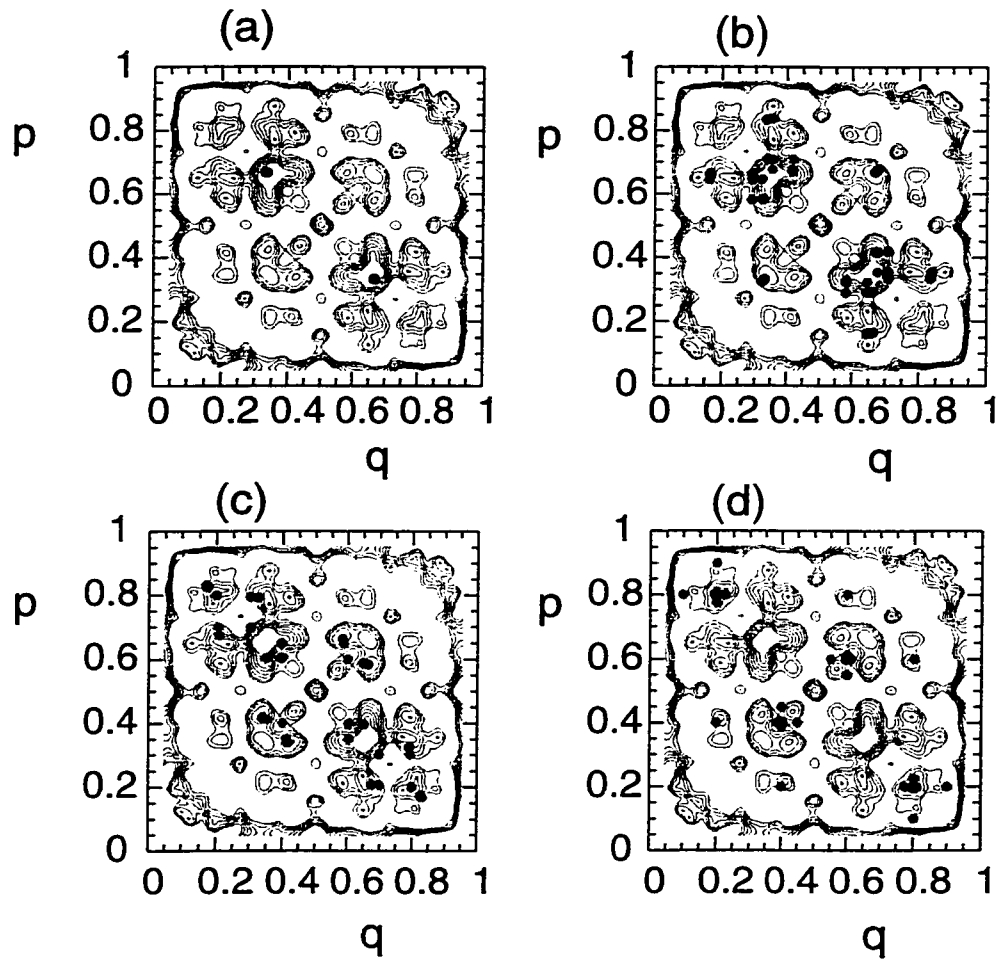


Figure 5.3: Comparison of classical structures in the correlation at  $N = 100$ . Details in the text.

- i) the period-2 orbit at  $(1/3, 2/3)$ ,  $(2/3, 1/3)$  is by far the most prominent structure. This is shown in Fig. (5.3a) by two circular dots. Also, we can look at these structures closely through 1-d slices. In Fig. (5.2a), the correlation is seen to be large and negative at  $(q_\alpha = .66)$ . The period-2 structure is dominating the landscape;
- ii) next in importance is the primary homoclinic orbit to the period 2 orbit in i),  $(1/3, 1/3)$ , which goes to  $(2/3, 1/6)$ , quickly gets into the region of the period two orbit and is difficult to resolve. The parity and time-reversal symmetric image points are also indicated. It turns out that there is an infinite set of periodic orbits which approximate this orbit more and more closely. Its effects may be present simultaneously, and indistinguishable from the homoclinic orbit itself [12]. The relevant family (set) is denoted by  $(001)_{01}$  which is based on a complete binary coding of the orbits [26]. For example, the first few periodic orbits of the family are associated with the binary codes  $(00101)$ ,  $(0010101)$ , and  $(001010101)$ . They are also shown in Fig. (5.3b), including the symmetric image points. In the 1-d slice of Fig. (5.2a) we see this orbit as well;
- iii) there is an infinite number of orbits homoclinic to the period-2 orbit. They become increasingly more complicated. The next associated periodic orbit family,  $(0011)_{01}$ , is shown in Fig. (5.3c), including the symmetric image points. This family was noted by Saraceno to scar eigenfunctions [12]. Also shown in this figure is the period-4 along the diagonal lines:  $(3/5, 3/5) \rightarrow (1/5, 4/5) \rightarrow (2/5, 2/5) \rightarrow (4/5, 1/5)$ . Figure (5.4) shows sections at  $p_\alpha = 3/5, 4/5, 2/5$  to highlight this orbit. In Figs. (4a)  $p_\alpha = 3/5$  and has a local minimum at  $q_\alpha = 3/5$ ; (b)  $p_\alpha = 4/5$  and has a local minimum at  $q_\alpha = 1/5$ ;

and (c)  $p_\alpha = 2/5$  and has a local minimum at  $q_\alpha = 2/5$ . These are marked, to indicate location along  $q_\alpha$  by filled circles. The other minima are due to competing nearby structures of the period-2 orbit and its principal homoclinic excursion;

iv) the orbit homoclinic to the period-4 orbit included in Fig. (5.3c) with the initial condition  $(1/5, 2/5)$  (and its symmetric partners) is shown in Fig. (5.3d); and

v) points, such as  $(0, 1/4)$ , which are homoclinic to the fixed points  $(0, 0)$ ,  $(1, 1)$  also show prominently.

That these structures are in a sense invariant, i.e. not specific to  $N = 100$  is shown in Fig. (5.5a,b) where the correlation (absolute value) is shown for  $N = 128$  and 200 respectively. The phase-space resolution of the correlation is increasing with  $N$ , while the overall magnitude is decreasing as  $1/N$ . The peculiar properties of the quantum baker's map for  $N$  equaling a power of two [12, 26, 27] is tested by  $N = 128$ . Here the correlation is "cleaner" and the stable and unstable manifolds at  $1/4$ ,  $1/2$ , and  $3/4$  of the fixed points are clearly visible. The peaks are well enunciated as well. Both Figs. (5.5a,b) have contours up to  $2/3$  peak height, so a direct comparison is meaningful. Higher  $N$  values show more clearly the secondary homoclinic orbit to the period-2 orbit.

We may compare these structures with the inverse participation ratio defined as:

$$P(\alpha) = \sum_{i=0}^{N-1} |\langle \alpha | \psi_i \rangle|^4. \quad (5.22)$$

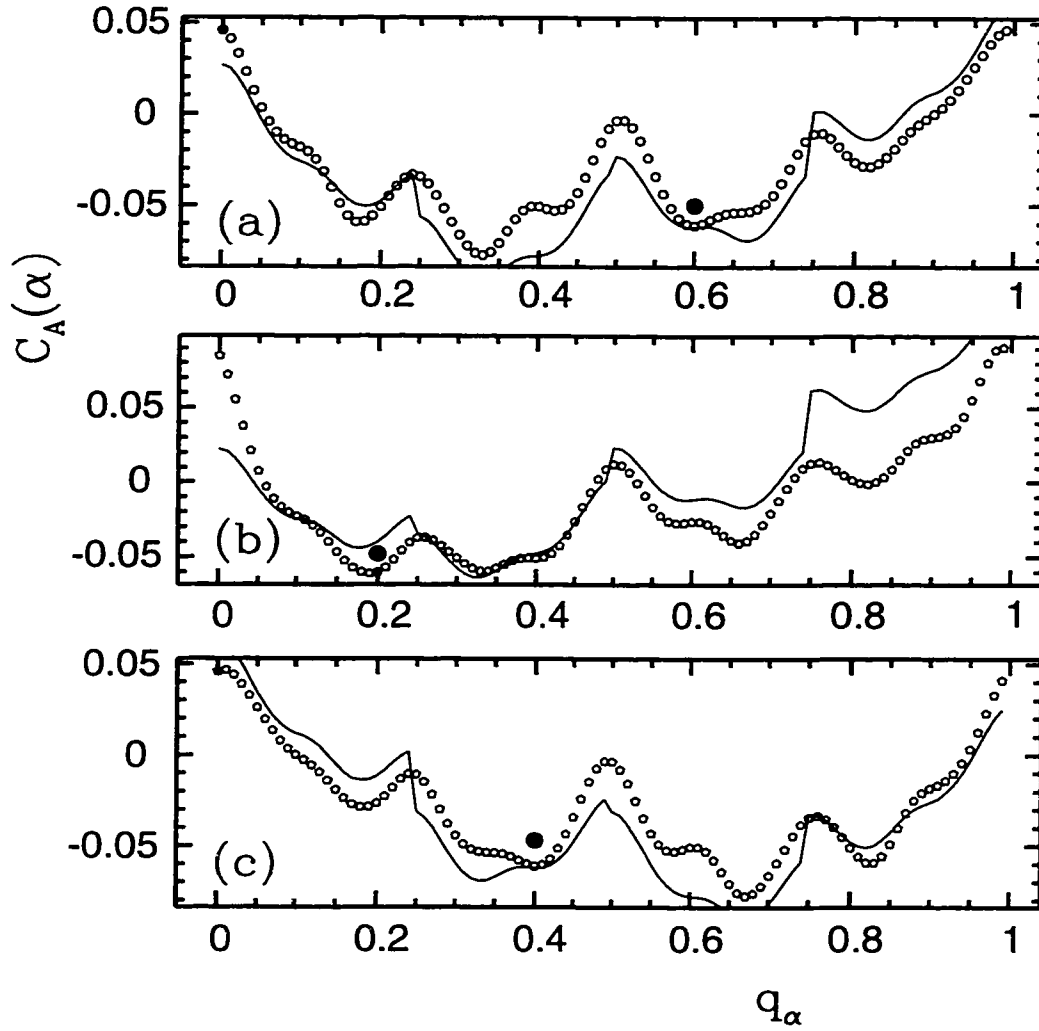


Figure 5.4: Sections of the correlation ( $N = 100$ ) to highlight the period-4 orbit. (a)  $p_\alpha = 3/5$  and has a local minimum at  $q_\alpha = 3/5$  (b)  $p_\alpha = 4/5$  and has a local minimum at  $q_\alpha = 1/5$  (c)  $p_\alpha = 2/5$  and has a local minimum at  $q_\alpha = 2/5$ .

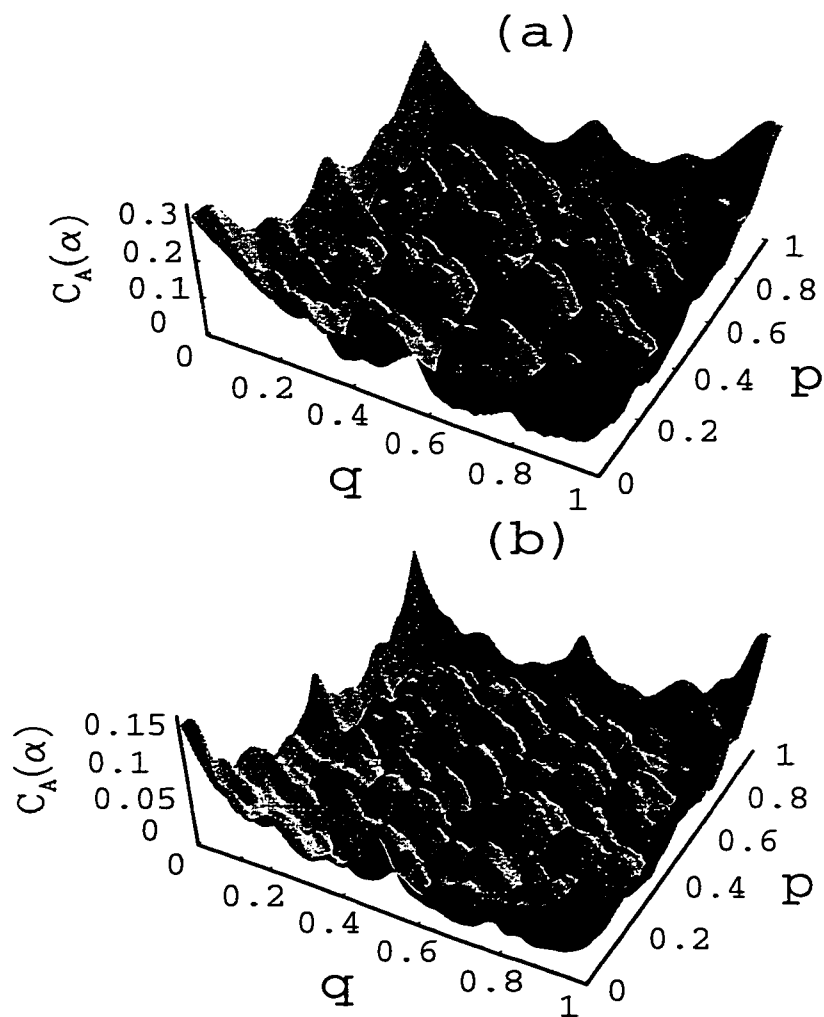


Figure 5.5: The correlation at (a)  $N = 128$  and (b)  $N = 200$ . Note the sharp features in (a), where the peak height is about twice as large as that in (b).

It is illustrated in Fig. (5.6). It shows marked enhancements at the period-2 and period-4 (along the symmetry lines) orbits, and closer examination reveals all orbits up to period-4 are present and one orbit of period-6 along the symmetry lines (the diagonals); see Ref. [27] for a more detailed discussion.

#### 5.2.4 General operators and selective enhancements

The results so far have dealt with the special case  $A(q) = \cos(2\pi q)$ . It seems natural to suspect that the structures highlighted in the correlation are dependent on the choice of the operator. This turns out to be true, and we show here how this works in the bakers map. We reemphasize though that were the eigenstates behaving ergodically, the correlations would have been consistent with zero to within statistical uncertainties independent of the choice of the operator. In this sense, a complete view of the extent to which the eigenstates manifest phase space localization properties comes only from considering both the full phase plane of wave packets and enough operators to span roughly the space of possible perturbations of the energy surface. The flexibility of operator choice does provide a means to enhance selectively particular features of interest supposing one had a specific localization question in mind. As an illustration, note that localization about the period-3 orbit barely appeared in the contour plot of Fig. (5.3), and yet, we show below that it can be made to show up prominently with other operators.

Since the case  $A(q) = \sin(2\pi nq)$  has vanishing correlations for any integer  $n$  due to symmetry, the other cases of interest are the higher harmonics of the cosine. Therefore

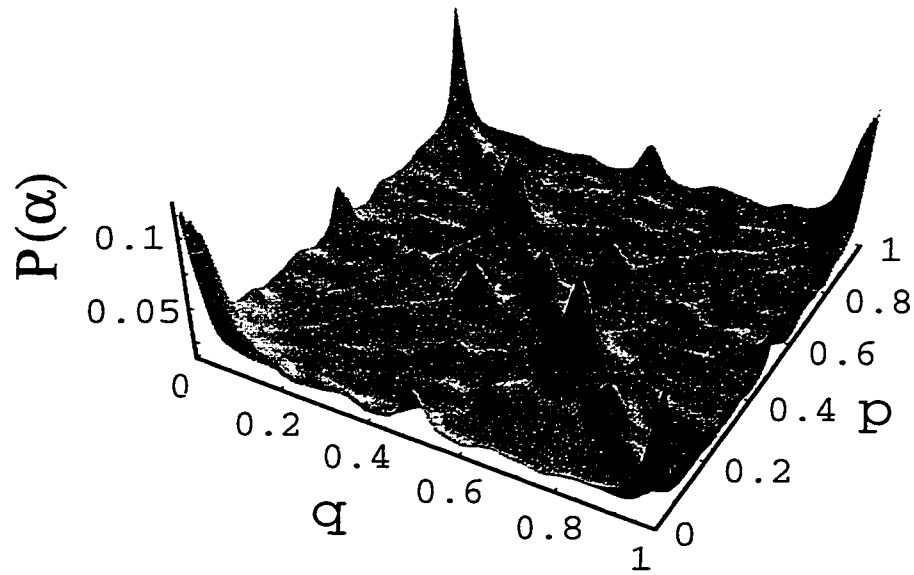


Figure 5.6: The inverse participation ratio for the baker's map. Classical structures are present in this quantity as well.

consider:

$$A(q) = \cos(2\pi nq). \quad (5.23)$$

If  $n = 2^m$  for some positive integer  $m$ , a rather remarkable scaling property of the quantum bakers map is revealed that is actually implicit in the way the bakers map was originally quantized in [26]. Semiclassically, the correlations are *identical* to the case  $m = 0$ . For example, consider  $A(q) = \cos(4\pi q)$ . Then the one-step back classical correlation becomes identical to the zero-th order correlation corresponding to  $A(q) = \cos(2\pi q)$ . The correlations all shift by  $m$  in the sense that  $C(l) \rightarrow C(l + m)$ . Thus, there is a kind of scale invariance in the correlation like classical fractals, although this is not self-similarity in the same curve. Quantum calculations reflect this invariance to a remarkable degree as seen in Fig. (5.7) where the  $N = 200$  and  $p_\alpha = 1/3$  case is shown.

Other harmonics do weight differently the same localization effects (classical structures). In Fig. (5.8),  $N$  and  $p_\alpha$  are taken the same as in Fig. (5.7). The cases  $n = 1, 3, 5$  are all very different from each other, but note that the case  $n = 6$  almost coincides with  $n = 3$  for the same reason that powers of two harmonics are nearly same. Thus only operators of odd harmonics give the possibility of providing new or unique information about the nonergodicity in the eigenstates. The period-2 orbit localization is accentuated at  $n = 3$ , since for  $n = 3m$  where  $m$  is a positive integer,  $\cos(6\pi m q)$  has a maximum of  $+1$  at  $q = 2/3$ , whereas for all other integers  $n$ ,  $\cos(2\pi n q) = -1/2$  at the same point. In short the perturbation (or measurement) is more significant at the location of the period-2 orbit for  $n = 3$ . On the other hand, the case  $n = 5$  is similar to the fundamental harmonic case at



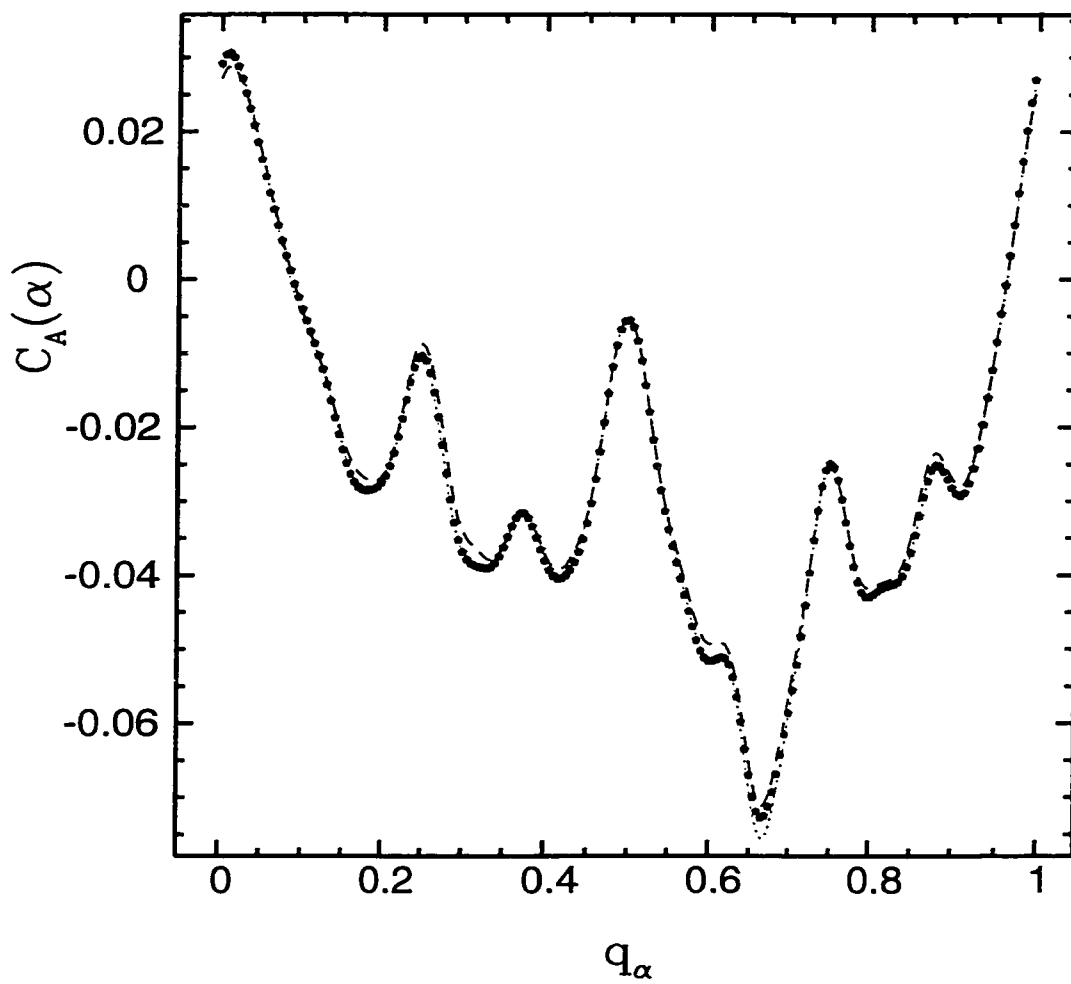


Figure 5.7: The correlation for the series of operators  $A = \cos(2\pi 2^m q)$ . Shown are  $m = 0$  (large dot),  $m = 1$  (small dot),  $m = 2$  (dashed line).

$q = 2/3$  where the perturbation is also equal to  $-1/2$ .

The case  $n = 7$  is interesting as  $\cos(14\pi q)$  has a maximum at  $q = 1/7$  which coincides with a period-3 orbit at  $(1/7, 4/7)$ . In Fig. (5.9), we see the correlation ( $N = 100$ ) corresponding to this operator and the dominant structure is this period-3 orbit and its symmetric partner. Also visible are the stable and unstable manifolds of these orbits. In fact, it is the multiples of the  $2^m - 1$  harmonics which selectively highlights the period  $m$  orbits.

Summarizing then, the correlations reflect that the bakers map eigenstates are not ergodic, and manifest strongly phase space localization properties. There do not exist transport barriers such as cantori or diffusive dynamics in the bakers map, so whatever localization that exists should be due to scarring by the short periodic orbits. This is confirmed in the examples shown with connections to their homoclinic orbits illustrated as well. The perturbation or observable determines the regions of phase space that will light up in the correlation measure. A semiclassical theory predicts reasonably well many of these structures. The correlation is semiclassically written as a sum of classical correlations that are super-exponentially cut off after about half the log-time scale.

## 5.3 The standard map

### 5.3.1 The map and the mixed phase space regime

The standard map (a review is found in [35]) has many complications that can arise in more generic models and we turn to their study. It is also an area-preserving, two-dimensional

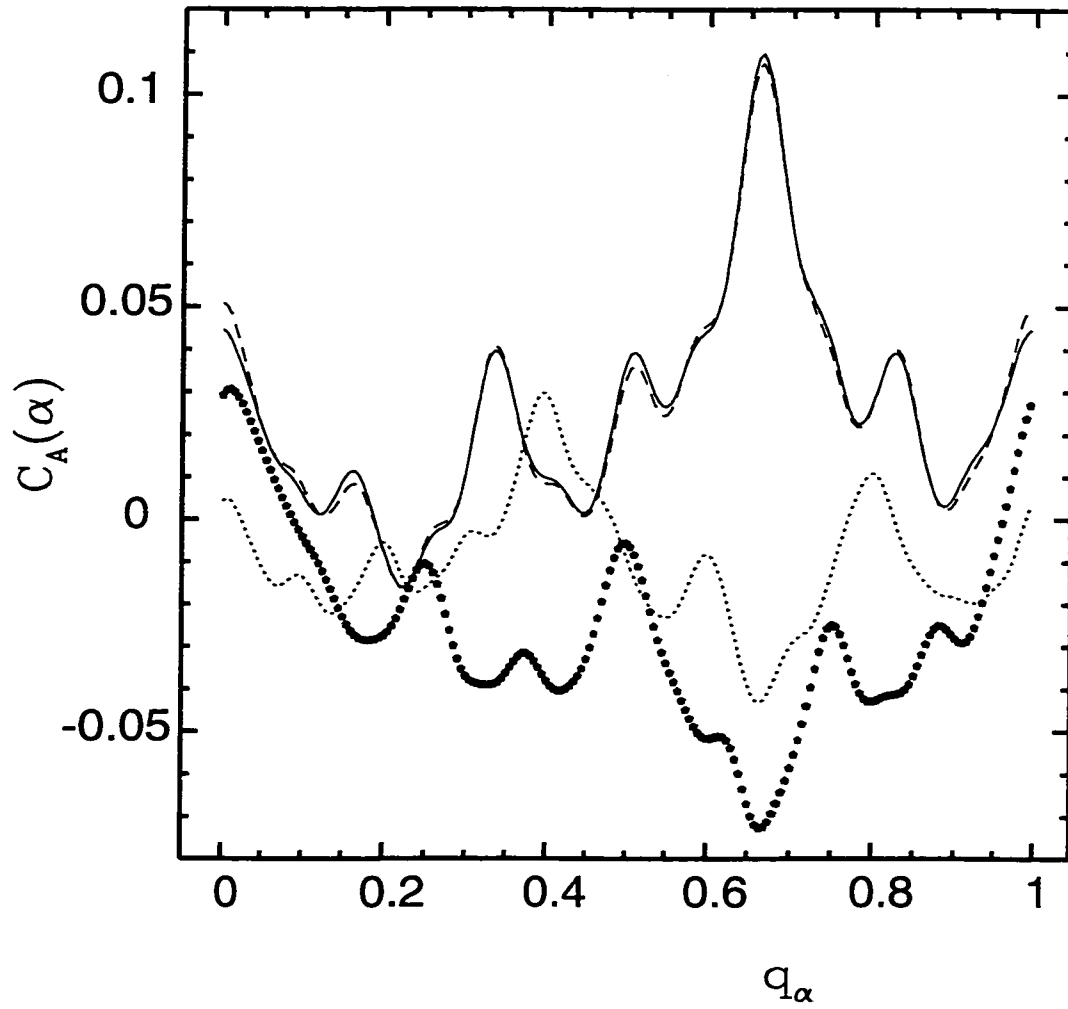


Figure 5.8: The correlation for different harmonics  $A = \cos(2\pi nq)$ . Shown are  $n = 1$  (solid large dots),  $n = 3$  (solid line),  $n = 5$  (dotted line), and  $n = 6$  (dashed line).

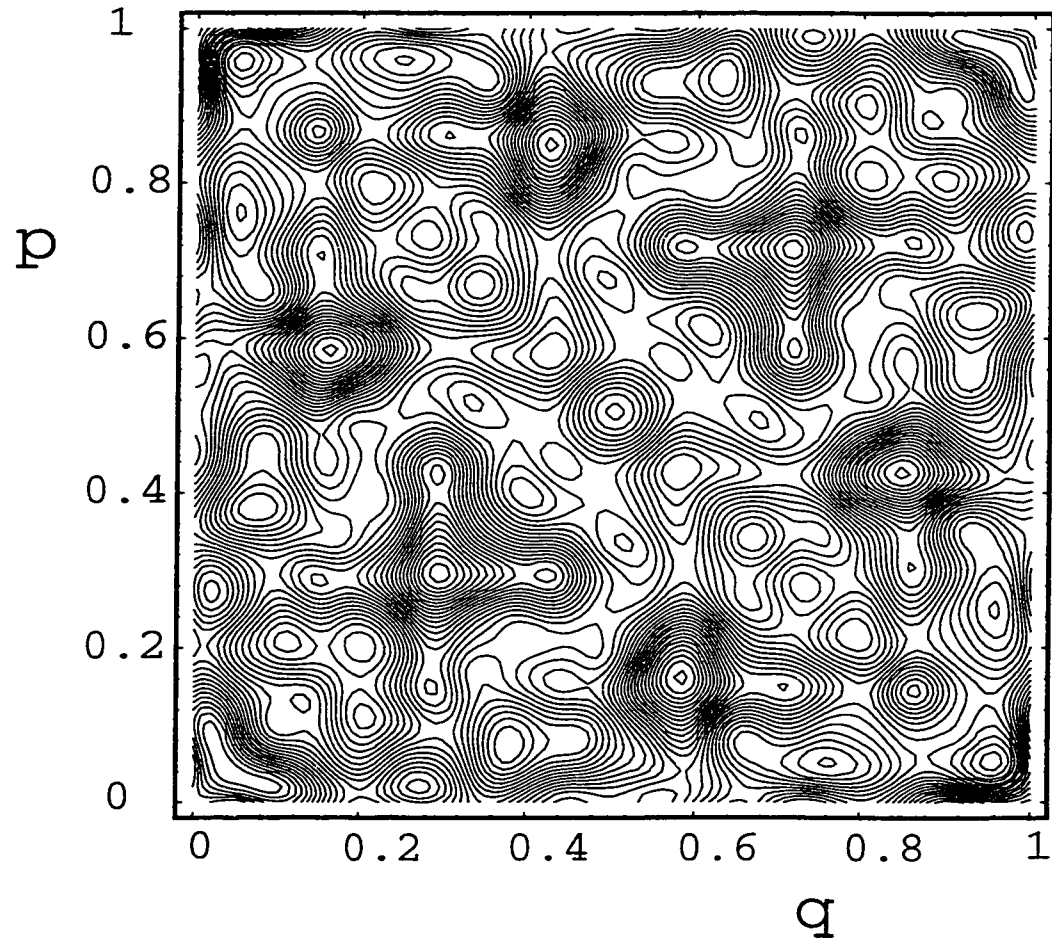


Figure 5.9: The correlation for the operator  $A = \cos(14\pi q)$  and case  $N = 100$ . The highlighted areas are in the region of classical period-3 orbits.

map of the cylinder onto itself that may be wrapped on a torus. We will consider identical settings of the phase space and Hilbert space as for the bakers map discussed above. The standard map has a parameter that controls the degree of chaos and thus we can study the effect of regular regions in phase space, *i.e.* the generic case of mixed dynamics.

The classical standard map is given by the recursion

$$\begin{aligned} q_{i+1} &= (q_i + p_{i+1}) \bmod(1) \\ p_{i+1} &= (p_i - (k/2\pi) \sin(2\pi q_i)) \bmod(1), \end{aligned} \tag{5.24}$$

where  $i$  is the discrete time. The parameter  $k$  is of principal interest and it controls the degree of chaos in the map. Classically speaking, an almost complete transition to ergodicity and mixing is attained above values of  $k \approx 5$ , while the last rotational KAM torus breaks around  $k \approx .971$ .

The quantum map in the discrete position basis is given by [36]

$$\langle n|U|n'\rangle = \frac{1}{\sqrt{iN}} \exp\left(i\pi(n-n')^2/N\right) \exp\left(i\frac{kN}{2\pi} \cos(2\pi(n+a)/N)\right). \tag{5.25}$$

The parameter to be varied will be the “kicking strength”  $k$ , while the phase  $a = 1/2$  for maximal quantum symmetries, and  $n, n' = 0, \dots, N - 1$ .

We use the unitary operator and evaluate the correlation as in Eq. (5.3) with  $A(q) = \cos(2\pi q)$  here as well. This corresponds exactly to the level velocity induced by a change in the parameter  $k$ . In Fig. (5.10) is shown the absolute value of the correlation for various

values of parameter  $k$ . Case (a) corresponds to  $k = .1 \times (2\pi)$  and is dominated by the KAM curves as the perturbation has not yet led to significant chaos. Highlighted is the fixed point resonance region at the origin that is initially stable. An unstable point is located at the point  $(1/2, 0 \text{ or } 1)$ . The separatrix or the stable and the unstable manifolds of this point are aligned along the local ridges seen in the correlation. Also the period-2 resonance region is visible. Higher resolution not shown here, corresponding to higher values of  $N$  reveal weakly the period-3 resonance as well. Case (b) corresponds to  $k = .3 \times (2\pi)$  while (c) and (d) to  $k = .9 \times (2\pi)$  and  $k = 2.3 \times (2\pi)$  respectively. We note the gradual destruction of the KAM tori and the emergence of structures that are dominated by hyperbolic orbits. A more detailed classical-quantum correspondence is however not attempted here.

These contour plots do not reveal the difference in the magnitude between the correlations in the stable and unstable regions. In Fig. (5.11), we have plotted the correlation at the origin  $(0, 0)$ , which is also a fixed point, as a function of the parameter. The value  $k/(2\pi) \sim 1$  corresponds to a transition to complete classical chaos and is reflected in this plot as erratic and small oscillations. The large correlation in the mixed phase space regime arises from the non-ergodic nature of the classical dynamics. The classical fixed point loses stability at  $k^*/(2\pi) = 4/(2\pi) \approx .63$  and this is roughly the region at which the correlation starts to dip away from unity toward lower values.

The gross features and principal  $\hbar$  behavior in this regime is easy to derive in terms of

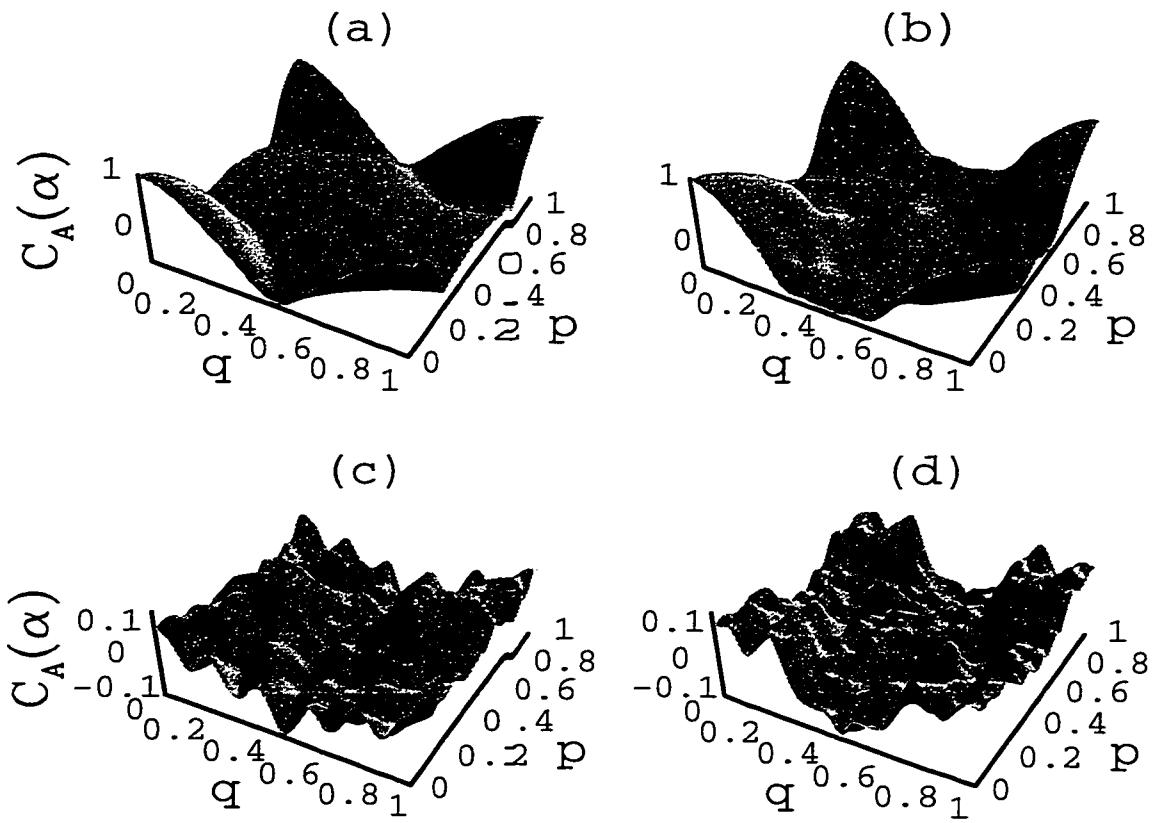


Figure 5.10: The quantum correlation for the standard map ( $N = 100$ ), (a)  $k/(2\pi) = .1$ , (b)  $k/(2\pi) = .3$ , (c)  $k/(2\pi) = .9$ , (d)  $k/(2\pi) = 2.3$ .

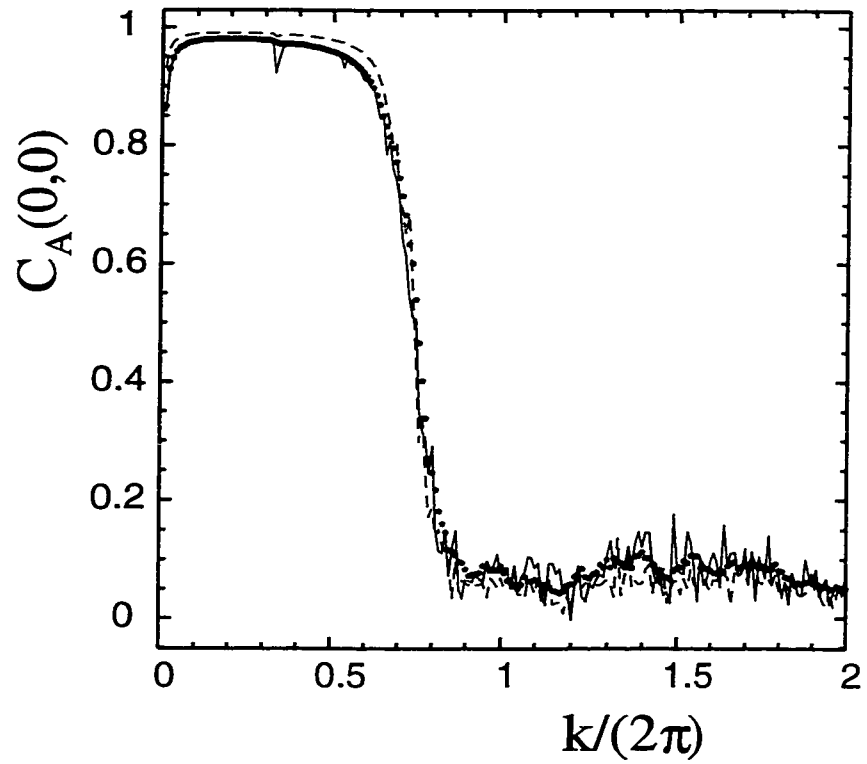


Figure 5.11: The quantum correlation for the standard map at  $\alpha = (0, 0)$  as a function of the parameter  $k$  ( $N = 100$  is the solid line and  $N = 200$  is the dashed one). The dotted line is a classical estimate based on Eq. (5.27) and averaged over twenty time steps with  $N = 100$ .



purely classical correlations as follows:

$$C_A(\alpha) = \left\langle \text{Tr} \left( |\alpha\rangle\langle\alpha| \hat{A}(n) \right) \right\rangle_n = \left\langle \int dq dp [|\alpha\rangle\langle\alpha|]_W [\hat{A}(n)]_W \right\rangle_n \quad (5.26)$$

where  $[\cdot]_W$  is the Weyl-Wigner transform of the operator in the brackets and  $\hat{A}(n)$  is the operator after a time  $n$ . Without worrying about the toral nature of the phase space and the Weyl-Wigner transforms, we treat the problem as in a plane. This is justified by the use of localized, Gaussian wave packets. Otherwise, we could imagine that the Wigner transform of the projector would follow from an infinite series of Gaussian states that is equivalent to discretizing the Gaussian. We use a normalized, “circular” Gaussian of width  $\sqrt{\hbar}$ . The approximation comes in when we replace  $[\hat{A}(n)]_W$  by  $A(f^n(q, p))$  where the latter is the classical function evaluated at the classically iterated point  $q_n = f^n(q, p)$ . We expect this approximation to be valid in the case of regular dynamics over a much longer time scale than found with chaotic dynamics. To a good approximation,

$$C_A(\alpha) \sim \left\langle \int dq dp \left( \frac{1}{\pi\hbar} \right) \exp \left[ -\frac{1}{\hbar} \left( (q - q_\alpha)^2 + (p - p_\alpha)^2 \right) \right] A(f^n(q, p)) \right\rangle_n \quad (5.27)$$

As intuitively expected, there is no principal  $\hbar$  dependence in the correlation since there is a non-zero classical limit. At  $\hbar = 0$ , we could replace the Gaussian forms by  $\delta$ -functions and would get simply  $C_A(\alpha) = \langle A(f^n(q_\alpha, p_\alpha)) \rangle_n$ .

This however vanishes as the classical system becomes more ergodic and is no more capable of predicting the correlation. Higher-order corrections are needed. It is in this

regime that we studied the bakers map and found that the correlation has a principal part that scales (almost) as  $\hbar$  and classical correlations based on periodic orbits predict the localization features that arise out of quantum interference.

We return to Fig. (5.11) to remark on some of these properties. Notice that the simple estimate of Eq. (5.27) performs very well, even as the phase space is becoming increasingly chaotic. It is quite unexpected that the oscillations after the onset of full mixing (around  $k/(2\pi) = 1$ ) should follow this estimate. However, after the transition to chaos the classical estimate will depend on the times over which the averaging is done and as this increases the estimate would vanish.

### 5.3.2 Chaotic regime

We attempt in some measure a semiclassical theory for the correlation in the chaotic regime along the lines adopted for the quantum bakers map. Of the two ingredients in Eq. (5.4) one of them remains the same, namely Eq. (5.7). However the diagonal elements of the propagator in Eq. (5.6) have to be generalized.

In [32] a semiclassical expression for the matrix elements of the propagator as a homoclinic orbit sum is given. Although this was derived with the example of the billiard in mind, it can be interpreted as a generalization of Eq. (5.6) for area-preserving, two-dimensional maps. We, however, interpret the sum not as a homoclinic orbit sum, but as a periodic orbit sum. To each homoclinic orbit there is a neighboring periodic orbit that we will use instead. This will form the points around which the expansions are carried out and the result is identical

to that in [32]. Thus we write

$$\langle \alpha | U^n | \alpha \rangle \sim \sum_{\gamma} \exp(iS_{\gamma}/\hbar - i\pi\nu/2) \sum_j B_j \quad (5.28)$$

where

$$B_j = \sqrt{\frac{2}{A_0}} \exp \left\{ \frac{-1}{2\hbar A_0} \left[ (\text{tr} - 2)(\delta q^2 + \delta p^2) + 2i(m_{21} \delta p^2 - m_{12} \delta q^2 + \delta q \delta p (m_{22} - m_{11})) \right] \right\}. \quad (5.29)$$

$B_j$  generalizes the Gaussian form (including the prefactor) in Eq. (5.6). Again  $j$  labels points along the periodic orbit and  $\delta q = q_j - q_{\alpha}$ ,  $\delta p = p_j - p_{\alpha}$  are as before deviations from the centroid of the wave packet. The two dimensional matrix elements,  $m_{ij}$ , are the elements of the stability matrix at the periodic point  $j$  along the periodic orbit  $\gamma$ . The deviations  $\delta q$  and  $\delta p$  after  $n$  iterations of the map are given by:

$$\begin{pmatrix} \delta p_n \\ \delta q_n \end{pmatrix} = \begin{pmatrix} m_{11} & m_{12} \\ m_{21} & m_{22} \end{pmatrix} \begin{pmatrix} \delta p \\ \delta q \end{pmatrix} \quad (5.30)$$

The invariant is the trace of this matrix that is denoted  $\text{tr}$ . While  $A_0 = m_{11} + m_{22} + i(m_{21} - m_{12})$ ,  $\nu$  is a phase that will not play a crucial role below. In the case of the bakers map  $m_{12} = m_{21} = 0$  and  $m_{11} = 2^{-n}$ ,  $m_{22} = 2^n$  uniformly at all points in phase space, as well as  $\nu = 0$ . On substitution of this in Eq. (5.28) we get Eq. (5.6).

The dependence on individual matrix elements of the stability matrix complicates the use of this formula in general. However we note that the Gaussian is effectively cutting

off periodic points that are not close to  $\alpha$  and therefore we may take the  $m_{ij}$  elements to be the stability matrix at this point. In the chaotic regime each of the matrix elements grow exponentially with time  $n$ . Thus we have that  $\exp(-\lambda n) m_{ij} \rightarrow \text{constant}$ , where  $\lambda$  is the Lyapunov exponent. We call this saturated constant  $m_{ij}$  as well. Below we will assume that the exponential growth has been factored out of these elements. Also we use  $\exp(-\lambda n) A_0 \rightarrow a_0$ . The terms inside the exponential function in Eq. (5.29) saturate in time  $n$  while the prefactor goes as  $\exp(-\lambda n/2)$ . It follows then that

$$B_j \rightarrow \sqrt{\frac{2}{a_0}} \exp(-\lambda n/2) F(q_j, p_j) \quad (5.31)$$

where  $F(q_j, p_j)$  is

$$F(q_j, p_j) = \exp \left\{ \frac{-1}{2\hbar a_0} \left[ (\delta q^2 + \delta p^2) + 2i(m_{21} \delta p^2 - m_{12} \delta q^2 + \delta q \delta p (m_{22} - m_{11})) \right] \right\}. \quad (5.32)$$

Here the  $m_{ij}$  elements already have the exponential behavior factored out. For example in the case of the bakers map  $m_{22} = 1$  while all the other elements are zero and this gives consistently the approximated Gaussian form in Eq. (5.9). Further steps are identical to the case of the bakers map and leads to the generalization of Eq. (5.10):

$$C_A(\alpha) = \sqrt{\frac{2}{a_0}} \sum_T \sum_{l=-M}^M \tilde{C}_T(l), \quad (5.33)$$

where the classical correlations are calculated as in Eq. (5.11) with the function  $F$  being that

in Eq. (5.32). We may then expect all the principal conclusions from the study of the bakers map to be carried over, principally the decrease in the correlation as  $\hbar$ , the correlations being cut off after half the log-time scale, and the effects of classical orbits.

More detailed analysis in the lines of the special case discussed in case of the bakers map will run into the following difficulties. First, the  $m_{ij}$  elements will depend on  $\alpha$  in general. Exceptions are uniformly hyperbolic systems such as the cat or sawtooth maps (and, of course, the bakers map). A second difficulty is that the correlations have to be evaluated to half the log-time while classically iterating the map (analytically) over such times is often not possible. The classical correlations that arise in the study of rms values of level velocities [25] involved correlations that exponentially decreased in time while here we are likely to get generalizations of forms such as in Eq. (5.15) that will require us to go up to log-times. We have calculated the correlations for times 1, -1, and 2 but will not display them as they are by themselves not very useful. A third problem with this form of the generalization is that it is not explicitly real.

We have used Eq. (5.33) and for the  $m_{ij}$  used either those calculated at one point in phase space (such as the origin) or in fact assumed those that are relevant for the bakers map. While fine structures are not reproduced, the general features are captured equally well in both these approaches. To illustrate the quality of the approximation we again look at the correlation at the point (0,0) as a function of  $k$  in Fig. (5.12) (as in the previous figure). The solid line is the semiclassical prediction based upon using the *same*  $m_{ij}$  values at all values of  $k$ . It is seen that even with these (over) simplifications the semiclassical

expressions capture much of the oscillations with the parameter and the magnitude.

## 5.4 Summary and conclusions

We have studied the details of phase space localization present in the quantum time evolution of operators. This was related to a measure of localization involving the correlation between the level velocities and wavefunction intensities. While individual quantum states show well known interesting scars of classical orbits, groups of states weighted appropriately provide both a convenient and important quantity to study semiclassically. We were interested principally in those features whose origins were quantum mechanical. The quantities studied had both a vanishing classical limit as well as vanishing RMT averages.

We studied simple maps as a way to understand the general features that will appear. We found that the operator dictated to a large extent which parts of phase space will display prominent localization features and further that these localization features are often related to classical periodic orbits and their homoclinic structures. The time average of the operator for wave packets was explicitly related semiclassically to classical correlations. These were shown to be cut off super-exponentially after half the log-time in the quantum baker's map. Thus the localization features in quantum systems associated with scars were reproduced using long (periodic) orbits but short time correlations. The localization would disappear in the classical limit as the magnitude of the quantum correlations or time averages are proportional to (scaled)  $\hbar$ .

General systems were approached using the quantum standard map and complications

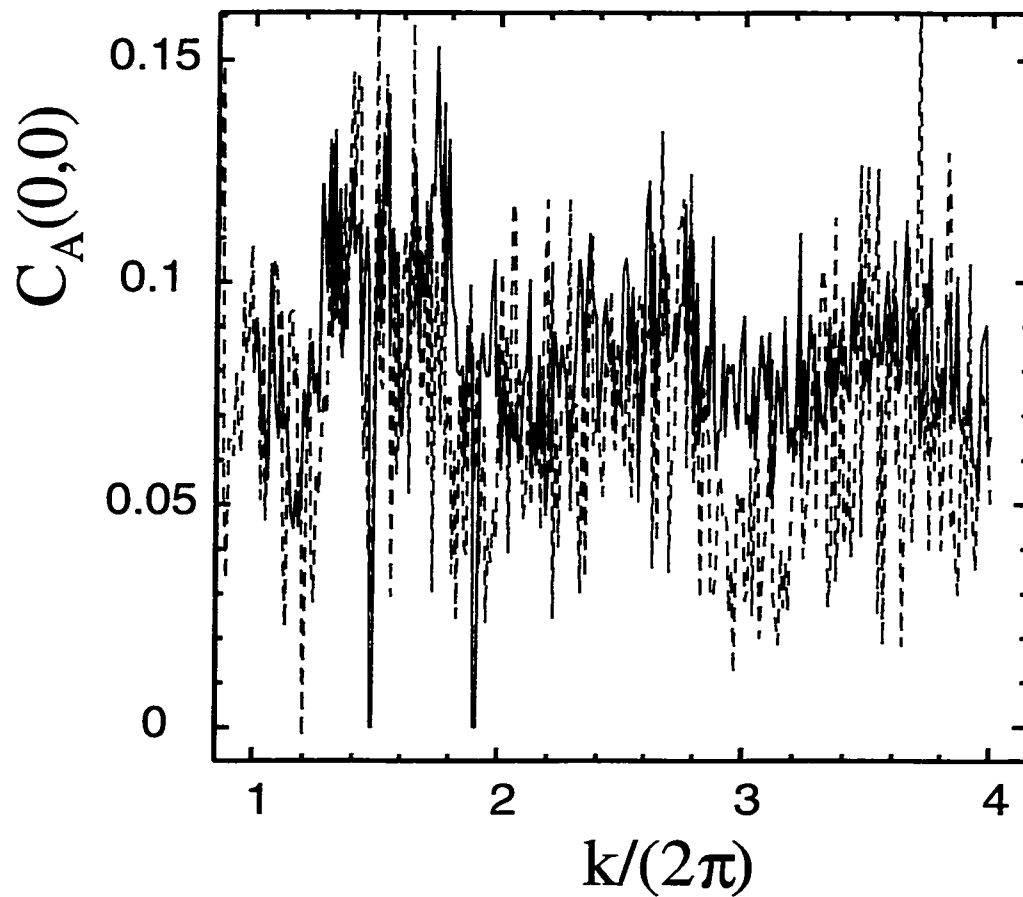


Figure 5.12: The quantum correlation for the standard map ( $N = 100$ ) at  $\alpha = (0, 0)$  as a function of the parameter  $k$  (dashed line). The solid line is the semiclassical estimate.

that would arise were discussed. Also the case of mixed phase space was seen to be well reproduced by a simple classical argument. The generalization to Hamiltonian systems [22] contains many of the features and structures are also (not surprisingly) present in this case.

We gratefully acknowledge support from the National Science Foundation under Grant No. NSF-PHY-9800106 and the Office of Naval Research under Grant No. N00014-98-1-0079.



## References

- [1] M. V. Berry, *J. Phys. A* **10**, 2083 (1977).
- [2] A. Voros, In *Stochastic Behaviour in Classical and Quantum Hamiltonian Systems*, edited by G. Casati and J. Ford (Springer, Berlin, 1979).
- [3] E. B. Stechel and E. J. Heller, *Ann. Rev. Phys. Chem.* **35**, 563 (1984); E. B. Stechel, *J. Chem. Phys.* **82**, 364 (1985).
- [4] L. Kaplan and E. J. Heller, *Physica D* **121**, 1 (1998); *Ann. Phys. (N. Y.)* **264**, 171 (1998); L. Kaplan, *Phys. Rev. Lett.* **80**, 2582 (1998).
- [5] N. L. Balazs and B. K. Jennings, *Physics Reports* **104** (6), 347 (1984).
- [6] E. J. Heller, *Phys. Rev. Lett.* **53**, 1515 (1984).
- [7] E. J. Heller, in *Les Houches LII, Chaos and Quantum Physics*, edited by M.-J. Giannoni, A. Voros, and J. Zinn-Justin (North-Holland, Amsterdam 1991).
- [8] E. J. Heller, in *Quantum Chaos and Statistical Nuclear Physics*, edited by T. H. Selgman and H. Nishioka, *Lecture Notes in Physics* 263. (Springer, Berlin, 1986).

- [9] E. B. Bogomolny, *Physica D* **31**, 169 (1988).
- [10] M. V. Berry, *Proc. R. Soc. Lond. A* **423**, 219 (1989).
- [11] B. Eckhardt, G. Hose, E. Pollak, *Phys. Rev. A* **39**, 3776 (1989).
- [12] M. Saraceno, *Ann. Phys. (N. Y.)* **199**, 37 (1990).
- [13] M. S. Santhanam, V. B. Sheorey, and A. Lakshminarayan, *Phys. Rev. E* **57**, 345 (1998).
- [14] T. M. Fromhold *et al.*, *Phys. Rev. Lett.* **72**, 2608 (1994).
- [15] G. Muller *et al.*, *Phys. Rev. Lett.* **75**, 2875 (1995).
- [16] R. S. McKay and J. D. Meiss, *Phys. Rev. A* **37**, 4702 (1988).
- [17] R. Ketzmerick, G. Petshel, and T. Geisel, *Phys. Rev. Lett.* **69**, 695 (1995).
- [18] O. Bohigas, S. Tomsovic, and D. Ullmo, *Physics Reports* **223** (2), 43 (1993).
- [19] S. Tomsovic and E. J. Heller, *Phys. Rev. Lett.* **70**, 1405 (1993).
- [20] O. L. De Lange and R. E. Raab, *Operator Methods in Quantum Mechanics*, (Oxford Science Publications, Oxford, 1991).
- [21] S. Tomsovic, *Phys. Rev. Lett.* **77**, 4158 (1996).
- [22] N. R. Cerruti, A. Lakshminarayan, J. H. Lefebvre, and S. Tomsovic, submitted to *Phys. Rev. E*.
- [23] P. W. O'Connor, S. Tomsovic and E. J. Heller, *Physica D* **55**, 340 (1992).

- [24] T. A. Brody, J. Flores, J. B. French, P. A. Mello, A. Pandey, and S.S.M. Wong, Rev. Mod. Phys. **53**, 385 (1981).
- [25] A. Lakshminarayan, N. R. Cerruti and S. Tomsovic, Phys. Rev. E **60**, 3992 (1999).
- [26] N. L. Balazs and A. Voros, Ann. Phys. (N. Y.) **190**, 1 (1989).
- [27] P. W. O'Connor and S. Tomsovic, Ann. Phys. (N. Y.) **207**, 218 (1991).
- [28] A. M. Ozorio de Almeida and M. Saraceno, Ann. Phys. (N. Y.) **210**, 1 (1991).
- [29] M. Saraceno and A. Voros, Physica D **79**, 206 (1994).
- [30] J. Schwinger, *Quantum Kinematics and Dynamics*, (Benjamin, New York, 1970).
- [31] J. H. Hannay and M. V. Berry, Physica D **1**, 267 (1980).
- [32] S. Tomsovic and E. J. Heller, Phys. Rev. E **47**, 282 (1993).
- [33] B. Eckhardt, S. Fishman, K. Muller and D. Wintgen, Phys. Rev. A **45**, 3531 (1992).
- [34] J. H. Hannay and A. M. Ozorio de Almeida, J. Phys. A **17**, 3429 (1984).
- [35] F. M. Izrailev, Phys. Rep. **196**, 299 (1990).
- [36] A. Lakshminarayan, Pramana **48**, 517 (1997).

## Chapter 6

# Chaos in Quantum Dots: Dynamical Modulation of Coulomb Blockade Peak Heights

By Evgenii E. Narimanov,<sup>1</sup> Nicholas R. Cerruti,<sup>2</sup> Harold U. Baranger<sup>1</sup>

and Steven Tomsovic<sup>2</sup>

<sup>1</sup>Bell Laboratories – Lucent Technologies, 700 Mountain Ave.,

Murray Hill, NJ 07974

<sup>2</sup>Dept. of Physics, Washington State University, Pullman, WA 99164-2814

Physical Review Letters **83**, 2640 (1999)

Copyright 1999 by the American Physical Society.

## 6.0 Abstract

We develop a semiclassical theory of Coulomb blockade peak heights in quantum dots and show that the dynamics in the dot leads to a large modulation of the peak height. The corrections to the standard statistical theory of peak height distributions, power spectra, and correlation functions are non-universal and can be expressed in terms of the classical periodic orbits of the dot that are well coupled to the leads. The resulting correlation function oscillates as a function of peak number in a way defined by such orbits; in addition,

the correlation of adjacent conductance peaks is enhanced. Both of these effects are in agreement with recent experiments.

## 6.1 Letter

The electrostatic energy of an additional electron on a quantum dot— a mesoscopic island of confined charge with quantized states— blocks the flow of current through the dot, an effect known as the Coulomb blockade [1]. Current can flow only if two different charge states of the quantum dot are tuned to have the same energy; this produces a peak in the the conductance of the dot whose magnitude is directly related to the magnitude of the wavefunction near the contacts to the dot. Since dots are generally irregular in shape, the dynamics of the electrons is chaotic, and the characteristics of Coulomb blockade peaks reflect those of wavefunctions in chaotic systems [2–4]. Previously, a statistical theory for the peaks was derived [2, 3] by assuming these wavefunctions to be completely random and uncorrelated with each other. The experimental data [5, 6] for the distribution of the Coulomb blockade peak heights were found to be in excellent agreement with the predictions of the statistical theory, thus giving a solid foundation to the conjecture of effective “randomness” of the quantum dot wavefunctions.

It therefore came as a surprise when several recent experiments [6–8] demonstrated large correlations between the heights of adjacent peaks. The effect of nonzero temperature (when several resonances contribute to the same peak) was found to be insufficient to account for these correlations [9]. To explain the correlations, the enhancement due to spin-paired

levels [8, 9], due to a decrease of the effective level spacing found in density functional calculations [10], and due to level anticrossings in interacting many-particle systems [11] were proposed. However, we show here that peak height correlations arise already within an effective single-particle picture of the electrons in the quantum dot. The specific internal dynamics of the dot, even though it is chaotic, modulates the peaks: because all systems have short-time features, chaos is not equivalent to randomness. The predicted dynamical modulation is exactly of the type needed to explain the experiments [6–8].

To study the non-universal effects of the dynamics of a particular dot, we derive a relation between the quantum conductance peak height and the classical periodic orbits in the dot. The main effect is that as a system parameter varies— the magnetic field or the number of electrons in the dot in response to a gate voltage, for instance— the interference around each periodic orbit oscillates between being destructive and constructive. When the interference is constructive for those periodic orbits which come close to the leads used to contact the dot, the wavefunction is enhanced near the leads, the dot-lead coupling is stronger, and so the conductance is larger. Likewise, destructive interference produces a smaller conductance. The resulting modulation can be substantial, as shown in Fig. 1. Similar short-time dynamical effects have been noted in other contexts such as atomic and molecular spectra [12–14], eigenfunction scarring [14, 15], magnetotransport in antidot lattices [16], and tunneling into quantum wells [17–19]. Such modulation is completely omitted in theories in which the wavefunction is assumed to change randomly as the system changes [2, 3].

Our starting point is the connection between the peak height and the width of the level

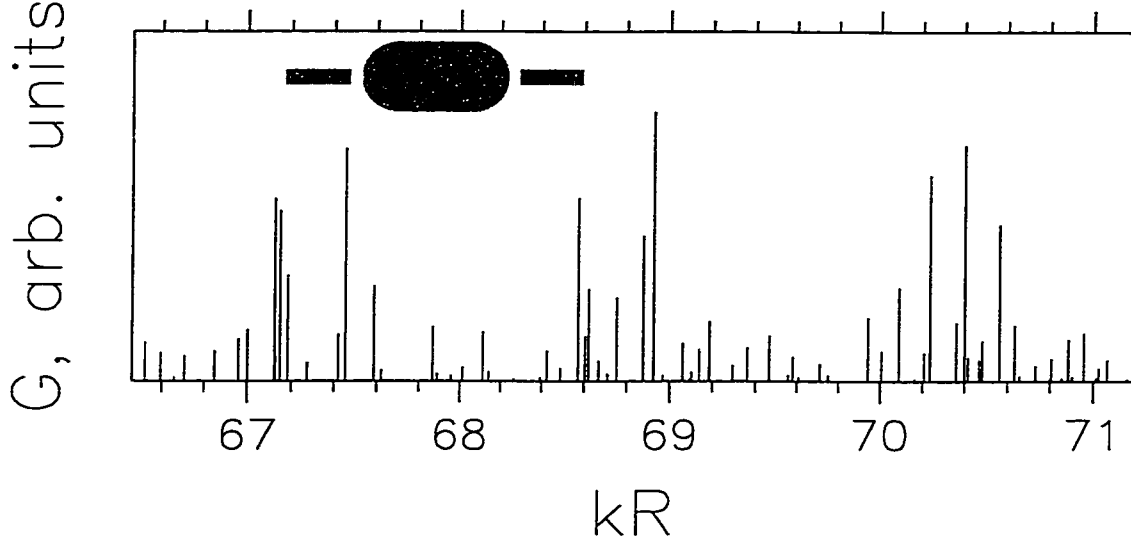


Figure 6.1: The peak conductance from tunneling through subsequent energy levels for the stadium billiard shown in the inset. Each peak is placed at the wavevector  $k$  corresponding to its level;  $R$  is the radius of the half-circle parts of the stadium. A Gaussian lead wavefunction appropriate for tunneling from a single transverse mode is used with width  $ka_{\text{eff}} = 15$ .

in the quantum dot. We consider a dot close to two leads (Fig. 1 inset) so that the width,  $\Gamma$ , of a level comes from tunneling of the electron to either lead. When the mean separation of levels is larger than the temperature  $T$  which itself is much larger than the mean width, the electrons pass through a single quantized level in the dot. The conductance peak height in this regime is [20]

$$G_{\text{peak}} = \frac{e^2}{h} \frac{\pi\Gamma}{4kT}. \quad (6.1)$$

Here for simplicity we consider symmetrically placed leads— the total width is equally split between tunneling to the right and left leads— spinless particles, and temperature much smaller than the level spacing.

The width of the level is related by Fermi's Golden Rule to the square of the matrix element for tunneling between the lead and the dot,  $M^{\ell \rightarrow d}$ . A convenient expression for the matrix element in terms of the lead and dot wavefunctions,  $\Psi_\ell$  and  $\Psi_d$  respectively, was derived by Bardeen [21] and can be expressed as [17, 18]

$$M^{\ell \rightarrow d} = \frac{\hbar^2}{m^*} \int_S d\mathbf{S} \Psi_\ell(r) \nabla \Psi_d(r) \quad (6.2)$$

where the surface  $S$  is the edge of the quantum dot.  $\Gamma$ , then, depends on the square of the normal derivative of the dot wavefunction at the edge weighted by the lead wavefunction. Writing the product of the two  $\Psi_d$ 's in  $\Gamma$  as a Green function  $G(r, r')$  and using the standard semiclassical expression for the latter [12], we express  $\Gamma$  as a sum over the classical trajectories which start at  $r$  on the edge of the dot near the lead and end at  $r'$  which is also on the edge near the lead.

Tunneling from the lead to the dot is dominated by the lowest transverse energy subband in the constriction between the lead and the dot [3]. Therefore, for the calculation of the tunneling matrix element the transverse potential in the tunneling region can be taken quadratic:  $U_\ell \sim \kappa (y - y_\ell)^2$ . In this case the transverse dependence of the lead wavefunction is simply a harmonic oscillator wavefunction, so that at the edge of the dot  $\Psi_\ell \sim c_\ell \exp[-(y - y_\ell)^2 / 2a_{\text{eff}}^2]$ , where  $\hat{y}$  represents the direction tangential to the boundary of the dot,  $y_\ell$  is the center of the lead and constriction, and the effective width is  $a_{\text{eff}} = \sqrt{\hbar / \sqrt[4]{2\kappa m^*}}$ . While the exact form of the lead wavefunction is not crucial, the  $\hbar$ -dependence of the width is important for the semiclassical argument which follows; note that  $a_{\text{eff}} \sim \sqrt{\hbar}$  does not depend



on a particular transverse potential.

Using this information about  $\Psi_\ell$  in the expression for  $M^{\ell \rightarrow d}$ , we see that the lead wavefunction restricts the integration to a semiclassically narrow region of width  $a_{\text{eff}} \sim \sqrt{\hbar}$ . This allows one to express the contribution of the open trajectories entering the Green function in terms of an expansion near their closed neighbors. In the resulting expression for  $\Gamma$ , the contribution of each of these closed orbits is suppressed by a factor exponentially small in  $\Delta p_y^2$ , where  $\Delta p_y$  is the change of transverse momentum after one traversal. This suppression is the effect of the mismatch of the closed orbit (momentum) with the distribution of transverse momentum at the lead, which is centered at zero with width  $\delta p_\ell \sim \hbar/a_{\text{eff}} \sim \sqrt{\hbar}$  for the lowest subband. Therefore, only closed orbits with *semiclassically* small momentum change  $\Delta p$  contribute to the width. This in turn implies that the closed orbit is located semiclassically close (within a distance  $\sim \sqrt{\hbar}$ ) to a *periodic orbit* for which  $\Delta p \equiv 0$ . Thus, one can express the tunneling width in terms of the properties of these periodic orbits, obtaining [22]

$$\Gamma = \bar{\Gamma} + \sum_{\mu:\text{p.o.}} A_\mu \cos\left(\frac{S_\mu}{\hbar} + \phi_\mu\right) \quad (6.3)$$

where the monotonic part is

$$\bar{\Gamma} = \frac{\sqrt{\pi}}{2} c_\ell^2 a_{\text{eff}} \frac{p^2}{m^*} e^{-\zeta} [I_0(\zeta) + I_1(\zeta)], \quad \zeta = \frac{p^2 a_{\text{eff}}^2}{2\hbar^2},$$

the amplitude is

$$A_\mu = 4\sqrt{2} \frac{\hbar c_\ell^2 p_z^\mu}{m^*} \left[ \text{Tr}^2 [M_\mu] (1 + \sigma_+^2) (1 + \sigma_-^2) \right]^{-1/4} \\ \times \exp \left( -\frac{\sigma_+^2 \bar{p}^2}{(1 + \sigma_+^2)} - \frac{\sigma_-^2 \bar{y}^2}{(1 + \sigma_-^2)} \right)$$

with

$$\sigma_\pm \equiv \frac{1}{2} \left[ \bar{m}_{12} - \bar{m}_{21} \pm \sqrt{(\bar{m}_{22} - \bar{m}_{11})^2 + (\bar{m}_{21} + \bar{m}_{12})^2} \right] \\ \bar{m}_{ij} \equiv \frac{2m_{ij}^\mu}{\text{Tr} [M_\mu] + 2} \left( \frac{a_{\text{eff}}^2}{\hbar} \right)^{\frac{i-j}{2}} \\ \theta \equiv \frac{1}{2} \arctan \left( \frac{\bar{m}_{22} - \bar{m}_{11}}{\bar{m}_{21} + \bar{m}_{12}} \right) \\ \bar{y} \equiv \cos \theta (y_\mu - y_\ell) / a_{\text{eff}} + \sin \theta p_y^\mu a_{\text{eff}} / \hbar \\ \bar{p} \equiv \cos \theta p_y^\mu a_{\text{eff}} / \hbar - \sin \theta (y_\mu - y_\ell) / a_{\text{eff}} ,$$

and, finally, the result for the slowly varying phase  $\phi_\mu$  will be given elsewhere. Here  $I_n$  is the Bessel function of complex argument,  $\mathbf{p}^\mu$  is the electron momentum for the periodic orbit  $\mu$  at the bounce point,  $y_\mu$  is the bounce point coordinate,  $S_\mu$  is the action of the periodic orbit, and  $M_\mu \equiv (m_{ij}^\mu)$  is the corresponding monodromy matrix [12]. The semiclassical approach used here is similar to the calculation of the tunneling current in a resonant tunneling diode in a magnetic field developed in Ref. [17] and [19].

The equation above is the main result of this paper: it expresses the modulation of the heights of the Coulomb blockade peaks by the classical periodic orbits. Note that the result

(6.3) is valid not only for chaotic but also for both integrable and mixed systems (for an integrable system or for the contributions of the remaining unbroken tori of a mixed system  $\text{Tr}[M] \equiv 2$ ).

In order to assess the validity of the semiclassical expression (6.3), we compare it to numerical calculations for two simple billiards, one integrable— the circle— and one chaotic— the stadium. The stadium billiard (Fig. 1 inset) is one of the canonical examples of a completely chaotic system [12]. From the dot wavefunctions (numerically obtained using the method of Ref. [23]),  $\Gamma$  can be calculated from Eq. (6.2) using the  $\Psi_\ell$  given above. To observe the variation in peak height, we vary the energy, or equivalently the wavevector  $k=p/\hbar$ , which changes the number of electrons on the dot as more levels are filled.

In Fig. 1 we show an example trace of  $G$  for the stadium. The calculation clearly demonstrates both strong peak-to-peak fluctuations and an oscillatory modulation of the heights (3 periods are observed). While the former comes from the quasi-random fluctuations in the wavefunctions near the leads, the large oscillatory modulation is caused by interference along the horizontal orbit which connects both leads.

Since the main theoretical result concerns the periodic modulation of the peak heights, it is natural to consider the Fourier power spectrum of  $G_{\text{peak}}(k)$ . In Fig. 2 we present a comparison of the numerical and semiclassical power spectra, calculated for both integrable (circular) and chaotic (stadium) dots. The data show that for both the circle and the stadium the power spectrum has sharp peaks corresponding to periodic orbits. More peaks appear for narrow leads [Fig. 2(a)] because the lack of momentum constraint in this regime

allows coupling to more periodic orbits. The excellent agreement between the semiclassical expression and the numerical result in all cases is a striking demonstration of the validity of our theory.

Further characterization of the peak fluctuations is shown in Fig. 3. The peak-to-peak correlation function is

$$\text{Corr}_m [\delta G, \delta G] \equiv \frac{\langle \delta G (E_{n+m}) \delta G (E_n) \rangle_n}{\langle \delta G (E_n)^2 \rangle_n}, \quad (6.4)$$

where  $\delta G (E_m) \equiv G (E_m) - \langle G (E_n) \rangle_n$  is a natural measure of the statistics of nearby peaks. A semiclassical expression for this quantity can be derived by assuming that the distribution of individual peak heights is locally Porter-Thomas [24], with the mean given by the semiclassical envelope (6.3). Indeed, as was first shown by Kaplan and Heller [15], this is generally true for wavefunction fluctuations in chaotic systems. We obtain

$$\text{Corr}_m = \delta_{m,0} + (1 - \delta_{m,0}) \times \frac{\sum_{\mu} A_{\mu}^2 \cos \left( \frac{\tau_{\mu} \Delta}{\hbar} m \right)}{4\bar{\Gamma}^2 + 3 \sum_{\mu} A_{\mu}^2}. \quad (6.5)$$

In Fig. 3(a) we compare the semiclassical correlation function with numerical data for the stadium dot. The oscillatory behavior for large separations reflects the peak in the corresponding power spectrum in Fig. 2 and is in agreement with the semiclassical result. The positive correlation for nearest neighbors is also in agreement with the semiclassical theory, demonstrating the influence of dynamics even in this apparently non-semiclassical regime.

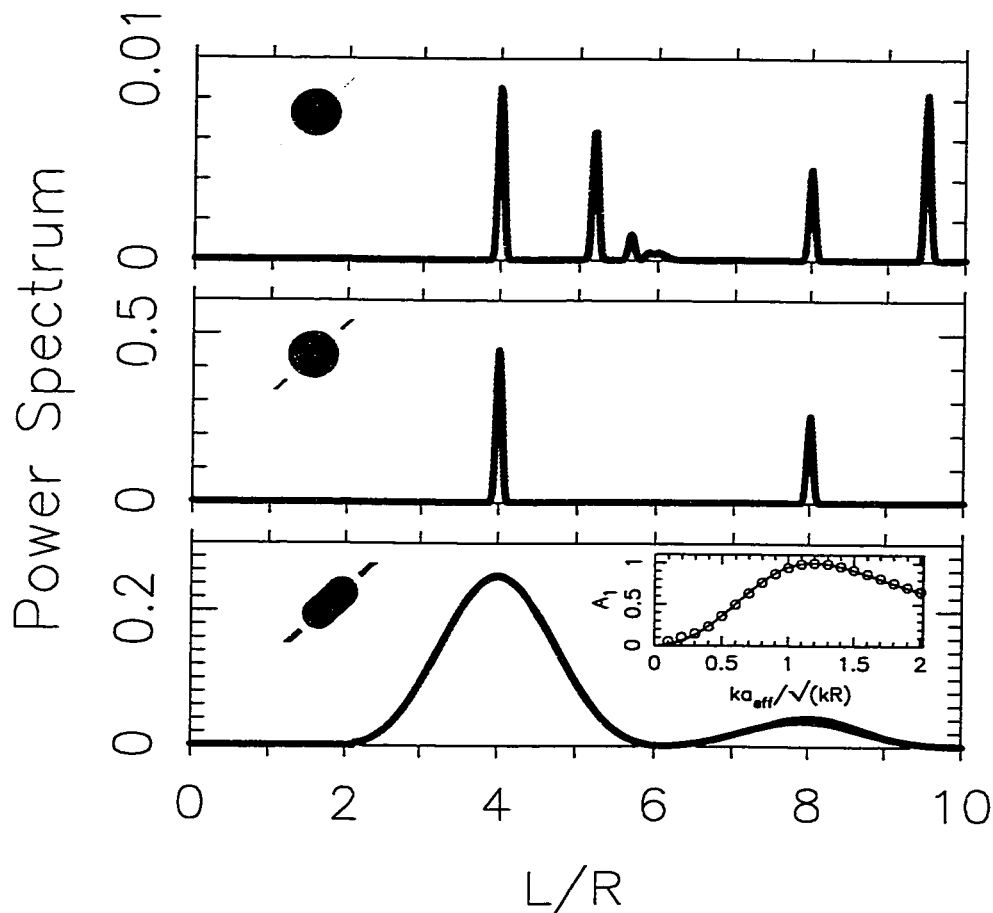


Figure 6.2: Length spectrum of the oscillations in  $G(k)$  obtained from the Fourier power, numerical (blue) and semiclassical (red) results compared. The power is normalized to the mean conductance and then this mean is removed for clarity. (a) Circular dot with narrow leads,  $ka_{\text{eff}} \approx 1.2$ , where  $a_{\text{eff}}$  is the width of the lead wavefunction. (b) Circular dot with wider leads,  $ka_{\text{eff}} \approx 12$ . (c) Stadium dot using data in Fig. 1; dependence of amplitude at  $L/R=4$  on  $ka_{\text{eff}}$  in inset. The width of the peaks reflects the length of  $G(k)$  used. More data was available for the circle because it is integrable; conservation of angular momentum allows a simple representation of the wavefunctions in terms of Bessel functions. In (a) the peak at  $L/R=4$  is the diameter, that at 8 is its repetition, those accumulating to  $2\pi$  are the whispering gallery trajectories, and the largest length peak is the star orbit. The magnitude of the oscillatory part compared to the mean depends on the strength of the coupling to the periodic orbit and so on  $a_{\text{eff}}$  as well. For the stadium, (c), the principal peak corresponds to the horizontal orbit, which appears at 4 because we use only the wavefunctions symmetric about the vertical symmetry axis (equivalent to using a half-stadium). Note the excellent agreement between the semiclassical theory and the numerical results in all cases.

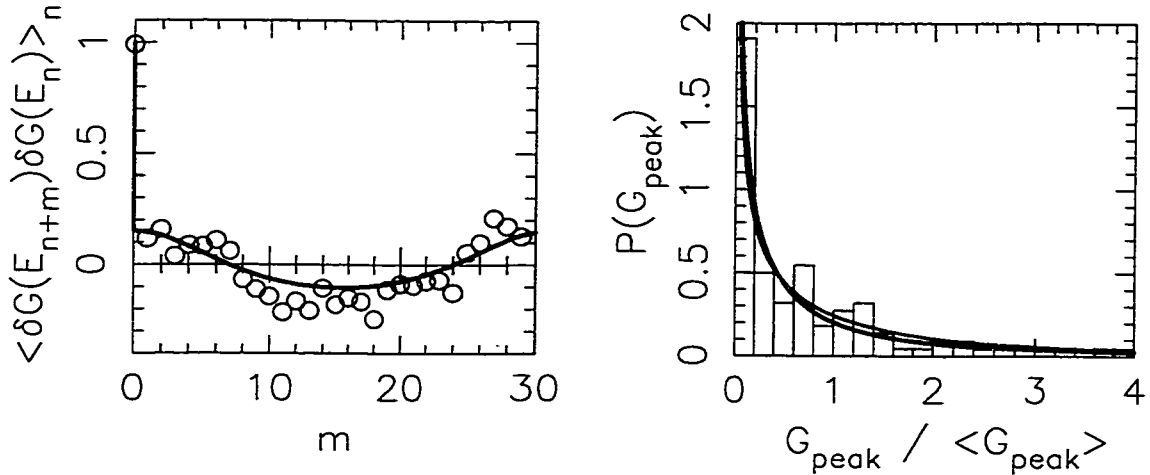


Figure 6.3: Conductance statistics: (a) peak-to-peak correlation function and (b) probability distribution of  $G$  for the stadium data in Fig. 1. The numerical correlation function (circles with typical error bars)– the average of all pairs of peaks  $m$  peaks apart– is in good agreement with the semiclassical theory (red). The agreement for small  $m$  is surprising since this regime is not semiclassical, but shows how dynamics can give rise to correlations even between nearest-neighbors. The numerical probability distribution (histogram) is for the entire range of data in Fig. 1 and is compared to both the semiclassical theory (red) and the standard statistical theory based on random wavefunctions (blue). The two theories predict nearly the same result for this quantity, and both are consistent with the numerics.

When  $T \gg \Delta$ , the major source of correlations between neighboring peaks is the joint contribution of several resonances to the same conductance peak [9]. In this regime the “nearest-neighbor” correlator is  $\text{Corr}_{m=1} \sim 1$ , and the dynamical effect accounts for only a small correction to the correlation function. However, for low temperature  $T \leq \Delta$ , the correlations due to temperature are exponentially suppressed. In this regime, the correlations induced by dynamical modulation dominate, and they account for the experimentally observed enhancement of correlations at low temperatures [8].

The probability distribution of  $G_{\text{peak}}$  over a large energy range is the main quantity considered in the previous statistical theories [2, 3]. They predict no peak-to-peak correlation or periodic modulation of the heights, and a Porter-Thomas distribution:  $P(G_{\text{peak}}) = \sqrt{4/\pi G_{\text{peak}}} \exp(-G_{\text{peak}})$ . Considering an energy range larger than any period in Eq. (6.3), we find, in contrast, that the distribution should be locally Porter-Thomas but with the mean modulated by the periodic components, as in Ref. [15]. Curiously, the resulting distribution is not very different from Porter-Thomas: Fig. 3 (b) shows that the two theories predict nearly the same result, and both are consistent with numerical calculation. This explains why no dynamical effect was observed in the experimental peak-height probability distribution [5, 6].

In contrast, the periodic modulation of the peak heights has been observed in several recent experiments [6–8]. The clearest observation is in Ref. [8]: the data in their Fig. 1 show modulated peak heights as a function of the number of electrons in the dot. In their trace of 90 peaks, approximately six oscillations are visible, yielding a period of  $\sim 15$  peaks.

In our treatment, this period is the ratio of the period of fundamental oscillation in Eq. (6.3) to the level spacing  $\Delta$ . The fundamental period is given by  $(\frac{1}{\hbar} \frac{\partial S_\mu}{\partial \epsilon})^{-1} \equiv \hbar/\tau_\mu$  where  $\tau_\mu$  is the period of the relevant orbit. To determine  $\tau_\mu$ , we use the billiard approximation:  $L_\mu \equiv v_F \tau_\mu$ , where  $L_\mu$  is the length of the shortest orbit and  $v_F$  is the Fermi velocity. We use the micrograph of the dot to estimate  $L_\mu$  for the  $V$ -shaped orbit connecting the two leads, and calculate  $v_F$  from the experimental density [25]. Using the appropriate spin-resolved level spacing  $\Delta = 10 \mu\text{eV}$  (which is half of the spin-full value from excitation measurements in Ref. [8]), we find  $\hbar/\tau_\mu \Delta \approx 12$ . Because the billiard approximation underestimates the period in a soft wall potential, this is a lower bound for the modulation period, and therefore our theory is in good agreement with the experiment.

Similarly, we make estimates which are consistent with the other two experiments showing variation as a function of number of electrons [5, 6]. A similar approach to the peak modulation as a function of magnetic field is in agreement with the experimental results [6, 7] as well.

We close with two further experiments suggested by our results. First, if the tuning parameter used to change the number of electrons, such as a gate voltage, does not change the action of the dominant periodic orbit, then no modulation connected to that orbit should be seen. In particular, gates which affect different parts of the dot may produce different oscillatory behavior. Second, several samples made in a robust geometry— a circle with directly opposite leads, for example— should show the same modulation. Any deviations from the same behavior would be a sensitive indication of the material quality.



We gratefully acknowledge stadium eigenfunction calculations by J. H. Lefebvre, helpful discussions with C. M. Marcus, the hospitality of the Aspen Center for Physics where this work was initiated, and support from the US ONR and the US NSF.

## References

- [1] H. Grabert and M. H. Devoret, *Single Charge Tunneling: Coulomb Blockade Phenomena in Nanostructures* (Plenum Press, New York, 1992).
- [2] R. A. Jalabert, A. D. Stone, and Y. Alhassid, *Phys. Rev. Lett.* **68**, 3468 (1992).
- [3] L. P. Kouwenhoven, C. M. Marcus, P. L. McEuen, S. Tarucha, R. M. Westervelt, and N. S. Wingreen, in *Mesoscopic Electron Transport*, edited by L. L. Sohn, L. P. Kouwenhoven, and G. Schön (Kluwer, Dordrecht, 1997) pp. 105-214.
- [4] M. Stopa, *Physica B* **251**, 228 (1998).
- [5] A. M. Chang, H. U. Baranger, L. N. Pfeiffer, K. W. West, and T. Y. Chang, *Phys. Rev. Lett.* **76**, 1695 (1996).
- [6] J. A. Folk, S. R. Patel, S. F. Godijn, A. G. Huibers, S. M. Cronenwett, and C. M. Marcus, *Phys. Rev. Lett.* **76**, 1699 (1996).
- [7] S. M. Cronenwett, S. R. Patel, C. M. Marcus, K. Campman, and A. G. Gossard, *Phys. Rev. Lett.* **79**, 2312 (1997).

- [8] S. R. Patel, D. R. Stewart, C. M. Marcus, M. Gökcedag, Y. Alhassid, A. D. Stone, C. I. Duruöz, and J. S. Harris, Jr., *Phys. Rev Lett.* **81**, 5900 (1998).
- [9] Y. Alhassid, M. Gokcedag, and A. D. Stone, *Phys. Rev. B* **58**, 7524 (1998).
- [10] M. Stopa, *Phys. Rev. B* **54**, 13767 (1996).
- [11] G. Hackenbroich, W. D. Heiss, and H. A. Weidenmüller, *Phys. Rev. Lett.* **79**, 127 (1997).
- [12] M. Gutzwiller, *Chaos in Classical and Quantum Mechanics* (Springer, New York, 1990).
- [13] J. B. Delos and C. D. Schwieters, in *Classical, Semiclassical and Quantum Dynamics in Atoms*, Lecture notes in physics **485**, ed. by H. Friedrich and B. Eckhardt, p. 223-247, Springer (1997); M. W. Beims, V. Kondratovich, and J. B. Delos, *Phys. Rev. Lett.* **81**, 4537 (1998).
- [14] E. J. Heller, in *Chaos and Quantum Physics*, edited by M. J. Giannoni, A. Voros, and J. Zinn-Justin (Elsevier, Amsterdam, 1991) pp. 547-663.
- [15] L. Kaplan, *Phys. Rev. Lett* **80**, 2582 (1998); L. Kaplan, and E. J. Heller, *Annals of Phys.* **264**, 171 (1998).
- [16] D. Weiss, K. Richter, A. Menschig, R. Bergmann, H. Schweizer, K. von Klitzing and G. Weimann, *Phys. Rev. Lett.* **70**, 4118 (1993); G. Hackenbroich, and F. von Oppen, *Europhys. Lett.*, **29**, 151 (1995); K. Richter, *Europhys. Lett.* **29**, 7 (1995).

- [17] E. E. Narimanov, A. D. Stone, and G. S. Boebinger, *Phys. Rev. Lett.* **80**, 4024 (1998);  
an alternative semiclassical theory of resonant magnetotunneling was developed by  
E. B. Bogomolny, and D. C. Rouben, *Europhys. Lett.* **43**, 111 (1998).
- [18] T. S. Monteiro, D. Delande, A. J. Fisher, G. S. Boebinger, *Phys. Rev. B* **56**, 3913 (1996).
- [19] E. E. Narimanov, and A. D. Stone, to be published in *Physica D*; also preprint cond-  
mat/9808161.
- [20] C. W. J. Beenakker, *Phys. Rev. B* **44**, 1646 (1991).
- [21] J. Bardeen, *Phys. Rev. Lett.* **6**, 57 (1961).
- [22] The expressions given for  $\bar{\Gamma}$  and  $A$  are for tunneling from a single subband in the lead.  
The generalization to many subbands is straightforward.
- [23] T. Szeredi, J. H. Lefebvre, D. A. Goodings, *Nonlinearity* **7**, 1463 (1994).
- [24] L. E. Reichl, *The Transition To Chaos* (Springer-Verlag, New York, 1992).
- [25] C. M. Marcus, private communication.

## Chapter 7

# Semiclassical Theory of Coulomb Blockade Peak Heights in Chaotic Quantum Dots \*

By Evgenii E. Narimanov,<sup>1</sup> Harold U. Baranger,<sup>2</sup> Nicholas R. Cerruti<sup>3</sup>

and Steven Tomsovic<sup>3</sup>

<sup>1</sup>Bell Laboratories – Lucent Technologies, 700 Mountain Ave.,

Murray Hill, NJ 07974

<sup>2</sup>Dept. of Physics, Duke University, Durham, NC 27708

<sup>3</sup>Dept. of Physics, Washington State University, Pullman, WA 99164-2814

In Preparation for Submittal to Physical Review B

## 7.0 Abstract

We develop a semiclassical theory of Coulomb blockade peak heights in chaotic quantum dots. Using Berry's conjecture, we calculate the peak height distributions and the correlation functions. We demonstrate that the corrections to the corresponding results of the standard statistical theory are non-universal and can be expressed in terms of the classical periodic

---

\*Modifications have been made to the manuscript without two of the authors reviewing the changes.

orbits of the dot that are well coupled to the leads. The effect is substantial for both symmetric and asymmetric lead placement.

## 7.1 Introduction

The Coulomb blockade is a fundamentally classical effect in microstructures—the addition of an electron to an isolated microstructure requires a certain amount of electrostatic energy, the charging energy  $e^2/2C$  where  $C$  is the capacitance of the structure. It is the simplest effect of electron charge in microstructures and has been extensively studied with regard to both fundamentals and applications in single electron transistors [1]. One common way to study the Coulomb blockade is by measuring the conductance through a nearly isolated nanoparticle (using tunneling contacts) as a function of a gate voltage which tunes the electrostatic potential of the particle. For most values of the gate voltage, the conductance is very small since the flow of electrons is blocked because the charging energy is not available. However, when the gate voltage is tuned so that states differing by one charge have the same energy, there is a peak in the conductance. The height of this peak is simply the conductance of the two tunnel barriers in series, and the spacing of the peaks is uniform with separation  $e^2/C$ .

For the smallest quantum dots and at low temperature, however, quantum mechanical interference becomes important. Interference causes variation in both the height and spacing of the conductance peaks. For the spacing, single particle quantization and the residual interactions among the electrons are important. For the height, the nature of the wave-

functions become critical: if the wave function of the state at the chemical potential is poorly coupled to the leads—if it has nodes at the leads—then the conductance peak is small, but if the wave function is well coupled to the leads then the peak is large. In this paper, we restrict our attention to fluctuations in the conductance peak heights and investigate what this tells us about wave functions in quantum dots.

Since dots are generally irregular in shape, the classical dynamics of the electrons is chaotic, and so the characteristics of Coulomb blockade peaks reflect those of wave functions in chaotic systems [2–4]. Previously, a statistical theory for the peaks was developed [2, 3] by assuming these wave functions to be completely random and uncorrelated with each other. The random matrix theory used was known to be a good description of energy level statistics, and so likely to be reasonable for wave functions. The experimental data [5, 6] for the distribution of the Coulomb blockade peak heights were found to be in excellent agreement with the predictions of the statistical theory, thus supporting the conjecture of effective “randomness” of the quantum dot wave functions.

A potential problem with the statistical theory was, however, evident in one of the first experiments: there is no correlation between wave-functions in random matrix theory so the statistical theory predicted zero correlation between neighboring conductance peaks, but in one of the experiments [6] correlation was clearly present in the form of a slowly varying envelope modulating the peak heights. In subsequent years a number of different effects were investigated as candidates to explain this correlation. The simplest is the effect of nonzero temperature: since excitation above the Fermi level is possible, several resonances contribute

to each peak and a given resonance contributes to several neighboring conductance peaks, inducing correlation. However, in a detailed study, this was found to be insufficient to account for the observed correlations [7]. Other explanations that were explored include correlation due to spin-paired levels [7, 8], due to a decrease of the effective level spacing found in density functional calculations [9], and due to level anticrossings in interacting many-particle systems [10]. While these latter explanations rely on subtle electron-electron interaction effects, here we argue that peak height correlations already arise within an effective single-particle picture of the electrons in the quantum dot. The specific internal dynamics of the dot, even though it is chaotic, modulates the peaks: because all systems have short-time dynamical features, chaos is not equivalent to randomness.

While the statistical theory is “universal” in that it depends on no specific features of the quantum dot at hand, the classical dynamics in the dot is clearly not universal. Thus, while correlations between the conductance peak heights are generally present in quantum dots, the particular correlations in a given dot are not universal but rather involve detailed information about the dot. The simplest information to include is the spatial correlation function of the wave functions: this is very short length dynamical information. Going beyond this, we use semiclassical techniques to derive a relation between the quantum conductance peak height and the classical periodic orbits in the dot.

The main result is that as a system parameter varies—the magnetic field, for instance, or the number of electrons in the dot (controlled by varying a gate voltage)—the interference around each periodic orbit oscillates between being destructive and constructive. When



the interference is constructive for those periodic orbits which come close to the leads used to contact the dot, the wave function is enhanced near the leads, the dot-lead coupling is stronger, and so the conductance is larger. Likewise, destructive interference produces a smaller conductance. The resulting modulation at frequencies corresponding to the periodic orbits can be substantial. Because of dephasing effects, only the short periodic orbits, indeed perhaps only the shortest one, is likely to be significant.

Similar short-time dynamical effects have been noted in other contexts such as atomic and molecular spectra [11–13], eigenfunction scarring [13, 14], magnetotransport in antidot lattices [15], and tunneling into quantum wells [16–19]. The periodic orbit modulation that we discuss here is completely omitted in theories in which the wave function is assumed to change randomly as the system changes [2, 3]. Reassuringly, the predicted dynamical modulation is of the type in the original anomalous experiment [6]. More recently, other experimental data has been published which show the effect [8, 20], but to date no systematic experimental study of this effect has been performed.

In the rest of this paper, we present the calculation of the periodic modulation of the conductance peak heights and then compare it to numerical results. A few of the results have been briefly reported previously [21]. However, the derivation given here is completely different from the previous one which relied on the methods of Ref. [19]: here our approach in terms of a statistical ansatz for the wave functions yields more results for chaotic systems but misses the results for regular systems that we obtained previously. In the first section we express the height of the conductance peak in terms of the resonant wave function.

The basic ansatz for the distribution of the wave functions, including dynamical effects, is presented in Section 7.3. In Section 7.4 our results for the conductance peak heights are obtained. Comparison to numerical results for the stadium billiard in Section 7.5 confirms the adequacy of the semiclassical approach. Finally, we close with a summary and discussion of future directions.

## 7.2 The Height of a Conductance Peak in Coulomb Blockade

Our starting point is the connection between the Coulomb blockade peak heights and the width of the level in the quantum dot. This connection is well-known [22]; it allows us to express the conductance in terms of single-particle quantities. We consider a dot close to two leads so that the width,  $\Gamma$ , of a level comes from tunneling of the electron to either lead. When the mean separation of levels is larger than the temperature  $T$  which itself is much larger than the mean width, the electrons pass through a single quantized level in the dot, and the conductance peak height is [22]

$$G_{\text{peak}} = \frac{e^2}{h} \frac{\pi}{2kT} \frac{\Gamma_1 \Gamma_2}{\Gamma_1 + \Gamma_2} \quad (7.1)$$

where  $\Gamma_1$  and  $\Gamma_2$  are the partial decay widths due to the tunneling into a single lead and spin degrees of freedom are neglected. In particular, when the leads are identical and sym-

metrically attached to the dot,

$$G_{\text{peak}} = \frac{e^2}{h} \frac{\pi}{4kT} \Gamma_1 \quad (7.2)$$

The partial width is related by Fermi's Golden Rule to the square of the matrix element for tunneling between the lead and the dot,  $M^{\ell \rightarrow d}$ . A convenient expression for the matrix element in terms of the lead and dot wave functions,  $\Psi_\ell$  and  $\Psi_d$ , respectively, was derived by Bardeen [23] and can be expressed as [16, 17]

$$M^{\ell \rightarrow d} = \frac{\hbar^2}{m_*} \int_S d\mathbf{r} \Psi_\ell(\mathbf{r}) \nabla \Psi_d(\mathbf{r}) \quad (7.3)$$

where the surface  $S$  is the edge of the quantum dot. The partial width,  $\Gamma$ , then, depends on the square of the normal derivative of the dot wave function at the edge weighted by the lead wave function. The dot wave function  $\Psi_d$  in (7.3) is calculated for the effective potential, which accounts for interactions in the dot in the mean-field approximation. For the partial width we then obtain

$$\Gamma_\alpha[\Psi_d] = \frac{2\pi\hbar^4}{m_*^2} \sum_\ell \rho_\ell^{(\alpha)} \int_S d\mathbf{r}_1 \cdot \nabla \Psi_d(\mathbf{r}_1) \int_S d\mathbf{r}_2 \cdot \nabla \Psi_d(\mathbf{r}_2)^* [\Psi_\ell^{(\alpha)}(\mathbf{r}_1)^* \Psi_\ell^{(\alpha)}(\mathbf{r}_2)] \quad (7.4)$$

where  $\alpha$  is the index of the lead, the integer  $\ell$  represents different transverse subbands in the lead, and  $\rho_\ell$  is the density of states in the lead for a given subband. To obtain the statistics of the conductance peak heights, we thus need to know the statistical properties of the dot

wave functions  $\Psi_d$ .

### 7.3 Wave functions in the Dot: The Statistical Description

For a *single* dot, we consider an ensemble of Coulomb blockade peaks—measured either in a narrow interval of gate voltage or obtained by following a single resonance under continuously changing magnetic field. The wave functions associated with the peaks of the conductance will vary—or “fluctuate”—in a way characterized by a distribution  $P[\psi]$  which we seek.

It was first conjectured by M. V. Berry that the wave functions of a classically chaotic system fluctuate with certain universal properties and can be characterized as random variables [24]. This is the foundation of the first statistical theory of peak heights [2]. Subsequently, the statistical ansatz made by Berry has been further developed. One direction of refinement is the incorporation of some short length-scale aspects of the real classical dynamics. First, a constraint of an arbitrary correlation function

$$C(\mathbf{r}_1, \mathbf{r}_2) \equiv \int \mathcal{D}\psi P[\psi] \psi^*(\mathbf{r}_1) \psi(\mathbf{r}_2) \quad (7.5)$$

was incorporated into the ansatz [25, 26]. By using the correlation function of a random superposition of plane waves, the probability distributions of level-widths and conductance peaks in the case of multi-mode leads to the quantum dot were found [25]. A distribution similar to this ansatz was derived microscopically for disordered systems, a specific kind of

chaotic system, using the nonlinear sigma model [27–30].

The next step was to constrain the correlation function by the short-time classical dynamics. Using the short-path semiclassical correlation, Srednicki and coworkers [31, 32] studied correlations in chaotic eigenfunctions at large separations and found that the predicted correlations are in excellent agreement with numerical calculations in chaotic billiards [31]. This semiclassically constrained ansatz for  $P[\psi]$  is much harder to justify—certainly no derivation in disordered systems can be made. However, progress towards this goal has been achieved by Kaplan and Heller by treating the nonlinear effects of classical recurrences [14]. In a recent paper by Kaplan [33] short-time dynamics were incorporated into the general probability distribution of Ref. [25] to improve the random matrix theory results for the conductance peak height statistics.

Here we use a maximum entropy technique to derive the specific form of the distribution  $P[\psi]$  that we need [34]. An advantage of this approach is that arbitrary constraints can be introduced, as in the case of normalization which we discuss below. We make the following ansatz: the distribution  $P[\psi]$  maximizes the information entropy [35]

$$H = - \int \mathcal{D}\psi P[\psi] \log P[\psi] \quad (7.6)$$

within the space allowed by the constraints. Here the measure corresponding to the distribution  $P[\psi]$  is defined in the standard way [32]

$$\mathcal{D}\psi_d = \lim_{N \rightarrow \infty} \prod_{n=1}^N d\psi_d(\mathbf{r}_n) \quad (7.7)$$

so that the product  $P[\psi_d] \mathcal{D}\psi_d$  represents the probability that a wave function  $\psi(\mathbf{r})$  of the original ensemble is between  $\psi_d(\mathbf{r})$  and  $\psi_d(\mathbf{r}) + d\psi_d(\mathbf{r})$  for any point  $\mathbf{r}$  inside the dot.

Assuming that the *only* constraint imposed on the ensemble of wave functions is the correlation function  $C(\mathbf{r}_1, \mathbf{r}_2)$ , the maximum of the functional (7.6) under the constraint (7.5) is equivalent to the extremum of the functional

$$F[\psi] = \int \mathcal{D}\psi [-P[\psi] \log P[\psi] - \int d\mathbf{r}_1 \int d\mathbf{r}_2 \lambda(\mathbf{r}_1, \mathbf{r}_2) \{\psi^*(\mathbf{r}_1) \psi(\mathbf{r}_2) P[\psi] - C(\mathbf{r}_1, \mathbf{r}_2)\}] \quad (7.8)$$

where the Lagrange multiplier  $\lambda(\mathbf{r}_1, \mathbf{r}_2)$  can then be determined from Eq. (7.5). Setting the first variation of  $F[\psi]$  equal to zero, we find that  $P[\psi]$  is Gaussian. The final result, obtained by substituting Eq. (7.5) to find  $\lambda(\mathbf{r}_1, \mathbf{r}_2)$ , is

$$P[\psi] = A \exp \left[ -\frac{\beta}{2} \int d\mathbf{r}_1 \int d\mathbf{r}_2 \psi^*(\mathbf{r}_1) C^{-1}(\mathbf{r}_1, \mathbf{r}_2) \psi(\mathbf{r}_2) \right] \quad (7.9)$$

where  $A$  is the normalization (independent of  $\psi(\mathbf{r})$ ) and  $C^{-1}$  is the functional inverse of the of the two-point correlation function  $C(\mathbf{r}_2, \mathbf{r}_1 | \varepsilon)$

$$\int d\mathbf{r}_3 C^{-1}(\mathbf{r}_1, \mathbf{r}_3) C(\mathbf{r}_3, \mathbf{r}_2) = \delta(\mathbf{r}_1 - \mathbf{r}_2) . \quad (7.10)$$

The coefficient  $\beta = 1$  for a system with time-reversal invariance, when the wave functions can be chosen real, and  $\beta = 2$  otherwise.

It has been shown [32] that in the small- $\hbar$  limit for classically chaotic systems, the correlation function  $C(\mathbf{r}_2, \mathbf{r}_1)$  can be expressed in terms of the semiclassical approximation to the Green function [11]  $G_{\text{sc}}(\mathbf{r}_2, \mathbf{r}_1)$  as

$$C(\mathbf{r}_2, \mathbf{r}_1) = \frac{1}{\pi \bar{\rho}_{\text{sc}}} \text{Im} G_{\text{sc}}(\mathbf{r}_2, \mathbf{r}_1) + \mathcal{O}(\hbar^{3/2}), \quad (7.11)$$

where  $\bar{\rho}_{\text{sc}}(\varepsilon)$  is the smooth part of the density of states (DOS) in the dot, given by the leading order (Thomas-Fermi) semiclassical approximation to the DOS.

In the semiclassical approximation, the energy-averaged Green function can be expressed in terms of the classical trajectories (labeled by the index  $j$ ) [11, 36],

$$G_{\text{sc}}(\mathbf{r}_2, \mathbf{r}_1) = G_0(\mathbf{r}_2, \mathbf{r}_1) + \frac{1}{i\hbar} \frac{1}{\sqrt{2\pi i\hbar}} \sum_j \sqrt{|D_j|} \exp\left(i\frac{S_j}{\hbar} - in_j \frac{\pi}{4}\right) \exp\left(-\frac{\tau_j^2 W^2}{2\hbar^2}\right) \quad (7.12)$$

where  $S_j = S_j(\mathbf{r}_2, \mathbf{r}_1)$  is the classical action,  $\tau_j$  is the period, the integer  $n_j$  is the topological index [11] of the trajectory  $j$ , and the amplitude  $D_j$  is

$$D_j = \det \begin{pmatrix} \frac{\partial^2 S_j(\mathbf{r}_2, \mathbf{r}_1)}{\partial \mathbf{r}_2 \partial \mathbf{r}_1} & \frac{\partial^2 S_j(\mathbf{r}_2, \mathbf{r}_1)}{\partial \varepsilon \partial \mathbf{r}_1} \\ \frac{\partial^2 S_j(\mathbf{r}_2, \mathbf{r}_1)}{\partial \varepsilon \partial \mathbf{r}_2} & \frac{\partial^2 S_j(\mathbf{r}_2, \mathbf{r}_1)}{\partial \varepsilon^2} \end{pmatrix}. \quad (7.13)$$

The last exponential in Eq. (7.12) is due to a Gaussian averaging over an energy window of width  $W$ , and we have specialized to two spatial dimensions. The energy windowing includes only contributions from the short orbits; the oscillations caused by the longer orbits are damped out by the averaging, but their fluctuations are included in the statistical arguments.

Without the windowing every conductance peak would be uniquely defined by the Green function and we would have to calculate the orbits of every period. The function  $G_0(\mathbf{r}_2, \mathbf{r}_1)$  is the contribution of the non-classical so-called “zero-length” trajectories, those with actions less than or of order  $\hbar$ . Therefore,  $G_0(\mathbf{r}_2, \mathbf{r}_1)$  cannot be obtained using the stationary-phase approximation, but may be evaluated [24, 32] by replacing the actual propagator  $\langle \mathbf{r}_2 | \exp(-iHt/\hbar) | \mathbf{r}_1 \rangle$  by its free space analog

$$\langle \mathbf{r}_2 | \exp\left(-\frac{iHt}{\hbar}\right) | \mathbf{r}_1 \rangle \approx \int \frac{d\mathbf{p}}{(2\pi\hbar)^2} \exp\left(i\frac{\mathbf{p} \cdot (\mathbf{r}_2 - \mathbf{r}_1)}{\hbar}\right) \exp\left(-\frac{iH(\mathbf{p}, \mathbf{r}_0)t}{\hbar}\right) \quad (7.14)$$

where  $\mathbf{r}_0 \equiv (\mathbf{r}_2 + \mathbf{r}_1)/2$ . The corresponding Green function is then

$$G_0(\mathbf{r}_2, \mathbf{r}_1) = \int \frac{d\mathbf{p}}{(2\pi\hbar)^2} \exp\left(i\frac{\mathbf{p} \cdot (\mathbf{r}_2 - \mathbf{r}_1)}{\hbar}\right) \frac{1}{\varepsilon - H(\mathbf{p}, \mathbf{r}_0) + i0}. \quad (7.15)$$

Note that because of the short trajectory involved, this part of the Green function varies very smoothly as a function of energy. The smooth part of the correlation function which results is

$$C_0(\mathbf{r}_2, \mathbf{r}_1) = \frac{1}{\bar{\rho}_{sc}} \int \frac{d\mathbf{p}}{(2\pi\hbar)^2} \cos\left(\frac{\mathbf{p} \cdot (\mathbf{r}_2 - \mathbf{r}_1)}{\hbar}\right) \delta(\varepsilon - H(\mathbf{p}, \mathbf{r}_0)) \quad (7.16)$$

and so  $C_0(\mathbf{r}_2, \mathbf{r}_1) \propto J_0(p|\mathbf{r}_2 - \mathbf{r}_1|/\hbar)$ . This smooth part of the correlation function is rather local in that it decays monotonically with separation.



Having fully specified the correlation function we wish to use, we finally obtain

$$P(\psi_d|\varepsilon) \sim \exp \left[ -\frac{\beta}{2} \int d\mathbf{r}_1 \int d\mathbf{r}_2 \psi^*(\mathbf{r}_1) G_{sc}^{-1}(\mathbf{r}_2, \mathbf{r}_1|\varepsilon) \psi(\mathbf{r}_2) \right]. \quad (7.17)$$

The general ensemble defined by the distribution (7.9) has, however, certain limitations. Strictly speaking, in its general form this ensemble is only suitable for calculations of those observables which can be represented in terms of only two-point products  $\psi^*(\mathbf{r}_1)\psi(\mathbf{r}_2)$ . The reason for this problem is as follows: instead of the proper normalization of *each member of the ensemble*,

$$\int d\mathbf{r} |\psi(\mathbf{r})|^2 = 1, \quad (7.18)$$

the normalization of the wave functions is satisfied *only on average*,

$$\int \mathcal{D}\psi(\mathbf{r}) P[\psi(\mathbf{r})] \int d\mathbf{r} |\psi(\mathbf{r})|^2 = 1. \quad (7.19)$$

As a result, the higher order moments,  $\Delta_n \equiv \langle \int d\mathbf{r}_1 \dots \int d\mathbf{r}_n |\psi(\mathbf{r}_1)|^2 \dots |\psi(\mathbf{r}_n)|^2 \rangle_\psi$ , of the distribution are different from unity. Therefore, in its general form, the ensemble defined by (7.9) is not suitable for calculations which are sensitive to the  $n > 1$  moments of the distribution  $P[\psi]$ , such as for the description of the residual interactions in quantum dots [37–39].

The method developed in this section yields a straightforward way to generalize the

distribution (7.9) to properly account for the higher moments. For example, adding an additional constraint

$$\int \mathcal{D}\psi P[\psi] \int d\mathbf{r}_1 \int d\mathbf{r}_2 |\psi(\mathbf{r}_1)|^2 |\psi(\mathbf{r}_2)|^2 = 1, \quad (7.20)$$

to the variational problem (7.6) will yield a generalization of the distribution (7.17) which properly accounts for the moment  $\Delta_2$ .

Note in contrast that the errors in the higher moments,  $n > 1$ , produced by the *semi-classical* distribution (7.17) are of higher order in  $\hbar$ ,  $\delta_n \sim \mathcal{O}(\hbar^2)$ , than the terms taken into account in  $G_{sc}$  [40]. As long as these higher-order corrections are not relevant for the quantity under consideration, one can generally use the *semiclassical* distribution (7.17).

## 7.4 Peak Heights Distribution

Since the Coulomb blockade peak heights are uniquely determined by the corresponding dot wave functions  $\psi_d$ , the peak heights distribution function  $P(G)$  is given by

$$P(G) = \int \mathcal{D}\psi_d P(\psi_d) \delta(G - G_{\text{peak}}[\psi_d]) \quad (7.21)$$

where  $G_{\text{peak}}[\psi]$  is determined by Eqs. (7.1), (7.2), and (7.4).

The width  $\Gamma$  depends only on the wave function near the boundary of the quantum dot, as follows from Eq. (7.4). If the function  $P_S(\bar{\psi})$  represents the distribution of the wave

functions in a narrow strip  $S$  along the boundary of the quantum dot, so that

$$\psi(\mathbf{r}) = \begin{cases} \bar{\psi}(\mathbf{r}), & \mathbf{r} \in S \\ \hat{\psi}(\mathbf{r}), & \mathbf{r} \notin S \end{cases}, \quad (7.22)$$

then the conductance distribution is

$$P(G) = \int \mathcal{D}\bar{\psi} P_S[\bar{\psi}|\varepsilon] \delta(G - G_{\text{peak}}[\bar{\psi}]) . \quad (7.23)$$

The “edge” distribution  $P_S$  can be obtained from the general distribution  $P[\psi]$  by integrating out the values of  $\hat{\psi}$ ,

$$P_S[\bar{\psi}] = \int \mathcal{D}\hat{\psi} P[\psi\{\bar{\psi}, \hat{\psi}\}] . \quad (7.24)$$

As the distribution  $P[\psi]$  is Gaussian, the resulting functional integral can be calculated exactly, yielding

$$P_S[\bar{\psi}] = A_S \exp \left[ -\frac{\beta}{2} \int_S d\mathbf{q}_1 \int_S d\mathbf{q}_2 \bar{\psi}^*(\mathbf{q}_1) \bar{K}(\mathbf{q}_1, \mathbf{q}_2) \bar{\psi}(\mathbf{q}_2) \right] \quad (7.25)$$

where

$$\bar{K}(\mathbf{q}_1, \mathbf{q}_2) = C^{-1}(\mathbf{q}_1, \mathbf{q}_2) + \int_{\Omega \setminus S} d\mathbf{q}_3 \int_{\Omega \setminus S} d\mathbf{q}_4 C^{-1}(\mathbf{q}_1, \mathbf{q}_3) C(\mathbf{q}_3, \mathbf{q}_4) C^{-1}(\mathbf{q}_4, \mathbf{q}_2) \quad (7.26)$$

and  $A_S$  is the new normalization constant. The spatial integrals are over the part of the

total space  $\Omega$  which is orthogonal to the edge  $S$ .

As follows from Eqs. (7.11)-(7.12), the “non-diagonal” part of the correlation function is of a higher order in  $\hbar$ ,  $\sim \mathcal{O}(\sqrt{\hbar})$ , compared to the “diagonal” part,  $C_0 \sim \mathcal{O}(1)$ . The second term in Eq. (7.26) involves the correlation functions  $C(\mathbf{q}_1, \mathbf{q}_3)$  and  $C(\mathbf{q}_4, \mathbf{q}_2)$ , taken between the points of the *different* parts of the dot, the edge strip  $S$  for one coordinate and the internal region  $\Omega \setminus S$  for the other. It is therefore of higher order in  $\hbar$ ,  $\sim \mathcal{O}(\hbar)$ , than the first contribution,  $C^{-1}(\mathbf{q}_1, \mathbf{q}_2) \sim \delta(\mathbf{q}_2 - \mathbf{q}_1)\mathcal{O}(1) + \mathcal{O}(\sqrt{\hbar})$ . Keeping such higher-order terms is not consistent with the leading-order semiclassical approximation we used for  $C(\mathbf{q}_1, \mathbf{q}_2)$ .

We therefore obtain

$$P_S[\bar{\psi}] = A_S \exp \left[ -\frac{\beta}{2} \int_S d\mathbf{q}_1 \int_S d\mathbf{q}_2 \bar{\psi}^*(\mathbf{q}_1) C^{-1}(\mathbf{q}_1, \mathbf{q}_2) \bar{\psi}(\mathbf{q}_2) \right]. \quad (7.27)$$

An alternative to the argument given here proceeds by noting that integrating out  $\hat{\psi}$  should yield a Gaussian in  $\bar{\psi}$ , and that this Gaussian, by construction of the ensemble, must reproduce the correct two point correlation function  $C(\mathbf{q}_1, \mathbf{q}_2)$ . This alternative argument [26] immediately yields the functional form (7.27).

When the *closed* dot is defined by the Dirichlet boundary conditions, the wave function in the narrow strip  $S$  near the “edge” can be represented as

$$\bar{\psi} = z\varphi(y) \quad (7.28)$$

where  $y$  is the coordinate along the boundary of the dot and  $z$  is in the direction of the

normal. In this limit, the correlation function is

$$C(\mathbf{q}_1, \mathbf{q}_2) = z_2 z_1 \partial_n C(y_1, y_2) \quad (7.29)$$

where  $\partial_n C(y_1, y_2)$  is defined as the correlation function of the normal derivatives of the wave function at the boundary of the dot and can be obtained as

$$\partial_n C(y_2, y_1) = \frac{1}{\pi \bar{\rho}_{\text{sc}}} \text{Im} \partial_n G_{\text{sc}}(y_2, y_1) + \mathcal{O}(\hbar^{(d+1)/2}) \quad (7.30)$$

where

$$\partial_n G(y_2, y_1 | \varepsilon) \equiv \sum_m \frac{\partial_n \psi_m^*(y_2, 0) \partial_n \psi_m(y_1, 0)}{\varepsilon_m - \varepsilon + i0}. \quad (7.31)$$

The semiclassical approximation  $\partial_n G_{\text{sc}}$  for the normal derivative Green function was derived in Ref. [19]:

$$\begin{aligned} \partial_n G_{\text{sc}}(y_2, y_1) &= \partial_n G_0(y_2, y_1) + \frac{4}{i\hbar^3} \frac{1}{\sqrt{2\pi i\hbar}} \sum_j [\mathbf{p}_j(y_1)]_n [\mathbf{p}_j(y_2)]_n \\ &\quad \times \sqrt{|D_j|} \sin\left(\frac{S_j}{\hbar} - \bar{n}_j \frac{\pi}{4}\right) \exp\left(-\frac{\tau_j^2 W^2}{2\hbar^2}\right) \end{aligned} \quad (7.32)$$

where  $\bar{n}_j$  and  $[\mathbf{p}_j]_n$  are, respectively, the Maslov index [11] and the normal component of the classical momentum of the trajectory  $j$ .

In order to connect the dot wave functions to the lead, let  $\{\phi_m(y)\}$  be the complete

orthogonal set of the wave functions corresponding to the transverse potential of the lead. Using this basis, we represent the function  $\varphi(y)$  as

$$\varphi(y) = \sum_{m=0}^{\infty} a_m \phi_m(y - y_\ell) \quad (7.33)$$

where  $y_\ell$  is the contact point of the lead. Assuming that the tunneling between the lead and the dot is dominated by the contribution of the lowest transverse subband of the lead and using (7.4) for the partial width  $\Gamma_\alpha$ , we obtain

$$\Gamma_\alpha = 2\pi\rho_0^{(\alpha)} \left(\frac{\hbar^2}{m_*}\right)^2 \left| \int dy \phi_0(y) \sum_m a_m \phi_m(y) \right|^2 = \frac{2\pi\hbar^4}{m_*^2} \rho_0^{(\alpha)} |a_0|^2 \quad (7.34)$$

where  $\rho_0^{(\alpha)}$  is the density of states in the lead corresponding to the lowest transverse subband.

For an arbitrary moment of the partial width  $\langle \Gamma_\alpha^m \rangle$  we therefore find

$$\begin{aligned} \langle \Gamma_\alpha^m \rangle &\propto \int da_0 \left[ \frac{2\pi\hbar^4}{m_*^2} \rho_0^{(\alpha)} \right]^m |a_0|^{2m} \\ &\times \exp \left[ - |a_0|^2 \int dy_1 \int dy_2 \phi_0(y_1) \frac{1}{\partial_n C(y_1, y_2)} \phi_0(y_2) \right]. \end{aligned} \quad (7.35)$$

To give explicit expressions for the distribution of level widths and conductance, we specialize to the time-reversal symmetric case ( $\beta=1$ , GOE) for the rest of this paper; the case when time-reversal symmetry is broken by a magnetic field ( $\beta=2$ , GUE) can be treated in an analogous way. In the presence of time-reversal symmetry, the wave functions, and

hence the coefficient  $a_0$ , can be chosen real, yielding

$$\langle \Gamma^m \rangle \propto \int d\Gamma \Gamma^m \frac{\exp(-\Gamma/2\bar{\Gamma})}{\sqrt{\Gamma}} \quad (7.36)$$

where

$$\bar{\Gamma} = \frac{\hbar^4 \rho_0^{(\alpha)}}{m_*^2 \bar{\rho}_{sc}} \left( \int dy_1 \int dy_2 \phi_0(y_1) \frac{1}{\text{Im}[\partial_n G_{sc}(y_2, y_1 | \varepsilon)]} \phi_0(y_2) \right)^{-1}. \quad (7.37)$$

*Thus the partial width is characterized by the Porter-Thomas distribution*

$$P(\Gamma) \propto \frac{1}{\sqrt{\Gamma}} \exp\left(-\frac{\Gamma}{2\bar{\Gamma}}\right) \quad (7.38)$$

*with the slowly varying local average  $\bar{\Gamma}(\varepsilon)$ .* This explicit result for the distribution of level widths is the main result of this section.

The conductance distribution  $P(G)$  can now be simply derived in two limiting cases: (i) when the leads are placed symmetrically, so that  $\Gamma_1 = \Gamma_2$  [cf. Eq. (7.2)], and (ii) when one of the partial widths is substantially smaller than the other,  $\Gamma_1 \ll \Gamma_2$ . In both these cases  $G \sim \Gamma_1$  [as follows from Eq. (7.1)], and the conductance distribution is also Porter-Thomas. The “local average” conductance,  $\bar{G}$ , is given by

$$\bar{G}(\varepsilon) = \frac{e^2 \pi}{2\gamma \hbar k T} \bar{\Gamma}(\varepsilon) \quad (7.39)$$

where the “local average” width  $\bar{\Gamma}(\varepsilon)$  is defined by Eq. (7.37), and  $\gamma = 1$  for  $\Gamma_1 \ll \Gamma_2$ , while

$\gamma=2$  for  $\Gamma_1=\Gamma_2$ .

In the general case,  $\Gamma_1/\Gamma_2 \sim \mathcal{O}(1)$  but not identical, however, an exact calculation of the conductance distribution is complicated by the essentially nonlinear dependence of the conductance on the partial widths  $\Gamma_1$  and  $\Gamma_2$ . In order to calculate the actual conductance, we choose the area  $S$  as the composition of two narrow strips,  $S_1$  and  $S_2$ , near each of the leads. Using the transverse lead wave functions as the basis in each of the two strips,

$$\bar{\psi}(y, z) = z \left[ \sum_m a_m^{(1)} \phi_m^{(1)}(y - y_\ell^{(1)}) + \sum_m a_m^{(2)} \phi_m^{(2)}(y - y_\ell^{(2)}) \right] \quad (7.40)$$

where the coordinates  $y_\ell^{(1)}$  and  $y_\ell^{(2)}$  represent the ‘‘contact points’’ of the leads. The partial widths  $\Gamma_1$  and  $\Gamma_2$  are then given by

$$\Gamma_1 = \frac{2\pi\hbar^4}{m_*^2} \rho_0^{(1)} |a_0^{(1)}|^2 \quad (7.41)$$

$$\Gamma_2 = \frac{2\pi\hbar^4}{m_*^2} \rho_0^{(2)} |a_0^{(2)}|^2 . \quad (7.42)$$

Assuming equal density of states in the leads,  $\rho_0^{(1)}(\varepsilon) = \rho_0^{(2)}(\varepsilon)$ , for the conductance  $G$  we obtain

$$G = \frac{\pi e^2 \hbar^3}{2 m_*^2 k T} \rho_0 \frac{|a_0^{(1)}|^2 |a_0^{(2)}|^2}{|a_0^{(1)}|^2 + |a_0^{(2)}|^2} . \quad (7.43)$$

An arbitrary  $n^{\text{th}}$  moment of the conductance  $G$ ,  $\langle G^n \rangle$ , can now be calculated by inte-



grating over the coefficients  $\{a_m\}$  for  $m \neq 0$ , yielding

$$\begin{aligned} \langle G^n \rangle &\propto \int da_0^{(1)} \int da_0^{(2)} \left[ \frac{|a_0^{(1)}|^2 |a_0^{(2)}|^2}{|a_0^{(1)}|^2 + |a_0^{(2)}|^2} \right]^n \\ &\times \exp \left[ -a_0^{(1)} \mathcal{A}_{11} a_0^{(1)} - a_0^{(2)} \mathcal{A}_{22} a_0^{(2)} - 2a_0^{(1)*} \mathcal{A}_{12} a_0^{(2)} \right] \end{aligned} \quad (7.44)$$

where the matrix  $\mathcal{A}$  is

$$\mathcal{A}_{\alpha\beta} = \int dy_1 \int dy_2 \phi_0 \left( y_1 - y_\ell^{(\alpha)} \right) \partial_n C^{-1} (y_1, y_2) \phi_0 \left( y_2 - y_\ell^{(\beta)} \right) . \quad (7.45)$$

Note that the definition (7.45) implies that the diagonal elements of the matrix  $\mathcal{A}$  are proportional to the corresponding partial widths,  $\mathcal{A}_{11} \sim \Gamma_1$ ,  $\mathcal{A}_{22} \sim \Gamma_2$ . A straightforward evaluation of the integrals in Eq. (7.44) using the substitution

$$x = \left[ a_0^{(1)} \right]^2 - \frac{2m_*^2 k T G}{\pi e^2 \hbar^3 \rho_0} \quad (7.46)$$

yields

$$\langle G^n \rangle = \int dG G^n P(G) \quad (7.47)$$

where the distribution is

$$P(G) = \frac{1}{\sqrt{G}} \exp \left( -\frac{1}{2} \text{Tr} \mathcal{A} G \right)$$

$$\times \int_0^\infty dx \frac{G+x}{x^{3/2}} \exp \left[ -\frac{1}{2} \mathcal{A}_{11} x - \frac{1}{2} \mathcal{A}_{22} \frac{G^2}{x} \right] \cosh \left[ \mathcal{A}_{12} G \left( \sqrt{\frac{x}{G}} + \frac{G}{x} \right) \right]. \quad (7.48)$$

Note that it is only the term involving  $\mathcal{A}_{12}$  which makes the remaining integral non-Gaussian and so hard to perform. However, this term is semiclassically small: from Eq. (7.45) it follows that the leading semiclassical term in the off-diagonal part of the matrix  $\mathcal{A}$  is of next order in  $\hbar$  compared to the leading diagonal terms. The  $x$ -integral in Eq. (7.48) is therefore dominated by the interval between  $1/(G\mathcal{A}_{11})$  and  $G\mathcal{A}_{22}$ , where the off-diagonal matrix element  $\mathcal{A}$  makes only a small correction *quadratic* in  $\mathcal{A}_{12}$ . Such a correction corresponds, however, to higher-order terms in  $\hbar$ . Corrections of this order were already neglected in the original semiclassical expansion of the Green function, and so to be consistent we discard all effects of the off-diagonal matrix element  $\mathcal{A}_{12}$  here. The integral in Eq. (7.48) can now be easily performed.

The semiclassical approximation to the conductance distribution is, then, simply a Porter-Thomas distribution, even in the general case:

$$P(G) = \left( \frac{2\pi}{\bar{G}} \right)^{1/2} \frac{1}{\sqrt{\bar{G}}} \exp \left[ -\frac{G}{2\bar{G}} \right], \quad (7.49)$$

where the “local average” conductance  $\bar{G}$  is

$$\bar{G} \equiv \left[ \frac{1}{\sqrt{G_1}} + \frac{1}{\sqrt{G_2}} \right]^{-2}, \quad (7.50)$$

and the “partial conductance”  $G_\alpha$  is related to the partial width  $\Gamma_\alpha$  via the standard relation

$$G_\alpha \equiv \pi e^2 / (2\hbar kT) \Gamma_\alpha. \quad (7.51)$$

As the semiclassical Green function,  $G_{\text{sc}}$ , and, consequently, the correlator,  $\partial_n C$ , can be expressed as a sum of the contributions of “zero-length” and longer classical trajectories, similar decompositions hold for the average partial width and average partial conductance:

$$\bar{\Gamma}_\alpha = \bar{\Gamma}_\alpha^0 + \bar{\Gamma}_\alpha^{\text{osc}} \quad (7.52)$$

$$\bar{G}_\alpha = \bar{G}_\alpha^0 + \bar{G}_\alpha^{\text{osc}} \quad (7.53)$$

where the “oscillatory” parts,  $\bar{\Gamma}^{\text{osc}}$  and  $\bar{G}^{\text{osc}}$ , depend on the longer classical trajectories and are of next order in  $\hbar$  compared to the smooth contributions,  $\bar{\Gamma}^0$  and  $\bar{G}^0$  which are the zero-length contributions.

We now proceed to the semiclassical calculation of the “local average” partial width  $\bar{\Gamma}$ . The defining equation (7.37) involves the functional inverse of the Green function, which is a hard object to calculate. Instead, we will use the original definition (7.4), which for the local average partial width yields

$$\bar{\Gamma} = \frac{2\pi\hbar^4}{m_*^2} \sum_\beta \rho_\beta \int dy_1 \int dy_2 \phi_\beta(y_1 - y_\ell) \phi_\beta(y_2 - y_\ell)^* \partial_n C(y_1, y_2) \quad (7.54)$$

where the correlation function of the normal derivatives of the dot wave functions  $\partial_n C(y_1, y_2)$

is related to the semiclassical Green function by Eq. (7.30).

If we now use some information about the lead wave functions, we can obtain an explicit expression for the average width  $\bar{\Gamma}$  in terms of the classical dynamics in the dot. When, as we assumed above, the tunneling from the lead to the dot is dominated by the lowest transverse energy subband in the constriction between the lead and the dot [3], the transverse potential in the tunneling region can be taken quadratic:  $U_\ell \sim \kappa (y - y_\ell)^2$ . In this case, the transverse dependence of the lead wave function is simply a harmonic oscillator wave function, so that at the edge of the dot  $\phi_0 \simeq c_\ell \exp[-(y - y_\ell)^2/2a_{\text{eff}}^2]$ , where  $y_\ell$  is the center of the lead and constriction, and the effective width is  $a_{\text{eff}} = \sqrt{\hbar}/\sqrt[4]{2\kappa m^*}$ . While the exact form of the lead wave function is not crucial, the  $\hbar$ -dependence of the width is important for the semiclassical argument which follows; note that  $a_{\text{eff}} \sim \sqrt{\hbar}$  does not depend on a particular transverse potential.

Using this information about  $\phi_0$  in the expression for the diagonal matrix elements  $\mathcal{A}_{11}$ ,  $\mathcal{A}_{22}$ , we see that the lead wave function restricts the integration to a semiclassically narrow region of width  $a_{\text{eff}} \sim \sqrt{\hbar}$ . This allows one to express the contribution of the open trajectories entering the Green function in terms of an expansion near their closed neighbors:

$$\begin{aligned} \bar{\Gamma} &= \bar{\Gamma}_0 + \frac{16}{m^*} \int dy \int dp_y f_W(y, p_y) \sum_\alpha \sqrt{\frac{(p_i^\alpha)_n (p_f^\alpha)_n}{m_{11}^\alpha + m_{22}^\alpha + 2}} \\ &\times \exp\left[-\frac{i}{\hbar} \frac{2m_{12}^\alpha}{m_{11}^\alpha + m_{22}^\alpha + 2} (p_y - \bar{p}_y^\alpha)^2\right] \exp\left[i \frac{S_\alpha(y, 0; y, 0; \varepsilon)}{\hbar}\right] \exp\left(-\frac{\tau_\alpha^2 W^2}{2\hbar^2}\right) \end{aligned} \quad (7.55)$$

where  $\bar{\Gamma}_0$  is the monotonic part of the resonance width,  $(p_i)_n$  and  $(p_f)_n$  are the normal

components of the initial and the final momenta of the closed orbit  $\alpha$ , the momentum  $\bar{\mathbf{p}} \equiv (\mathbf{p}_i + \mathbf{p}_f) / 2$ , the  $2 \times 2$  monodromy matrix [11]  $M_\alpha \equiv (m_{ij}^\alpha)$  is defined via the linearization of the Poincaré map near the closed orbit  $\alpha$ , and calculated at the contact point near the lead. We have also introduced in Eq. (7.56) the Wigner transform  $f_W^e$  of the lead wave function

$$f_W^e(y, p_y) \equiv \hbar^{-1} \int d\Delta y \phi_0(y - \Delta y/2, 0) \phi_0^*(y + \Delta y/2, 0) \exp(ip_y \Delta y / \hbar) \quad (7.56)$$

which describes the distribution in transverse position and momentum of electrons tunneling into the dot.

In the leading order in the distance between the contact point  $y$  of the closed orbit  $\alpha$ , and the center of the lead  $y_\ell$ , the action of the closed orbit  $S_\alpha$  scales linearly:

$$S_\alpha(y, 0; y, 0) \propto S(y_\ell, 0; y_\ell, 0) + \Delta p_y^\alpha (y - y_\ell) \quad (7.57)$$

where  $\Delta p_y$  is the change of transverse momentum after the traversal of the closed orbit. Assuming e.g. a Gaussian form of the lead wave function, the contribution of each of these closed orbits is suppressed by a factor exponentially small in  $\Delta p_y^2$ . This suppression is the effect of the mismatch of the closed orbit (momentum) with the distribution of transverse momentum at the lead, which is centered at zero with width  $\delta p_\ell \sim \hbar/a_{\text{eff}} \sim \sqrt{\hbar}$  for the lowest subband. Therefore, only closed orbits with *semiclassically* small momentum change  $\Delta p$  contribute to the width. This in turn implies that the closed orbit is located semiclassically

close (within a distance  $\sim \sqrt{\hbar}$ ) to a *periodic orbit* for which  $\Delta p \equiv 0$ . Using this proximity to a periodic orbit we can re-express the actions and momenta of the injection orbits in terms of the properties of their periodic neighbors (labeled by the index  $\mu$ ) as follows:

$$S_\alpha(y, 0; y, 0) \simeq S_\mu + \frac{\text{Tr}[M_\mu] - 2}{2m_{12}^\mu} (y - y_\mu)^2, \quad (7.58)$$

$$\bar{p}_y^\alpha \simeq p_y^\mu + \frac{m_{11}^\mu - m_{22}^\mu}{2m_{12}^\mu} (y - y_\mu) \quad (7.59)$$

Substitution of (7.58) and (7.59) into Eq. (7.56) and integration over  $y$  yields [21]

$$\bar{\Gamma} = \bar{\Gamma}_0 + \sum_{\mu:\text{p.o.}} A_\mu \cos\left(\frac{S_\mu}{\hbar} + \phi_\mu\right) \exp\left(-\frac{\tau_\mu^2 W^2}{2\hbar^2}\right) \quad (7.60)$$

where the monotonic part is

$$\bar{\Gamma}_0 = \frac{\sqrt{\pi}}{2} c_\ell^2 a_{\text{eff}} \frac{p^2}{m^*} e^{-\zeta} [I_0(\zeta) + I_1(\zeta)], \quad \zeta = \frac{p^2 a_{\text{eff}}^2}{2\hbar^2}, \quad (7.61)$$

the amplitude is

$$\begin{aligned} A_\mu &= 4\sqrt{2} \frac{\hbar c_\ell^2 p_z^\mu}{m^*} [\text{Tr}^2[M_\mu] (1 + \sigma_+^2) (1 + \sigma_-^2)]^{-1/4} \\ &\times \exp\left(-\frac{\sigma_+^2 \bar{p}^2}{(1 + \sigma_+^2)} - \frac{\sigma_-^2 \bar{y}^2}{(1 + \sigma_-^2)}\right) \end{aligned} \quad (7.62)$$

with

$$\begin{aligned}
\sigma_{\pm} &\equiv \frac{1}{2} \left[ \overline{m}_{12} - \overline{m}_{21} \pm \sqrt{(\overline{m}_{22} - \overline{m}_{11})^2 + (\overline{m}_{21} + \overline{m}_{12})^2} \right] \\
\overline{m}_{ij} &\equiv \frac{2m_{ij}^{\mu}}{\text{Tr}[M_{\mu}] + 2} \left( \frac{a_{\text{eff}}^2}{\hbar} \right)^{\frac{i-j}{2}} \\
\theta &\equiv \frac{1}{2} \arctan \left( \frac{\overline{m}_{22} - \overline{m}_{11}}{\overline{m}_{21} + \overline{m}_{12}} \right) \\
\bar{y} &\equiv \cos \theta (y_{\mu} - y_{\ell}) / a_{\text{eff}} + \sin \theta p_y^{\mu} a_{\text{eff}} / \hbar \\
\bar{p} &\equiv \cos \theta p_y^{\mu} a_{\text{eff}} / \hbar - \sin \theta (y_{\mu} - y_{\ell}) / a_{\text{eff}} ,
\end{aligned} \tag{7.63}$$

and  $\phi_{\mu}$  is a slowly varying phase. Here  $I_n$  is the Bessel function of complex argument,  $p$  is the magnitude of the electron momentum,  $\mathbf{p}^{\mu}$  is the electron momentum for the periodic orbit  $\mu$  at the bounce point,  $y_{\mu}$  is the bounce point coordinate,  $S_{\mu}$  is the action of the periodic orbit, and  $M_{\mu} \equiv (m_{ij}^{\mu})$  is the corresponding monodromy matrix [11]. Note the sharp suppression of the oscillatory effects in Eq. (7.62) if the periodic orbit does not match up to the lead wave function in *both* position and momentum space. The mismatch is characterized by  $\bar{y}$  and  $\bar{p}$ ; the most favorable case is that of a perpendicular periodic orbit hitting the edge of the dot right at the center of the lead,  $p_y^{\mu} = 0$  and  $y_{\mu} = y_{\ell}$  so that  $\bar{y} = \bar{p} = 0$ .

Further characterization of the peak fluctuations can be obtained from the peak-to-peak correlation function: this is a particularly interesting quantity because of the correlations sometimes observed experimentally [5, 6], as discussed in the Introduction. A natural measure of the statistics of nearby peaks is given by  $\delta G(E_m) \equiv G(E_m) - \langle G(E_n) \rangle_n$  in terms of

which the correlation function is

$$\text{Corr}_m [\delta G, \delta G] = \langle \delta G (E_{n+m}) \delta G (E_n) \rangle_n / \langle [\delta G (E_n)]^2 \rangle_n . \quad (7.64)$$

Substituting the conductance distribution (7.49) into (7.64), we obtain for symmetric leads

$$\text{Corr}_m = \delta_{m,0} + (1 - \delta_{m,0}) \times \frac{\sum_{\mu} A_{\mu}^2 \cos \left( \frac{\tau_{\mu} \Delta}{\hbar} m \right) \exp \left( -\frac{\tau_{\mu}^2 W^2}{\hbar^2} \right)}{4\bar{G}_0^2 + 3 \sum_{\mu} A_{\mu}^2 \exp \left( -\frac{\tau_{\mu}^2 W^2}{\hbar^2} \right)} . \quad (7.65)$$

Similar oscillatory behavior is expected in the height of a given peak as a function of magnetic field with the frequency of the oscillations proportional to the area covered by the periodic orbit, with the period of the corresponding oscillations related to the *area*, covered by a given periodic orbit.

## 7.5 Comparison with numerics and experiment

Since one of the main theoretical results of the present paper concerns the periodic modulation of the Coulomb blockade peak heights, it is natural to consider the Fourier power spectrum of  $G_{\text{peak}}(k)$ . In Fig. 7.1 we present a comparison of the numerical and semiclassical power spectra, calculated for a chaotic (stadium) dot, for three different placements of the leads. The data clearly demonstrate that the power spectrum has well-defined peaks corresponding to periodic orbits. The numerical results for the symmetric leads show excellent agreement with the semiclassical prediction and adequate representation for the asymmetric



leads.

As follows from Eq. (7.60), the oscillatory component of the “local average” conductance and the height of the corresponding peak in the power spectrum nontrivially depends on the position and the width of the lead. This dependence is illustrated in Fig. 7.2, where we plot the amplitude of the “diameter” orbit contribution to the conductance as a function of  $ka_{\text{eff}}$  extracted from numerical length spectrum and the corresponding semiclassical prediction.

In Fig. 7.3 we compare the semiclassical correlation function with numerical data for the stadium dot. The oscillatory behavior for large separations reflects the peak in the corresponding power spectrum in Fig. 7.1 and is in agreement with the semiclassical result. The positive correlation for nearest neighbors is also in agreement with the semiclassical theory, demonstrating the influence of dynamics even in this apparently non-semiclassical regime.

When  $T \gg \Delta$ , the major source of correlations between neighboring peaks is the joint contribution of several resonances to the same conductance peak [7]. In this regime the “nearest-neighbor” correlator is  $\text{Corr}_{m=1} \sim 1$ , and the dynamical effect accounts for only a small correction to the correlation function. However, for low temperature  $T \leq \Delta$ , the correlations due to temperature are exponentially suppressed. In this regime, as illustrated in Fig. 7.4, the correlations induced by dynamical modulation dominate, and they account for the experimentally observed enhancement of correlations at low temperatures [8]. For finite temperature each resonance is weighted by combinations of Fermi-Dirac functions and occupation numbers [22]. The occupation numbers used in Fig. 7.4 were obtained by

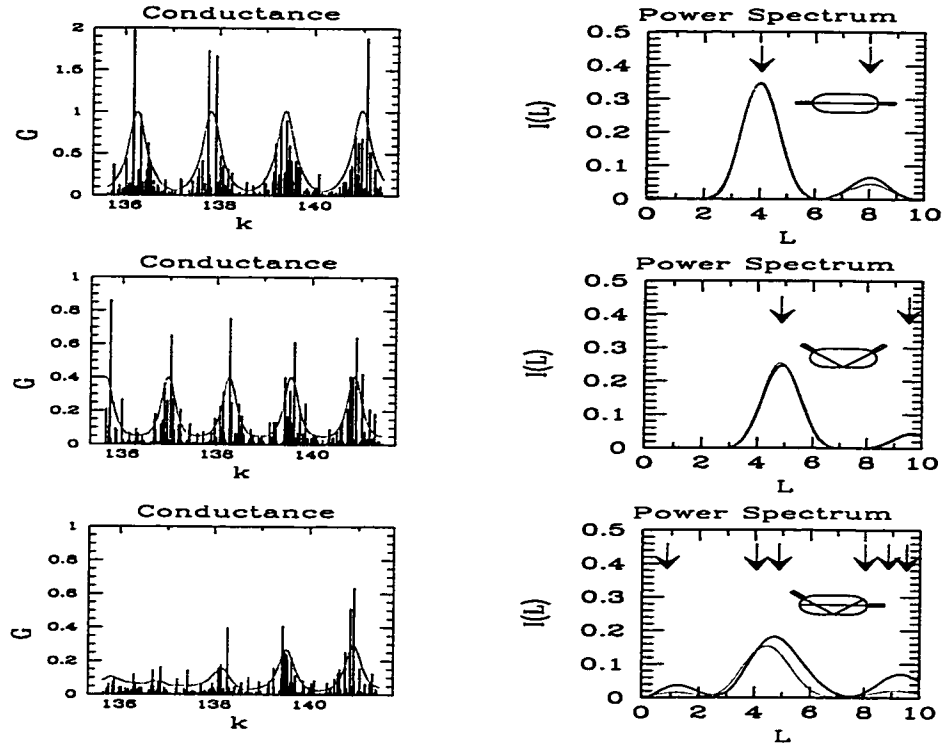


Figure 7.1: The peak conductances (left column) from tunneling through subsequent energy levels in the stadium quantum dot and the corresponding “length spectra”  $I(L)$  (right column) for different lead configurations (shown in the insets). In the peak conductance plots, each peak is placed at the wave vector  $k$  corresponding to its level;  $R$  is the radius of the half-circle parts of the stadium dot. A Gaussian lead wave function appropriate for tunneling from a single transverse mode is used with width  $ka_{\text{eff}} = 15$ . The red curves represent the semiclassical envelopes, defined by the contributions of the relevant periodic orbits (top: “diameter” orbit, middle: “V”-shaped orbit, bottom: both diameter- and V-orbits). Length spectrum of the oscillations in  $G(k)$  obtained from the Fourier power, numerical (black) and semiclassical (red) results are compared. The power is normalized to the mean conductance. The black arrows at the top show the positions of the relevant periodic orbits and their repetitions (black arrows), as well as the “combination lengths”  $L_1 \pm L_2$  (blue arrows). In the top panel, the peak at  $L/R \simeq 4$  is the diameter, that at 8 is its repetition. In the middle panel, the peak at  $L/R = 2(1 + \sqrt{2}) \approx 4.8$  corresponds to the V-shaped orbit, the peak at  $L/R \approx 9$  represents its repetition. In the bottom panel (asymmetric leads), the broad peak at  $L/R \simeq 4.5$  represents the total contribution of both diameter- and V-shaped orbits. For the stadium dot, the principal peaks appear at 4 and 4.8, because we use only the wave functions symmetric about the vertical symmetry axis (equivalent to using a half-stadium). Note the excellent agreement between the semiclassical theory and the numerical results for symmetric leads, and adequate representation for asymmetric leads.

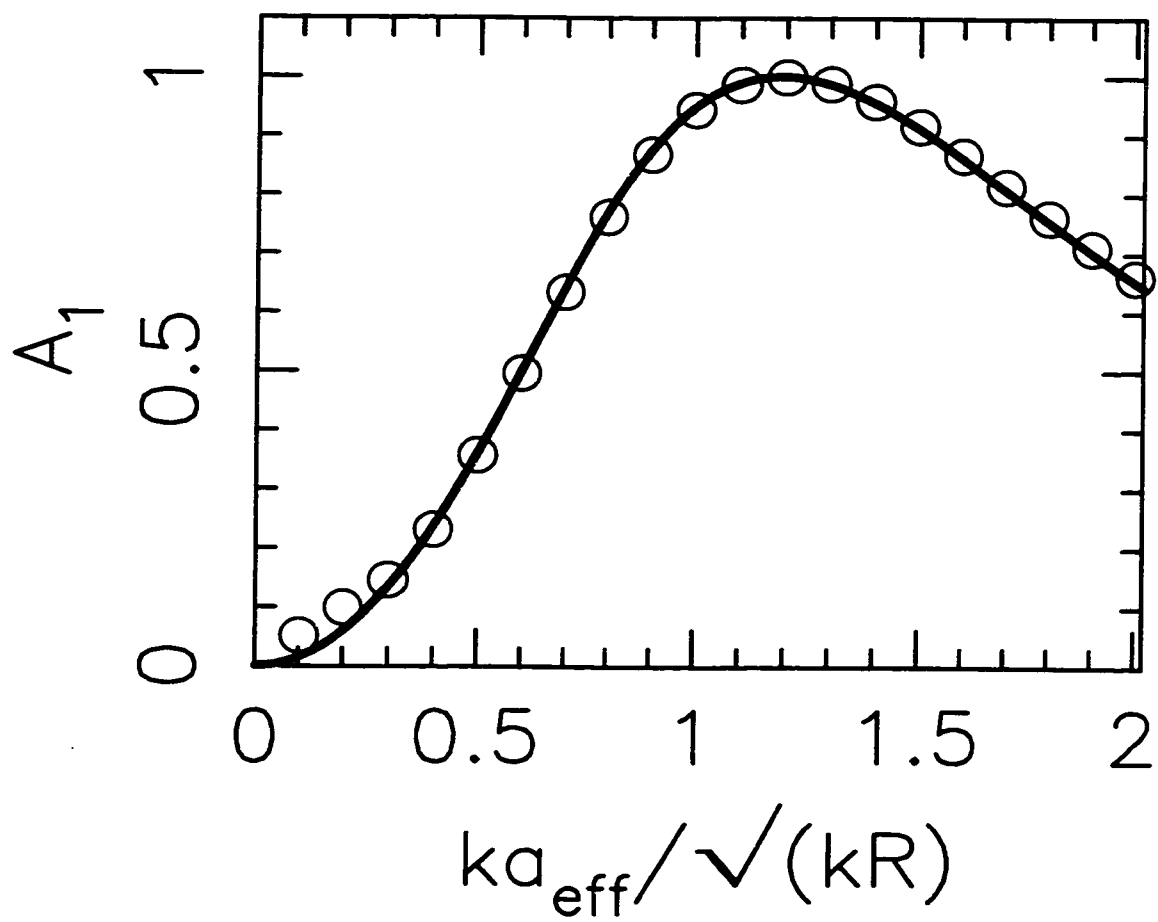


Figure 7.2: The dependence of amplitude of the length spectrum peak at  $L/R \simeq 4$  on  $ka_{\text{eff}}$ . The leads are symmetrically attached to the middle of the semicircle segments of the stadium dot.

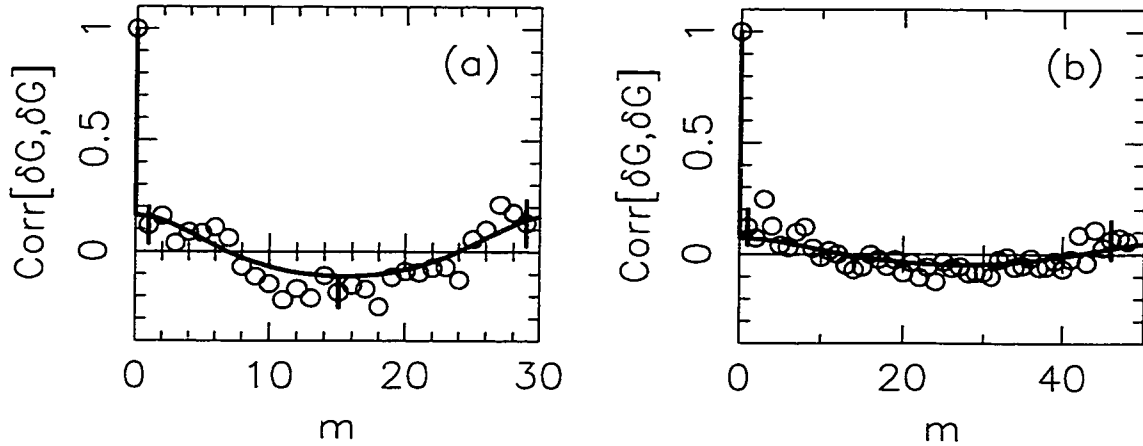


Figure 7.3: The peak-to-peak conductance correlation function for (a) symmetrically placed leads (attached to the “diameter” of the stadium dot), and (b) asymmetric leads (as in the inset to the length spectrum at the bottom of Fig. 7.1). The numerical correlation function (circles with typical error bars)—the average of all pairs of peaks  $m$  peaks apart—is in good agreement with the semiclassical theory (red). The agreement for small  $m$  is surprising since this regime is not semiclassical, but shows how dynamics can give rise to correlations even between nearest-neighbors. The difference between the periods of the modulation in (a) and (b) is accounted for by the difference in the values of  $kR$  used for the correlation function: the calculation for (a) is performed near  $kR = 70$ , while (b) corresponds to an interval near  $kR = 140$ .

employing a recursion relation [41] (see Appendix 7.A). As the temperature increases more resonances contribute to a single conductance peak, and thus dampening the effects of the longer orbits.

In Fig. 7.5 we present the results of the calculation of probability distribution of  $G_{\text{peak}}$  for a stadium quantum dot for both the “symmetric” and “asymmetric” placement of the leads. For comparison, we show both the actual distribution, Eqs. (7.49),(7.50), and the standard Porter-Thomas result without any account of the modulation of the average conductance:  $P(G_{\text{peak}}) = \sqrt{4/\pi G_{\text{peak}}} \exp(-G_{\text{peak}})$ . As the *individual* peak-height distribution is essentially a local measure, it’s not strongly sensitive to the correlations, and both the standard and the dynamical theories predict nearly the same result, and both are consistent with numerical calculation. This explains why no dynamical effect was observed in the experimental peak-height probability distribution [5, 6].

In contrast, the periodic modulation of the peak heights has been observed in several recent experiments [6, 8, 20]. The clearest observation is in Ref. [8]: the data in their Fig. 1 show modulated peak heights as a function of the number of electrons in the dot. In their trace of 90 peaks, approximately six oscillations are visible, yielding a period of  $\sim 15$  peaks. In our treatment, this period is the ratio of the period of fundamental oscillation in Eq. (7.60) to the level spacing  $\Delta$ . The fundamental period is given by  $(\frac{1}{h} \frac{\partial S_{\mu}}{\partial \epsilon})^{-1} \equiv h/\tau_{\mu}$  where  $\tau_{\mu}$  is the period of the relevant orbit. In the billiard approximation,  $\tau_{\mu} \equiv L_{\mu}/v_F$ , where  $L_{\mu}$  is the length of the periodic orbit and  $v_F$  is the Fermi velocity, which can be calculated from the experimental density [42]. Using the appropriate spin-resolved level spacing  $\Delta \simeq 10 \mu\text{eV}$

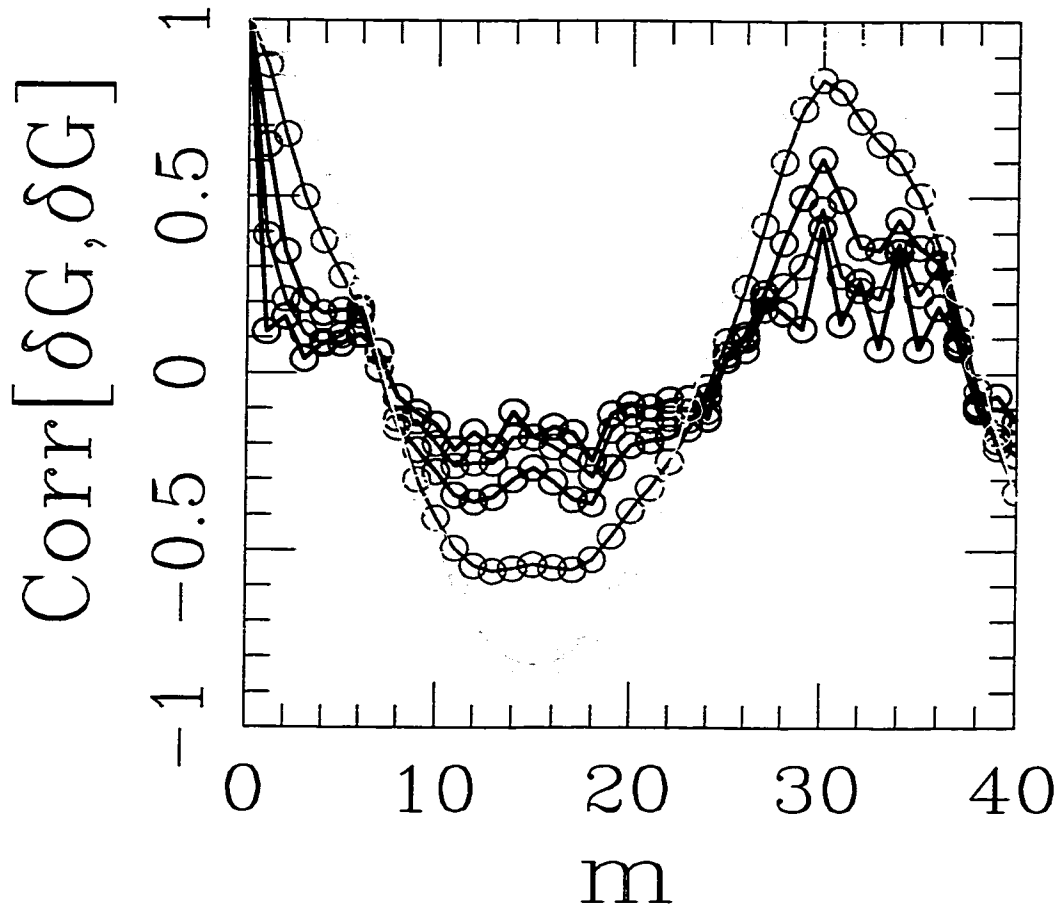


Figure 7.4: The peak amplitude correlation function for stadium-shaped quantum dot with symmetrically attached leads, for the temperature  $T = 0.25\Delta$ (red curve),  $0.5\Delta$ (blue),  $\Delta$ (green),  $2\Delta$ (yellow).

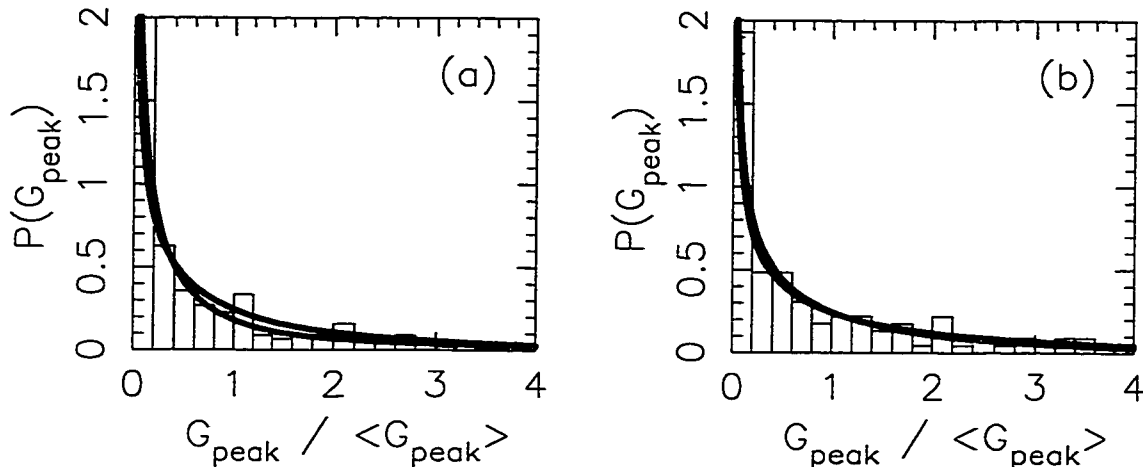


Figure 7.5: Conductance statistics: probability distribution function for (a) symmetrically and (b) asymmetrically placed leads. The numerical probability distribution (histogram) is for the entire range of data in Fig. 7.1 and is compared to both the semiclassical theory (red) and the standard statistical theory based on random wave functions (green). The two theories predict nearly the same result for this quantity (especially for asymmetric leads, where the dynamical modulation is weaker), and both are consistent with the numerics.

(which is half of the spin-full value from the measurements in Ref. [8]), we find  $L_\mu \simeq 5\mu m$ . This value is inconsistent with the typical size of the dot  $\leq 1\mu m$ . The above calculation assumes that the length of the orbit remained constant as additional electrons are added to the dot. By examining the configuration of the dot in the insert of Fig. 1 of [8], the gate voltage is situated on the shortest periodic orbit of each lead. By making the gate voltage more negative the electron will have a shorter path and thus contribute to the change of the action in Eq. (7.60). Also, it has been suggested [43] that the interaction of additional electrons cause the effective voltage of the dot to deform, increasing the size of the dot. This deformation will again change the path length of the periodic orbit.

A similar approach to the peak modulation as a function of magnetic field is also in

agreement with the experimental results [6, 20], where a quasi-periodic modulation of the peak heights was observed with the period  $\Delta B \simeq 35mT$ . In our treatment, this period is given by the ratio of flux quantum  $h/e$  to the area  $\mathcal{A}_0$  enclosed by the periodic orbit. We obtain  $\mathcal{A}_0 \simeq 0.12\mu m^2$ , which is consistent with the total area of the dot equal to  $0.32\mu m^2$  [6].

The dynamical modulation of the Coulomb Blockade peak heights however was not seen in the experiment of Ref. [5]. We attribute this behavior to a relatively small mean free path of  $\ell \sim 0.4\mu m$ , which only marginally exceeds the typical size of the dot  $d \simeq 0.3\mu m$ . As the length of the *shortest* periodic orbit is at least twice the effective “diameter”  $d$  of the dot,  $L_{\min} > 2d \simeq 0.6\mu m > \ell$ , in the experiment of Ref. [5] the dynamical effects are strongly suppressed by scattering and do not affect the Coulomb Blockade measurements.

The agreement of our semiclassical theory with experiment may seem surprising, since the adding of electrons may strongly influence the effective potential defining the dot. However, experiments on “magnetofingerprints” of the peaks [44] suggest robustness of the effective potential—its change from peak to peak is small. The energy levels undergo an overall shift in energy as an electron is added and smaller shifts in level spacings occur. These small deformations in the effective potential do not affect the action of the shortest periodic orbit substantially, but may still contribute to an action change.

## 7.6 Summary

In conclusion, using semiclassical methods, we developed a dynamical statistical theory of Coulomb blockade peak heights in chaotic quantum dots. We derived the peak height distri-



butions and the correlation functions, and showed that the corrections to the corresponding results of the standard statistical theory can be expressed in terms of the classical periodic orbits of the dot. Both our analytical results and numerical simulations clearly demonstrate that the dynamical effect is significant for both symmetric and asymmetric lead placements.

We close with two further experiments suggested by our results. First, if the tuning parameter used to change the number of electrons, such as a gate voltage, does not change the action of the dominant periodic orbit, then no modulation connected to that orbit should be seen. In particular, gates which affect different parts of the dot may produce different oscillatory behavior. Second, several samples made in a robust geometry—a circle with directly opposite leads, for example—should show the same modulation. Any deviations from the same behavior would be a sensitive indication of the material quality.

## Acknowledgments

We gratefully acknowledge stadium eigenfunction calculations by J. H. Lefebvre, and helpful discussions with C. M. Marcus and M. Srednicki. We thank L. Kaplan for making available Ref. [33] which we received during the final stages of this work.

## 7.A Temperature Calculations

For nonzero temperatures the conductance is obtained from a weighted sum over the zero temperature partial widths  $\Gamma_\lambda$  [22]. For symmetric leads this yields

$$G = \frac{e^2}{h} \frac{\pi}{4kT} \sum_\lambda w_\lambda \Gamma_\lambda \quad (7.66)$$

If  $kT, \Delta \ll e^2/C$ , then the weights are given by

$$w_\lambda = 4f(\Delta F_{N_0} - \tilde{E}_F) \langle n_\lambda \rangle_{N_0} [1 - f(E_\lambda - \tilde{E}_F)] \quad (7.67)$$

where  $\Delta F_N$  is the change in the canonical free energy from  $N - 1$  to  $N$ ,  $\langle n_\lambda \rangle_N$  is the canonical occupation,  $\tilde{E}_F = E_N + (N - 1/2)e^2/C$  is an effective Fermi energy and  $f(\epsilon) = [1 + \exp(\epsilon/kT)]^{-1}$  is the Fermi-Dirac function.

To obtain the canonical free energy and canonical occupation number we use a recurrence relation developed by Brack, Genzken and Hansen [41] for the partition function  $Z(N, M; \beta)$ .  $N$  is the number of particles,  $M$  is the number of levels and  $\beta = 1/kT$ . The final result for the partition function will not numerically depend upon  $M$ . The partition function is formally given by

$$Z(N, M; \beta) = \sum_{\alpha=1}^{I_{NM}} \exp(-\beta E_\alpha(N)) \quad (7.68)$$

where  $E_\alpha(N)$  is the sum of the energy of the occupied levels  $\epsilon_M$  and  $I_{NM}$  is the number of

partitions. The recurrence relation is as follows

$$Z(N, M; \beta) = Z(N, M - 1; \beta) + \exp(-\beta\epsilon_M)Z(N - 1, M - 1; \beta) \quad \text{for } N \geq 1, M \geq N \quad (7.69)$$

with the conditions

$$\begin{aligned} Z(0, M; \beta) &\equiv 1 \quad \forall M \geq 0 \\ Z(N, N - 1; \beta) &\equiv 0 \quad \forall N \geq 1 \end{aligned} \quad (7.70)$$

For the calculations of the conductance peaks the number of electrons in the dot exceeded 2500. This results in the recurrence relation ranging over many orders of magnitude; the range is beyond the precision of the computer. Since only small temperatures are considered, the partition function will be unity a few mean level spacing below the Fermi energy. Thus, we only need to calculate the partition function in the vicinity of the Fermi energy.

The occupation numbers  $\langle n_\lambda \rangle_N$  are obtained by recalculating the partition function with the  $\lambda$ th level removed from the spectrum, dividing by the total partition function and subtracting the result from one. The canonical free energy for  $N$  electrons is

$$F(N) = \frac{-1}{\beta} \ln Z(N, M; \beta) \quad (7.71)$$

## References

- [1] H. Grabert and M. H. Devoret, *Single Charge Tunneling: Coulomb Blockade Phenomena in Nanostructures* (Plenum Press, New York, 1992).
- [2] R. A. Jalabert, A. D. Stone, and Y. Alhassid, *Phys. Rev. Lett.* **68**, 3468 (1992).
- [3] L. P. Kouwenhoven, C. M. Marcus, P. L. McEuen, S. Tarucha, R. M. Westervelt, and N. S. Wingreen, in *Mesoscopic Electron Transport*, edited by L. L. Sohn, L. P. Kouwenhoven, and G. Schön (Kluwer, Dordrecht, 1997) pp. 105-214.
- [4] M. Stopa, *Physica B* **251**, 228 (1998).
- [5] A. M. Chang, H. U. Baranger, L. N. Pfeiffer, K. W. West, and T. Y. Chang, *Phys. Rev. Lett.* **76**, 1695 (1996).
- [6] J. A. Folk, S. R. Patel, S. F. Godijn, A. G. Huibers, S. M. Cronenwett, and C. M. Marcus, *Phys. Rev. Lett.* **76**, 1699 (1996).
- [7] Y. Alhassid, M. Gökçedag, and A. D. Stone, *Phys. Rev. B* **58**, 7524 (1998).
- [8] S. R. Patel, D. R. Stewart, C. M. Marcus, M. Gökçedag, Y. Alhassid, A. D. Stone, C. I. Duruöz, and J. S. Harris, Jr., *Phys. Rev. Lett.* **81**, 5900 (1998).

- [9] M. Stopa, *Phys. Rev. B* **54**, 13767 (1996).
- [10] G. Hackenbroich, W. D. Heiss, and H. A. Weidenmüller, *Phys. Rev. Lett.* **79**, 127 (1997).
- [11] M. Gutzwiller, *Chaos in Classical and Quantum Mechanics* (Springer, New York, 1990).
- [12] J. B. Delos and C. D. Schwieters, in *Classical, Semiclassical and Quantum Dynamics in Atoms*, ed. by H. Friedrich and B. Eckhardt, (Springer, Berlin, 1997) p. 223-247; M. W. Beims, V. Kondratovich, and J. B. Delos, *Phys. Rev. Lett.* **81**, 4537 (1998).
- [13] E. J. Heller, in *Chaos and Quantum Physics*, edited by M. J. Giannoni, A. Voros, and J. Zinn-Justin (Elsevier, Amsterdam, 1991) pp. 547-663.
- [14] L. Kaplan, *Phys. Rev. Lett* **80**, 2582 (1998); L. Kaplan, and E. J. Heller, *Annals of Phys.* **264**, 171 (1998).
- [15] D. Weiss, K. Richter, A. Menschig, R. Bergmann, H. Schweizer, K. von Klitzing and G. Weimann, *Phys. Rev. Lett.* **70**, 4118 (1993); G. Hackenbroich, and F. von Oppen, *Europhys. Lett.*, **29**, 151 (1995); K. Richter, *Europhys. Lett.* **29**, 7 (1995).
- [16] E. E. Narimanov, A. D. Stone, and G. S. Boebinger, *Phys. Rev. Lett.* **80**, 4024 (1998); an alternative semiclassical theory of resonant magnetotunneling was developed by E. B. Bogomolny and D. C. Rouben, *Europhys. Lett.* **43**, 111 (1998).
- [17] T. S. Monteiro, D. Delande, A. J. Fisher, G. S. Boebinger, *Phys. Rev. B* **56**, 3913 (1997).

- [18] D. Saraga and T. S. Monteiro, *Phys. Rev. Lett.* **81**, 5796 (1998).
- [19] E. E. Narimanov, and A. D. Stone, *Physica D* **131**, 220 (1999).
- [20] S. M. Cronenwett, S. R. Patel, C. M. Marcus, K. Campman, and A. G. Gossard, *Phys. Rev. Lett.* **79**, 2312 (1997).
- [21] E. E. Narimanov, N. R. Cerruti, H. U. Baranger, and S. Tomsovic, *Phys. Rev. Lett.* **83**, 2640 (1999).
- [22] C. W. J. Beenakker, *Phys. Rev. B* **44**, 1646 (1991).
- [23] J. Bardeen, *Phys. Rev. Lett.* **6**, 57 (1961).
- [24] M. V. Berry, *J. Phys. A* **10**, 2083 (1977).
- [25] Y. Alhassid and C. H. Lewenkopf, *Phys. Rev. Lett.* **75**, 3922 (1995).
- [26] M. Srednicki, *Phys. Rev. E* **54**, 954 (1996).
- [27] V. N. Prigodin, K. B. Efetov, and S. Idia, *Phys. Rev. Lett.* **71**, 1230 (1993).
- [28] V. N. Prigodin, B. L. Altshuler, K. B. Efetov, and S. Idia, *Phys. Rev. Lett.* **72**, 546 (1994).
- [29] V. N. Prigodin, *Phys. Rev. Lett.* **74**, 1566 (1995).
- [30] V. N. Prigodin, N. Taniguchi, A. Kudrolli, V. Kidambi, and S. Sridhar, *Phys. Rev. Lett.* **75**, 2392 (1995).

- [31] M. Srednicki and F. Stiernelof, *J. Phys. A* **29**, 5817 (1996).
- [32] S. Hortikar and M. Srednicki, *Phys. Rev. Lett.* **80**, 1646 (1998).
- [33] L. Kaplan, preprint, arXiv:nlin.CD/0003013 (2000).
- [34] C. Jarzynski, *Phys. Rev. E* **56**, 2254 (1997).
- [35] C. E. Shannon, *A Mathematical Theory of Communication*, The Bell System Technical Journal **27**, 379-423, 623-656 (1948).
- [36] L. E. Reichl, *The Transition to Chaos In Conservative Classical Systems: Quantum Manifestations* (Springer, New York, 1992).
- [37] P. W. Brouwer, Y. Oreg, and B. I. Halperin, *Phys. Rev. B* **60**, R13977 (1999).
- [38] H. U. Baranger, D. Ullmo, and L. I. Glazman, *Phys. Rev. B* **61**, R2425 (2000).
- [39] D. Ullmo and H. U. Baranger, in preparation.
- [40] M. Srednicki, private communication.
- [41] M. Brack, O. Genzken, and K. Hansen, *Z. Phys. D—Atoms, Molecules and Clusters* **21**, 65 (1991).
- [42] C. M. Marcus, private communication.
- [43] R. O. Vallejos, C. H. Lewenkopf, and E. R. Mucciolo, *Phys. Rev. Lett.* **81**, 677 (1998).

[44] D. R. Stewart, D. Sprinzak, C. M. Marcus, C. I. Duruöz, and J. S. Harris, *Science* **278**, 1784 (1997).



## Chapter 8

### Conclusion

In conclusion, we demonstrated that the variance of the level velocities are related to classical diffusion coefficients. This relation works well in both the mixed and chaotic regimes for the standard map. Also, the level velocities and overlap intensities are shown to be correlated which is contrary to ergodic theory. The regions of phase space where high correlation occurs are connected to specific classical features of the systems. For the stadium billiard, the high correlations corresponded to “gateways” into marginally stable regions of phase space, and for maps, they corresponded to homoclinic points of an orbit associated with the perturbation.

Moreover, a semiclassical theory of the modulation of the Coulomb blockade peak heights was developed. The theory agrees with the standard statistical theory for the peak height distributions and correctly yields the peak-to-peak correlations and peak modulations observed in experiments. The theory was developed for both symmetric and asymmetric leads and uses the periodic orbits of the system.

We have shown a few examples of how ergodicity is violated in quantum systems that are classically chaotic. These violations arose out of the short time dynamics and can be expressed as “corrections” to the ergodic model where the zero order approximations are the random matrix theory results. Thus, quantum chaotic systems have a richer display of features than suggested by the ergodic model for these systems.

The ergodic theory is still useful since it correctly predicts many of the statistics of chaotic systems. In approaching problems in quantum chaos it is advantageous to have a groundwork such as RMT that sets the background from which deviations take on meaning. RMT is extreme statistical model and does not represent any physical system. It is usually much easier to work out than the system based semiclassical theory which, in principle, is capable of seeing system specific features.

We close with a few suggestions for further research. In the mixed regime when most of the phase space is chaotic but a few small tori remain, a phenomenon called anomalous diffusion occurs. Normal diffusion is linear in time, while anomalous diffusion has an exponent of time greater than one. Our derivation of the variance of the level velocities in Chapter 3 did not include the presence of accelerator modes which cause anomalous diffusion. Accelerator modes occur when classical trajectories come close to the remaining tori. An interesting question is how these classical features manifest themselves in the quantum level velocities.

Throughout this dissertation, the parameters being varied have all been time independent. In the context of RMT, the diffusion constant has been worked out for the time dependent case [1], but a semiclassical theory is lacking. It has been shown that phase space localization causes deviations for RMT in the stadium billiard with moving boundaries [2]. The techniques used in Chapter 4 can be modified to cope with a time dependent parameter. This has applications in quantum dots with oscillating electric fields applied to them.

Other parametric correlators have also been developed along with their RMT predictions [3]. These correlators involve the eigenfunctions of the system and were found to be

universal in the framework of RMT. A detailed study of these correlators might show deviations from RMT and would suggest that the dynamics of the system gives corrections to the universal behavior.

Another area for further research is in the temperature dependence on the semiclassical theory of the conductance peak heights. As mentioned in Chapter 7 temperature enhances the correlation between the conductance peaks in the Coulomb blockade regime. A finite temperature will exponentially suppress the longer orbits and only the shortest periodic orbit will contribute. After subtracting out the modulation, the distribution of the peak heights collapses to a delta function as the temperature increases. Since all experiments are conducted at a finite temperature, knowing in more detail how the temperature affects the modulation of the conductance peaks is important.

The localization of classical electrons in a two-dimensional periodic potential has been studied [4]. The potential was taken as sinusoidal to simulate atoms on a crystalline surface. The transition from localized to delocalized motion occurred at energies well above the energy needed for an electron to escape from a single cell. A semiclassical analysis of this study might gain some more insight to physical problems of this nature; for instance, the motion of surface defects on a lattice could be analyzed with these methods.

## References

- [1] M. Wilkinson, *Phys. Rev. A* **41**, 4645 (1990).
- [2] D. A. Wisniacki and E. Vergini, *Phys. Rev. E* **59**, 6579 (1999).
- [3] Y. Alhassid and H. Attias, *Phys. Rev. Lett.* **74**, 4635 (1995).
- [4] R. Haydock, unpublished.